

ISSN 2187-2260

**Proceedings of the 22nd Meeting of
Japan CF Research Society
JCF 22**

March 5, 2022

Virtual Meeting

Japan CF-Research Society

Edited by Shinya Narita

Copyright © 2022 by Japan CF Research Society

All rights reserved. No part of this publication may be reproduced, stored in a retrieval system, or transmitted, in any form or by any means, electronic, mechanical, photocopying, recording or otherwise, without the prior permission of the copyright owner.

PREFACE

This is the proceedings of the 22nd Meeting of Japan CF-Research Society (JCF22). Since the pandemic of COVID-19 has not calmed down, the meeting was held in online format again, following JCF21. In this meeting, 8 presentations were given and 6 papers were submitted to the editorial board. They have been peer reviewed by the referees, and revised for the publication as the proceedings.

For all meetings, JCF1 through JCF21, we published the Proceedings. For the meetings after JCF4, we published electronic versions of the proceedings on our web-site http://jcfrs.org/proc_jcf.html in addition to their printed versions. In view of low efficiency and low effectiveness in distributing information, we decided to discontinue the printed version for the meetings, JCF12. Only the electronic versions have been published thereafter. Any comment and questions from the scientists all over the world are welcomed.

JCF22 was in part financially supported by The Thermal & Electric Energy Technology Foundation, which deserves special acknowledgements.

Finally, we would like to thank all the participants and the people who have collaborated in organizing this meeting.

Editor-in-Chief
Shinya Narita, Iwate University
Sep 2022

CONTENTS

Preface: S. Narita	i
New MHE Experiments by D-System <i>Y. Mori, A. Takahashi, M. Hasegawa, J. Hachisuka, Y. Furuyama</i>	1
Characteristics of Excess Power Generation in MHE Experiments by D-System <i>M. Hasegawa, A. Takahashi, Y. Mori, J. Hachisuka, Y. Furuyama</i>	13
Energy Generation using Nano-sized Multilayer Metal Composites with Hydrogen Gas; Intentional Induction of Heat Burst Phenomenon <i>Y. Iwamura, T. Itoh, T. Takahashi, S. Yamauchi, M. Saito, S. Murakami, J. Kasagi</i>	27
Heat generation of metal composite powder caused by the pulse flow of hydrogen gas <i>T. Kobayashi, K. Naitoh, J. Shigemura, D. Okada, Y. Nomura</i>	40
Recent Progress of Deuterium/Hydrogen Desorption Experiments Using Pd-Ni Samples <i>S. Narita, M. Endo, H. Matsuhashi, N. Yanagidate, A. Shoji</i>	50
Computer Simulation on the Metal Hydride Band Gaps of Pd, Ni and Cu Metal Lattices <i>H. Miura</i>	58

New MHE Experiments by D-System

Yutaka Mori¹, Akito Takahashi¹, Masahiko Hasegawa¹, Joji Hachisuka¹,
Yuichi Furuyama²

¹ Technova Inc. ² Kobe University,

*corresponding author e-mail: mori@technova.co.jp

Abstract We have studied the so-called AHE (anomalous heat effect) by calorimetry of our C-system. The C-system was designed to make accurate detection of excess thermal power larger than several W/kg-sample. By our latest data with significant increase of excess thermal power of the MHE (nano-metal hydrogen energy) experiment, we have met to needs for improving the system. Especially in cases of observing 200W/kg-sample level excess power evolution using re-calcined PNZ- and CNZ-type MHE powder-samples, we have found some drawbacks in calorimetry with the C-system. We have therefore developed a new system, called D-system. In our new system (D-system), we have made the following improvements:

- a) Heat recovery system to cover higher temperature conditions as over 500°C of hydrogen gas condition of reaction chamber
- b) Increase detection points of heat sensors
- c) Reaction chamber assembly with high temperature-tight performance

One drawback of the C-system was due to the problem that calorimetry inaccuracy became very large (underestimation) when coolant oil temperature reached at boiling point (ca. 350°C). In the D-system, we use the heat recovery by radiation heat transfer from the surface of reaction chamber settled in outer vacuum chamber. As a result, we can operate H-gas feeding runs with MHE sample powder to extend for much higher temperature conditions. We can take characteristic AHE data of excess thermal power with additional key data as evolution of H/Ni loading ratio. Characteristic feature of latest AHE data will be shown by another paper in this JCF22 meeting.

Key words: nano-metal hydrogen energy(MHE), the anomalous heat effect(AHE), C-system, D-system, calorimetry, H-loading ratio, excess heat, higher temperature run, sensor positions

1. INTRODUCTION

In our recent study on nano-metal hydrogen energy (MHE), we have observed a trend that reaction activity is increasing in higher temperature (around 500 °C). We need to study reaction characteristics in much higher temperature condition. We have observed also that excess power by reaction increased significantly by the repeated re-calcination of MHE powder samples (PNZ and CNZ types). Level of excess heat power by our latest experiments reached at the level of 200 W/kg-sample^{2, 4-6}.

The C-system⁴⁻⁶, which we have used for investigating anomalous heat effect (AHE) with calorimetry designed to detect excess thermal power level of several watts per kg MHE-sample, has been found with some drawbacks. When sample temperature in reaction chamber elevates far over the boiling point (near 350 °C) of coolant oil, there happened significant underestimation of heat power by mass flow calorimetry, and regular cooling of reaction chamber (RC) became difficult. We need an improved system to do experiments at higher RC temperatures than about 400 °C by avoiding oil boiling.

In addition, we need to reveal unresolved points on the AHE phenomenon mechanism, although we have obtained significant progress in recent studies by the C-system⁴⁻⁶). Especially, we need to know more detail of temperature distribution inside RC, for investigating heat generation distribution by the MHE reaction. Important detection points of temperatures are those at the highest temperature point (maybe at real mid-point) in RC, gas temperature in RC and various points in MHE powder sample region. To estimate amount of excess thermal power in RC, as accurate as possible, we need to study such various temperature-responses of RC points.

Our study has been concentrated in elucidating AHE generation mechanisms by the MHE experiments, under the guiding view of the TSC theory³). The 4H/TSC WS fusion theory predicts that dynamic evolution of hydrogen loading ratio (H/Ni value) should closely correlate to the generation pattern of excess heat power. Therefore, precise information of evolutionary dynamics of hydrogen absorption and desorption with MHE powder samples is of primary importance. To monitor precise evolution of H/Ni loading ratio, we need precise variation data of hydrogen gas in several points of the new D-system. The new D-system was designed to satisfy key points mentioned above, made and improved by start-up operation runs.

2. EXPERIMENTAL APPARATUS SYSTEM AND SENSORS

2.1 Previous MHE experimental system (called C-system)

Schematic views of our C-system which we have used in past^{1,4-6}) are shown in Fig.1 (whole view) and Fig.2(cross section of reaction chamber), respectively. The reaction chamber (RC) is thermally isolated by vacuum inside the outer chamber of cylindrical shape, and is set up vertically. There are two heaters called W1(wound outside of RC) and W2(set in lower central place of RC inside). Four temperature sensors (RTD) are placed at different heights with same radial distance from the center line. To monitor H-gas temperature, no direct measuring sensors in RC but a TC (thermos-couple) at H-gas inlet/outlet tube surface of RC outer flange. Heat removal of RC is made with oil flow through spirally wound oil coolant tube. Removed heat power is sum of heater powers and excess heat by AHE of the MHE reaction.

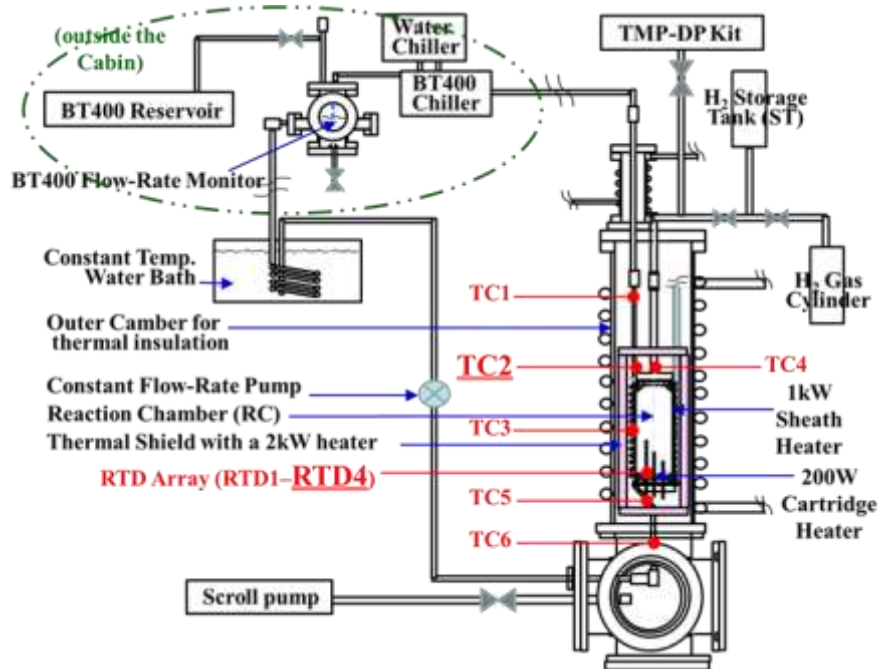


Fig.1; MHE experiment system (called C-system)

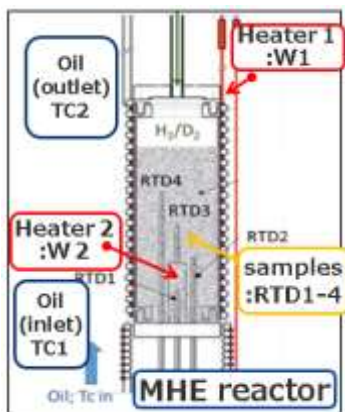


Fig.2; Cross-section of Reactor

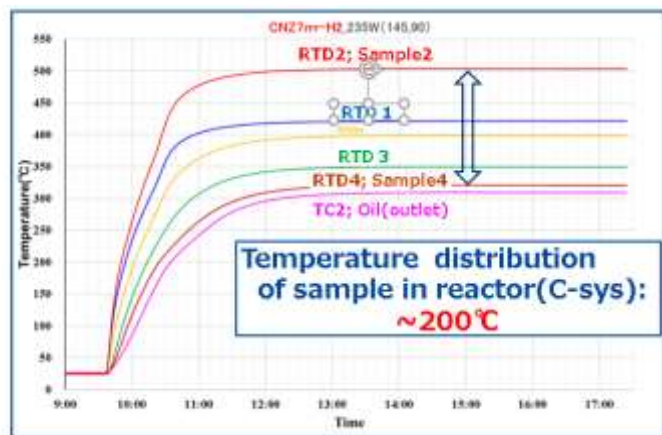


Fig.3; Temperature responses toward equilibrium after heater ON

In Fig.3, example of raw data is shown for temperature sensors as a function of elapsed time from start of heating to time region of rather equilibrium temperature distributions.

The highest temperature observed by RTD2 (60 mm high from the bottom of RC) reached 500 °C, which is over the coolant oil boiling point of 350 °C. Difference of temperatures for the highest point (RTD2) and the lowest point (RTD4 at 120mm high) is very large as 200 °C. Excess heat power levels by using latest MHE powder samples (CNZ: $\text{Cu}_1\text{Ni}_7/\text{ZrO}_2$ and PNZ: $\text{Pd}_1\text{Ni}_{10}/\text{ZrO}_2$) were observed with significant increment by repeated re-calcination of powder samples to have reached to the level of 200 W/kg-sample^{2, 4-6}. We can expect further scale increment of excess power by increasing reaction sites after calcination treatment and RC temperature elevation.

The design of the C-system was made based on conditions of RC temperature and smaller excess power level as several W/kg-sample, so as to carry out thoughtfully accurate calorimetry runs. Now we need an improved system for extending our study in much higher temperature zone and much larger excess power generation. Points of improvement are:

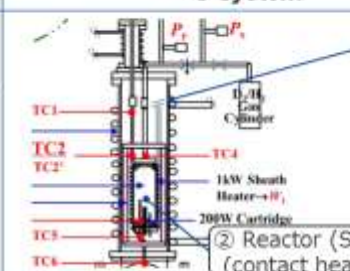
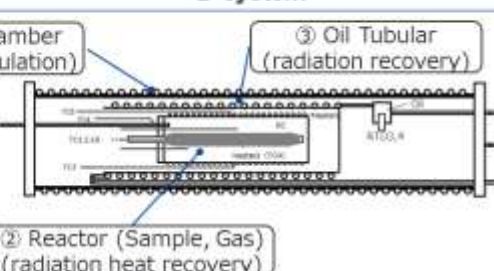
- 1) Heat recovery under keeping coolant oil temperature less than the boiling point (350 °C).
- 2) Sample mounting in RC to attain as homogeneous as possible temperature distribution in RC.
- 3) Addition of temperature sensors, particularly for H-gas temperature in RC and central zone temperature amid the RC cylinder.

2. 2 New MHE experimental system (called D-system)

With above mentioned subjective, new system called D-system was designed and constructed. Structures and main performances are compared in Table 1 in comparison between the C-system and the newer D-system. Major improvements in the D-system are as follows.

- 1) Oil coolant tube is separated by vacuum isolation, so that RC can be heated well over 500 °C.
- 2) MHE sample powder is set up inside a mesh holder, so that width of temperature distribution in sample zone can be narrowed with smaller amount of sample.
- 3) Temperature sensors are added for H-gas zone and RC center line's middle.
- 4) New H-gas valves in designated sections of near RC inlet and H-gas reservoir outlet points.

Table 1; Comparison of C-system and D-system

Apparatus	C-system	D-system
Structure		
Cross section		
points	◇precision heat power measurement (10~100W) Structure : longitudinal setting of two chambers	◇Higher heat power measurement at high temp. (10~1,000W) Structure : transvers setting of two chambers & oil tubular
Characteristics	Heat recovery : direct heat transfer on outside RC ● Issues of apparatus 1) [Material temp.] upper limit due to oil boiling 2) [Temp. distribution] large between top & bottom	Heat recovery : radiation heat transfer from outside RC ○ Modified in D-sys. 1) higher temperature for evaluation of MHE reaction 2) Smaller for precise analysis of MHE reaction

For the D-system RC setting, horizontal alignment was employed for easier working in sample changing works, while vertical alinement was employed for the C-system.

In addition, the horizontal alinement is expected to increase direct contact surface between sample zone and H-gas zone. In Fig. 4(1), over all schematic of the D-system

is shown. In Fig. 4(2), system control and sensors data logging are shown. Photographs of D-system are shown in Fig.5(1) and (2). Some detail explanation of improvement in D-system will be mentioned in the next section. Control method of MHE reaction activation and data logging are same with those for the C-system, except for RC-valve operation.

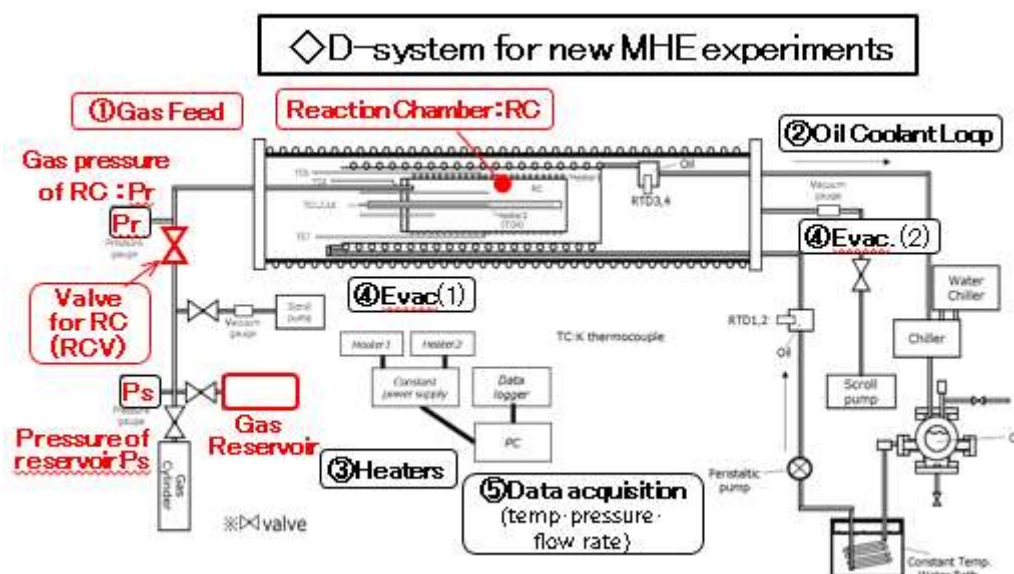


Fig.4(1); New MHE experiments apparatus; D-system

- ① **Gas Feed** : Hydrogen supply to reactor
 - Storage tank of hydrogen for test
 - Hydrogen valve between reservoir and reactor to confirm the situation of adsorption/desorption
- ② **Oil circulation, Heat recovery** :
 - Heat recovery by radiation from outside reactor
 - circulation by pump to control temperature constant through heat bath measuring flow rate
- ③ **Electrical Heater (W1,W2)** :
 - two heaters controlled by constant power supply
 - W1: outside of RC (sheathed heater)
 - W2: center of RC (cartridge heater)
- ④ **Vacuum**: 1)for RC 2)for outer chamber
- ⑤ **Sensor** : temperature, gas pressure, oil flow

Fig.4(2); Explanation of each system of control and measurement in D-system;



Fig.5(1); Overview of D-system Fig.5(2); Hydrogen valve and Pressure sensor

2.2-1 Configuration of Circulation oil tubular

Direct heat removal by coolant oil flow is used for the C-system (Fig.2), while heat removal via radiation from hotter RC surface to vacuum-isolated SS tube of oil flow is used in the new D-system (Fig. 4(1)). The oil cooling SS cylinder is set in evacuated zone inside the outer cylindrical chamber with cooling water through a constant temperature water bath. So, the D-system is of three layers system. By this radiation cooling system of RC under separation from oil flow, we can elevate RC temperature over 600 °C or more.

2.2-2 Mesh-holder for loading of MHE powder sample

In the C-system, sample powder plus dummy zirconia beads were mounted fully in RC volume (about 500 cc), as seen in Fig.2. In the D-system experiments, sample powder is set inside mesh holder which surrounds central W2 heater rod as shown in Fig.6(2). We expect for enhanced MHE reactions in sample powder surrounding closely the W2 heater rod. Another expectation is for homogeneous interaction between sample powder and hydrogen gas through mesh surface and enhanced heat conduction via hydrogen gas conduction flow to RC surface, from where radiation heat transfer takes place to the oil cooling cylinder. As a result, time-response of heat power generation became faster by reflecting the decrement of heat capacity of mounted sample volume. In these conditions, speculative analysis of MHE AHE reactions became easier with faster time response of temperatures and more simply monitored H/Ni response under rather homogeneous temperature distribution in sample zone. In present D-system runs, we used MHE sample amount as 50-200g, while in the past experiments by the C-system we used ca. 1kg sample + dummy beads. We can carry out R&D runs with smaller amount of MHE samples, and clearer data will be given for understanding physical mechanism of AHE.

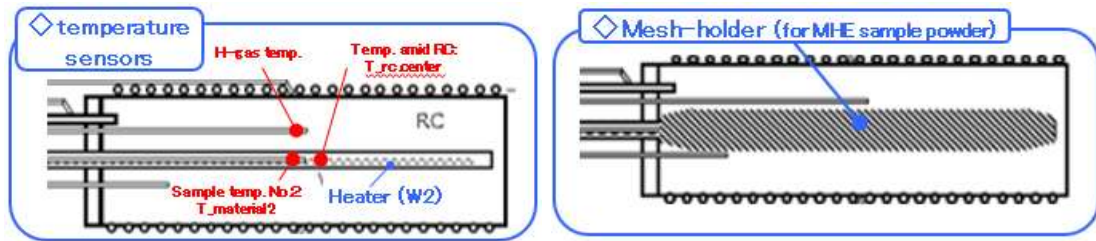


Fig.6(1); Cross Section of reaction chamber of D-system

Fig.6(2): Mesh Holder for MHE sample powder set-in

2.2-3 Temperature sensors of gas and reactor center

Two TC sensors were added in the D-system, for monitoring gas temperature directly and RC center temperature. Variation of RC temperature distribution along the axial direction of RC cylinder in D-system became ca. 30 °C, which is less than 200 °C in the C-system runs⁴⁻⁶). However, there remains considerable variation of temperature distribution in MHE sample zone for using three points average of sample TC temperatures to estimate excess power. We conceive that estimation of excess power by increment of H-gas temperature from calibration runs is most appropriate at the moment.

Time response of oil outlet temperature for removing heat by radiation transfer is found to be so slow (as more than 1 hour delay) that we cannot use for estimating time evolution of excess power generation. However, integral heat amount by oil mass flow is correctly estimated for very long time interval as several days. As a consequence, we decided to use excess power estimation by the H-gas temperature in RC for analysis of time evolution of excess power generation pattern, in correlation with dynamic evolution of H/Ni loading ratio¹). We found that evolution of temperature at the mid-point of RC is most sensitive to the evolution of excess power generation. We can see rapid and clear AHE indication by this temperature evolution, but accurate estimation for excess power is difficult due to very local variation of AHE status.

2.2-4 RC Hydrogen valve (RCV)

The D-system has a gas valve (RCV) at inlet/outlet place of hydrogen gas feeding tube to RC. The purpose of RCV is to check precise up/down of RC hydrogen pressure in the time elapsed duration of H/Ni loading ratio evolution, typically a few days after the initiation of elevated temperature run (ET run) of MHE experiments. Hydrogen loading ratio (H/Ni in the present work) is one of key measures in the MHE AHE study^{2,3}). Rate of hydrogen absorption by MHE sample powder is estimated by H-gas pressure decrease from initial H-gas pressure of reservoir cylinder in the open system of H-gas reservoir cylinder plus RC chamber (including connection pipe line). During the interval that hydrogen absorption rate is large, absorption rate can be easily calculated. In later time interval when absorption rate becomes very small, it becomes difficult to make precise estimation of absorption. During such later stage of hydrogen absorption getting close to saturation, we can check whether absorption is still going on or stopped by the simple RC valve closing treatment to watch H-gas pressure (Pr) evolution in RC, because large volume (8 L) of H-gas reservoir (pressure Ps) is isolated from a small effective gas-volume (ca. 0.3 L) of RC. Under this RCV-close mode,

hydrogen gas absorption rate by MHE powder is observed with 25 times magnification and we can observe the correlation between excess power generation and evolution of H/Ni loading ratio, for getting some key information of reaction mechanism.

3. DATA RESULTS AND DISCUSSIONS

3.1 Temperature response and correlation characteristics of D-system by Zirconia loading

We have done three kinds of calibration runs for estimating excess thermal power. First one is temperature calibration runs by using dummy zirconia beads and H₂ gas, for getting time response from start of W2 heater-on to 2-3 days elapsed time. Results by W2=100 W run is shown in Fig.7. Maximum (equilibrium) temperature of coolant oil outlet is about 100 °C, which is enough lower than the oil boiling point of 350 °C. We have confirmed that higher RC temperature runs can be safely done so far. Other two calibration methods are by using He-gas with MHE powder and by using H-gas with “dead” CNZ sample powder. We have found that the calibration by the third method is most precise in practical use, but the first one is enough accurate for resulting excess power level over 5 watts.

As written already in former section, time response of oil outlet temperature for removing heat by radiation transfer is found to be so slow (as more than 1 hour delay) that we cannot use for estimating time evolution of excess power generation. However, integral heat amount by oil mass flow is correctly estimated for very long time interval as several days. As a consequence, we decided to use excess power estimation by the H-gas temperature in RC for analysis of time evolution of excess power generation pattern, in correlation with dynamic evolution of H/Ni loading ratio¹⁾. Heat capacity of the present SS cylinder with spiral oil coolant tube is too large to reflect quick thermal power response of RC at high temperature.

Width of temperature variation along the axis of RC cylinder is ca. 30 °C, which is much smaller than ca. 200 °C by the C-system runs. The highest temperature in three TCs (TC1, TC2 and TC3) along the axis is at TC2 set on the middle of axis line, while the lowest temperature is at TC1 set near to RC flange. TC2 and TC3 are set on surface of mesh holder, so that these will reflect in outer-most temperatures of MHE sample powder. Gas temperatures in RC are monitored by TC6 and TC1 (see Fig.6). Since short SS sheath of TC1 makes larger heat leak to RC flange to indicate lower temperature than TC6 which is positioned at around mid distance of the RC axis. Therefore, we decided to use temperature by TC6 as H-gas temperature in RC. Temperature by TC6 is a relative measure of H-gas temperature in RC, but we can use it for estimating excess power indicating somewhat averaged values, by taking difference from TC6 data by calibration runs.

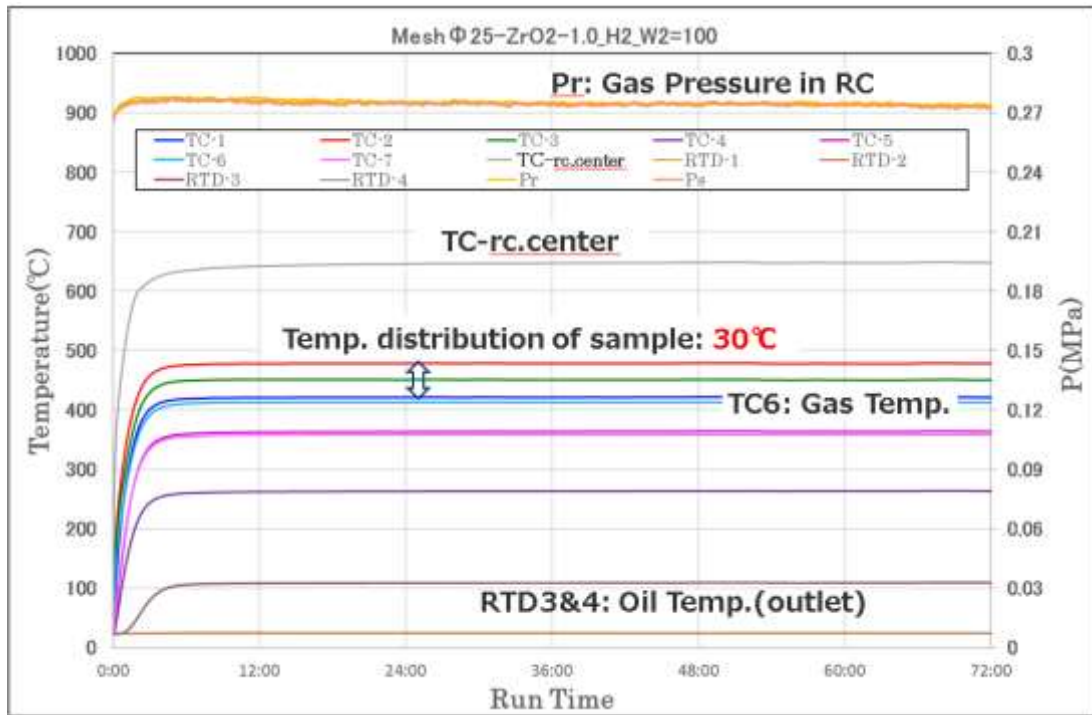


Fig.7; Temp. response and equilibrium in case of Zirconia beads and Hydrogen

3.2 Temperature response of heat generation by MHE reaction compared with ones by Cu1Ni7/Zirconia sample

In Fig.8, we show typical raw data of MHE H-gas run with ca. 150g CNZ9s-rr (Cu1Ni7/zirconia after twice re-calcinations) with W2=100 W heating. After about one hour of starting W2 heater-on, sample temperature (e.g., by TC2) reached at the level of 300 °C and then we saw the very steep and rapid elevation of temperature compared with the calibration curve, to show occurrence of excess thermal power of MHE AHE. Excess power shows rather plateau (around 20W typically with ca. 150g CNZ sample) evolution to continue for more than 20 hours in rather flat response.

Increment (over calibration line as shown by broken line) of TC6 gas temperature is in the range of 10-30 °C. Very sensitive indication of excess heat of MHE AHE is seen as ca. 150 °C increment (over calibration line as shown by broken line) of temperature at RC center (TC-rc.center in Fig.8). We found the response by TC-rc.center is the most easily seen monitor for excess thermal power generation by the MHE AHE phenomenon.

However, estimation of global excess power level of RC has been done by H-gas temperature data of TC6. In the case of Fig.8 run, $W_{ex} = 16$ W.

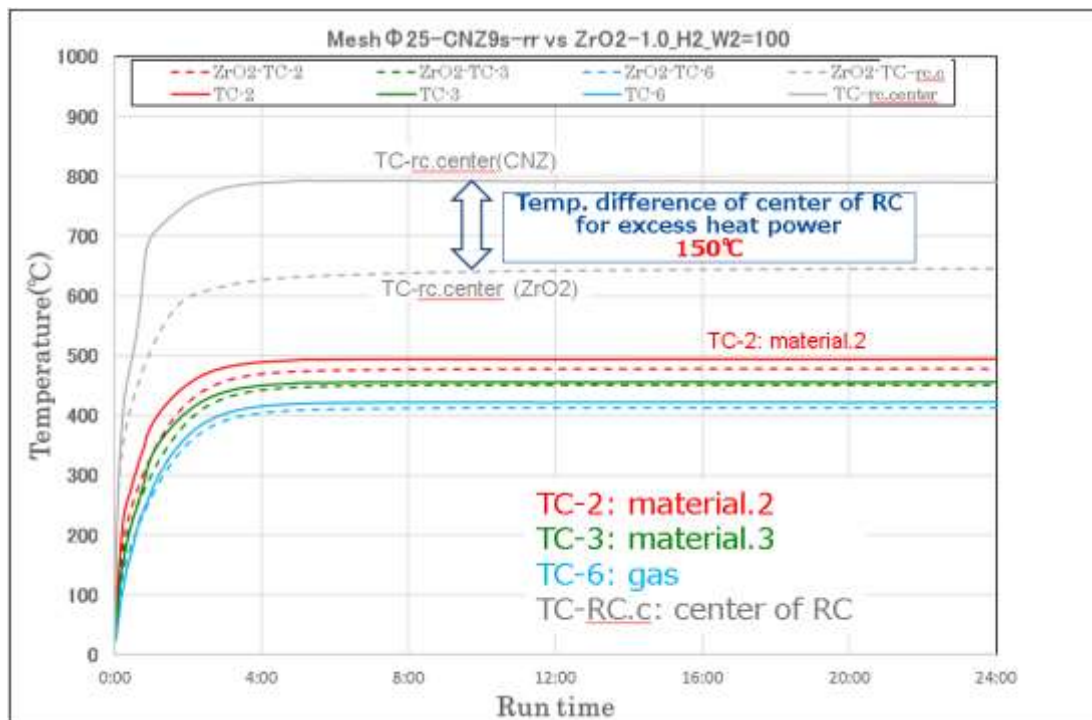


Fig.8; Temp. response and equilibrium in reactor of MHE reaction cf. calibration curves

3.3 Clarification of hydrogen absorption situation using change of hydrogen pressure by hydrogen valve RCV

In Fig.9, we show typical raw data by the RCV-close-to-open treatment. We tried to close RCV for several hours to measure RC gas pressure (P_r) variation (gradually decreasing) by very slow H-gas absorption by MHE powder. Then we opened RCV to see returning P_r pressure by direct path through to H-gas reservoir (P_s). During the RCV-close interval, speed of H-gas decrement by H-absorption was magnified by 25 times (see yellow line) due to diminished gas volume (0.3 L). More detail will be described in our second paper¹⁾ to this JCF22 Proceedings.

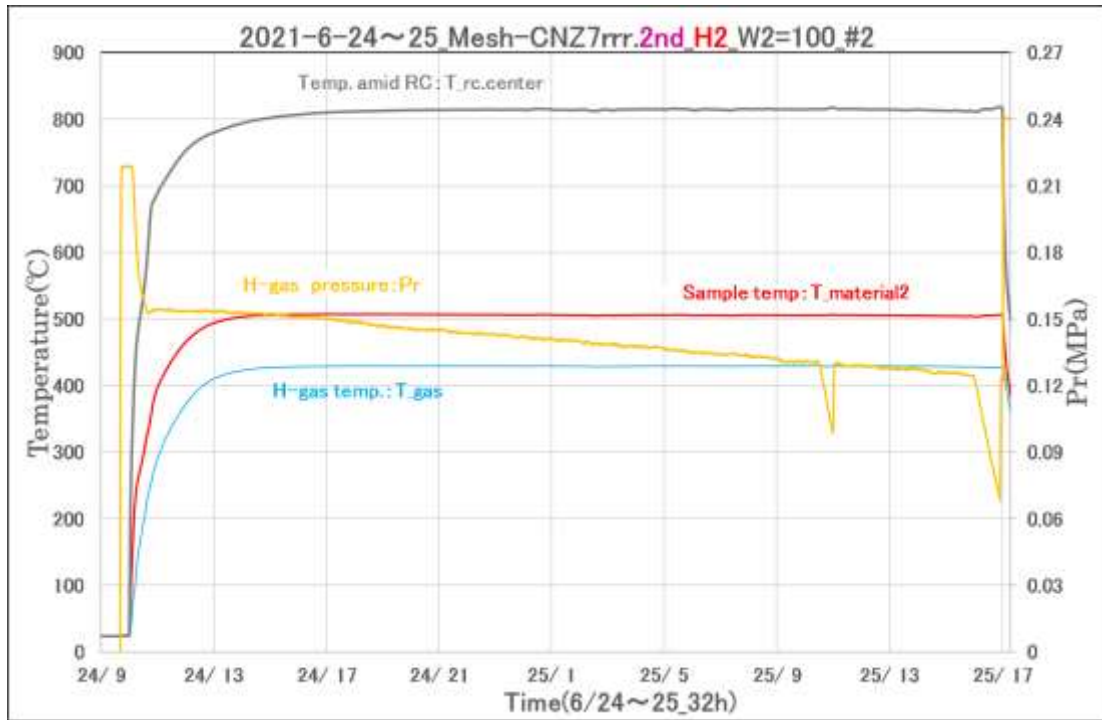


Fig.9; Pressure response of Hydrogen in RC by closing Hydrogen valve.

4. SUMMARY AND CONCLUDING REMARKS

Results of recent MHE experiments by our C-system has met limitation of performance for much higher temperatures runs with much more enhanced AHE data. We have developed the new system as called D-system. By the first step comparative study of calorimetry calibration runs with zirconia beads and MHE anomalous heat effect (AHE) runs with CNZ-type samples, we have confirmed that the D-system has satisfactory performances to implement further MHE studies at more elevated temperatures than the case of our C-system study. Merits of the D-system are summarized as follows.

- 1) Separation of oil cooling part from reaction chamber, for running RC over 500 °C
- 2) Set-up of mesh-holder for mounting MHE sample powder to realize less spread of temperature variation in sample zone with smaller amount of powder
- 3) Addition of sensors to observe RC center temperature evolution and H-gas temperature
- 4) Set-up of H-gas valve of RC to do close-to-open operation for precise monitoring of H-gas absorption stage phenomenon.

By further using this D-system, we report ^{1, 3)} some significant findings of excess power generation and AHE re-activation method.

References:

- 1) Masahiko Hasegawa, Yutaka Mori, Akito Takahashi, Joji Hachisuka, Yuichi Furuyama; Characteristics of MHE power generation by D-System, Proc. JCF-22 Meeting, 2022
- 2) Akito Takahashi; Physics of Cold Fusion by TSC Theory, *J. Condensed Matt. Nucl. Sci.*, 12, 191-198, 2013
- 3) See also: [\(PDF\) MHE nuclear-like thermal power generation and guiding TSC theory \(researchgate.net\)](#)
- 4) Akito Takahashi, Toyoshi Yokose, Yutaka Mori, Akira Taniike, Yuichi Furuyama, Hiroyuki Ido, Atsushi Hattori, Reiko Seto, Atsushi Kamei, Joji Hachisuka, “Latest Progress in Research on AHE and Circumstantial Nuclear Evidence by Interaction of Nano-Metal and H(D)-Gas”, *J. Condensed Matter Nucl. Sci.*, 33, 14-32, 2020
- 5) Akito Takahashi, Toyoshi Yokose, Yutaka Mori, Akira Taniike, Yuichi Furuyama, Hiroyuki Ido, Atsushi Hattori, Reiko Seto, Atsushi Kamei, Joji Hachisuka, “Enhancement of excess thermal power in interaction of nano-metal and H(D) gas”, Proc. JCF20, pp.9-27, 2020
- 6) Masahiko Hasegawa, Yutaka Mori, Akito Takahashi, Joji Hachisuka, Hiroyuki Ido, Reiko Seto, Akira Taniike, Yuichi Furuyama, “Comparison of AHE data between H2 and He runs for CNZ7rrr Sample”, Presentation at JCF21 Meeting, December 2020, web conference of JCFRS: [\(PDF\) Comparison of AHE data between H2 and He runs for CNZ7rrr sample - English version \(researchgate.net\)](#)

Characteristics of Excess Power Generation in MHE Experiments by D-System

*Masahiko Hasegawa¹, Akito Takahashi¹, Yutaka Mori¹, Joji Hachisuka¹,
Yuichi Furuyama²

¹ Technova Inc., ² Kobe University,

*corresponding author e-mail: hasegawa@technova.co.jp

Abstract By using our new experiment system (called D-system) of MHE (nano-metal hydrogen energy) reaction, it became able to measure and evaluate more clearly AHE (anomalous heat effect) by the elevated temperature interaction of nano-composite metal powder sample and hydrogen-gas. Two new characteristic phenomena of excess power evolution by the MHE reaction are reported in this paper. The first one is that the evolutionary generation of excess thermal power level is largely dependent on the dynamic absorption ratio of hydrogen (H/Ni loading ratio) in MHE sample-material (CNZ9; Cu₁Ni₇/zirconia, 140-150g by repeated calcination). After exceeding the turning point of H/Ni=0.9 (actual value), excess thermal power was started to increase steeply, and a few days later it started to decrease before the near full H/Ni loading ratio (H/Ni=2.0>>1.0, actual value). The characteristics of H/Ni evolution shows that the absorption of hydrogen in the MHE sample-material is important factor for the AHE excess thermal power generation in 200W/kg-sample level. And this is also the experimental evidence of the reported absorption mechanism of hydrogen into the Ni mesoscopic-size-catalyst islands.

The second one of new findings is that the AHE power level can be re-activated from the low-active state under the near full H-absorption rate (nominal value of H/Ni =3.5 locally is conceived). The control/trigger method is by the operation of RCV (the hydrogen-gas valve of RC) to be closed for a few hours and then to be re-opened. This control of triggering re-activation is repeatable for many times with significant excess power increase (10-15W in present actual runs) lasting a day or so per each triggering. The conceived mechanism of this phenomena is that the feeding of hydrogen-gas after re-opening of RCV from hydrogen reservoir would be some stimulus toward connected several processes of MHE reactions which would be occurred on the face of Cu-Ni nano-islands lattice and inside of nano scale core of Ni lattice.

Key words: nano-metal hydrogen energy(MHE), the anomalous heat effect(AHE), nano-composite-metals, hydrogen gas, C-system, D-system, excess thermal power, the absorption rate of hydrogen (H/Ni loading ratio), re-activation, burst of Pr, the hydrogen-gas valve of RC(RCV), 4H/TSC WS fusion

I. INTRODUCTION

The R&D of MHE had been performed so far by indicating the relative heat power generation (Wex: W/kg-sample) and COP (Coefficient of Performance: Wout/Win) as a performance of MHE reaction and an index of achieved R&D level of MHE technology. The levels have been increased as Wex was 240W/kg-sample and COP was around 1.4¹⁻⁵.

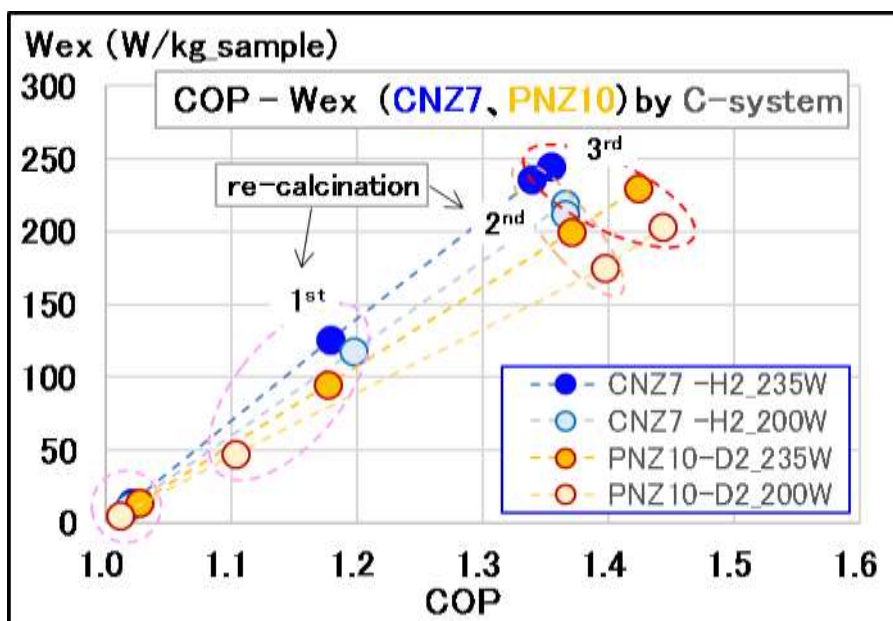


Fig.1; Performance index of MHE reaction: COP vs. Wex (W/kg-sample) by C-system

The former experiment apparatus (so called C-system^{1,2)}) has the upper limitation of reaction temperature. In order to execute the experiment at higher temperature, some part of apparatus and system was improved (so called D-system)⁶⁾. And in order to clarify the working-factors of MHE reaction and its mechanism, the sample was loaded in smaller size mesh holder in the RC (Reactor Chamber) and several additional temperature sensors were installed for the analysis of its reaction.

The treatment procedures of MHE sample and the conditions of generation of excess heat were clarified so far, but there exist still many unsolved factors. Regarding the continuous period of the generation of excess heat, it was lasting over a week in some cases and a few days in other cases. The effective factors were not well specified yet for the elongation of reaction life or for the decrease of MHE reaction.

It was clarified in the MHE R&D so far that hydrogen loading ratio per Nickel (H/Ni) was affected to the generation of excess heat in some way. It was one clarified fact that hydrogen was absorbed in the MHE sample in the beginning phase and the excess heat generation was started after the desorption of some part of absorbed hydrogen. Another fact is that H/Ni is under 1.0 for the bulk metal of Nickel but it's over 3.0 which is far excess 1.0 for Nickel nano particle (2nm-20nm). It was actually confirmed that H/Ni was up to 3.5 for the some MHE sample by individual sample test in the past. But it is still unknown that the detail of correlation between the generation of excess heat by the MHE reaction and situation of H/Ni⁷⁾.

It is the big issue for actual use that it is not possible to continue the excess heat by the MHE reaction for long time. It is necessary to clarify the total mechanism and the factors of MHE reaction. The two new characteristics of AHE (Anomalous Heat Effect) of MHE reaction are reported in this paper as follows.

In our past studies, we have a hint of elucidation for close correlation between hydrogen loading ratio (H/Ni in our case) and AHE (anomalous heat effect) excess power generation^{7,8)}. We have seen the start of AHE power generation after desorption of absorbed hydrogens^{3,4)}. In conventional results for bulk Ni metal sample, hydrogen

loading ratio (H/Ni) cannot exceed 1.0. However, when we used binary nano-composite powder (2-20 nm size) samples as PNZ type as Pd₁Ni₇/zirconia, we have observed⁸⁾ very large saturated value of H-loading as H/Ni = 3.5. However, the experimental results of close correlation between AHE power generation/evolution and H/Ni loading ratio evolution are the first findings by the present study. It is very important knowledge for controlled generation of AHE power by the MHE tools.

For extending R&D works to industrial application on clean portable high heat density source devices, we need controlling know-hows for long time operation with high power density. In this respect, the second findings in this work for the MHE power re-activation method is of great importance.

II. EXPERIMENTAL METHODS AND PROCEDURE

2.1 New MHE Experiment Apparatus System

A schematic view of newly developed D-system by improving our C-system^{3,4)} is shown in Fig.2. More basic and detail information on the D-system is given in our paper in this Proceedings⁶⁾. Main points of improvement are as follows;

- 1) addition of temperature sensors as hydrogen-gas (T-gas) and RC center (T-rc.ctr), which are useful for excess power estimation and watching (T-gas) AHE evolution with high sensitivity (T-rc-ctr)
- 2) set-up of SS mesh holder for mounting MHE powder samples, which is useful to homogenize MHE sample zone temperature during elevated temperature runs, and making good condition to obtain gross evolution of H/Ni loading ratio
- 3) addition of gas valve (RCV) for monitoring gas pressure near reaction chamber, which is useful for investigation of very slow H-absorption in the duration near H/Ni ratio saturation, and a good tool for the re-activation of MHE excess power generation

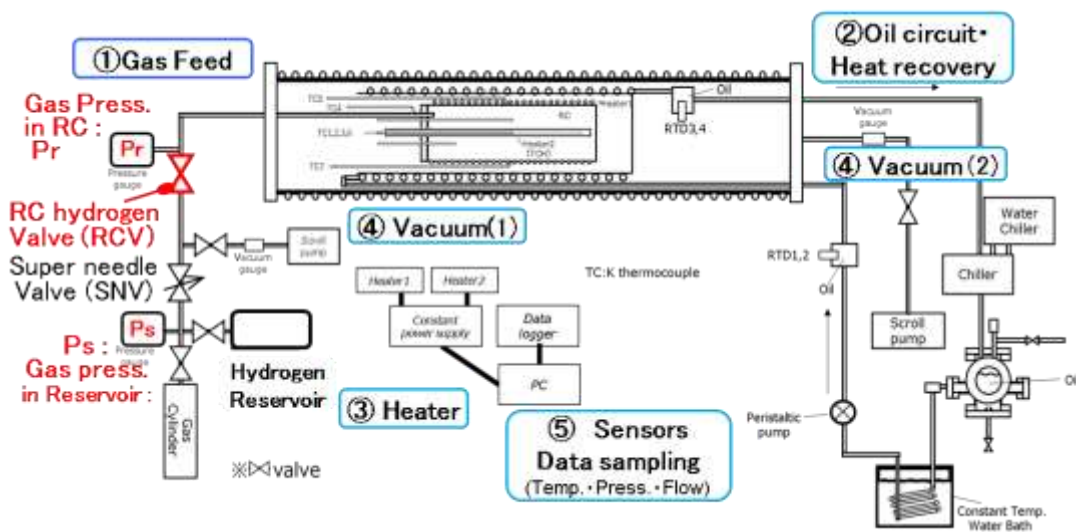


Fig.2; New MHE experiments apparatus; D-system⁶⁾

2.2 Mesh-Holder for Loading of MHE Powder Sample

In Fig.3, extended view of RC inside for positions of temperature sensors (TCs) and mesh holder. Along with the center line of RC, cartridge heater (W2-heater) is set to cover nearly whole horizontal region of RC. Gas temperature sensor (TC6 for T-gas monitor) is set at 5cm apart vertically from RC center axis and between central sample temperature sensor TC2 (near horizontally center) and near RC end point one TC3. TC6 locates in gas zone between mesh holder and RC chamber wall. We have observed in real runs that there happens about 30 °C temperature variation in sample zone. So far, we decided to use gas temperature (by TC6) for estimating gross excess power, by taking difference from TC6 values with dummy samples⁶⁾ for calorimetry calibration. T-rc.ctr is set at very center of RC in horizontal axis of RC. It is actually inside the cartridge heater tube of W2. As we will show in the following, temperature evolution data by T-rc.ctr is observed as very sensitive information for watching excess thermal power evolution by the MHE reaction. MHE sample powder are mounted inside of mesh holder in this study.

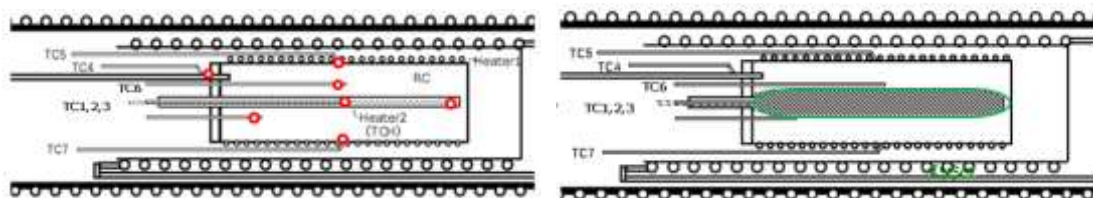


Fig.3; Cross Section of reactor and Mesh Holder for sample loading (D-system)

2.3 RC Hydrogen Valve (RCV)

We set up the RCV (reaction chamber hydrogen gas valve) in gas pipe line position very close to RC chamber (0.3 L effective gas volume) inlet/outlet point, it is apart from the H₂ gas reservoir (7.6 L). In the condition of usual ET (elevated temperature) runs, RCV is open. When we want to check very slow hydrogen absorption state, we will close RCV to monitor magnified change of Pr. By closing RCV, speed of Pr decrement is 25 times magnified by isolating 7.6 L volume of H₂ gas reservoir cylinder. This RCV close-to-open treatment is found to be surprisingly effective for re-activation of MHE thermal power generation as we will show later (the second findings).

2.4 Experiment Procedure

In the present work, we used CNZ-type samples^{3,4,5)} as labelled CNZ7 and CNZ9 both of which have nano-composite powder structure of Cu₁Ni₇/zirconia.

Sample 1 : CNZ7rrr after 3rd re-calcination

Sample 2 : CNZ9rr after 1st 3rd 2nd re-calcination

Mounted amount of CNZ powders in the mesh holder were 140-150 g.

After mounting CNZ sample in mesh holder with SS flange, we set it in RC chamber. We evacuate RC gas (air) by scroll pump to be Pr less than 1 Pa. Then, by using W1 outer RC heater and inner W2 heater, we start the so called baking treatment for out-gas (mostly moisture stuck with CNZ powder) reduction under evacuation. We make then cooling of RC for a day or so until RC temperature becomes RT (room temperature) around 25 °C. We fill H₂ gas into reservoir cylinder to the pressure around Ps = 0.4 MPa. Then we start

RT run by feeding H₂ gas to RC through a super needle valve, to take data of temperature rises and H/Ni loading ratio. After several hours of RT run, we start ET (elevated temperature) run with power-on of W2 heater (100 to 160 W typically). Data logging is continued for many days to record/monitor temperatures and gas pressures at many points, and oil flow rate of cooling SS tube (via radiation heat transfer).

III. RESULTS AND DISCUSSIONS

3.1 Fast H-Loading in Rise-Up and Slow Loading After

(1) Two Phases of H-Loading (Fast and Slow Loading)

Data logging was continued for many days. We show typical example of raw data of temperatures and gas pressures in many points in Fig.4. During usual condition of ET run, the super needle valve is fully open, so that $P_s = P_r$ state is kept. In Fig.4, we show P_s only with yellow line curve. We observe apparent equilibrium temperatures of 505 °C at TC2 (T-material2) and 430 °C of gas temperature at TC6 (T-gas), respectively. Evolution of P_s change is impressive. When temperature exceeds around 200 °C, fast H-absorption phase (① in Fig.4) starts and ends after around 40 min. During that fast H-absorption phase, gas temperature elevated to around 300 °C. Then we saw the second very slow H-absorption phase (② in Fig.4) starts and continued for over 30 hours. Hydrogen loading ratio H/Ni was 0.9 at the end of the first phase, and it slowly increased to 1.2 after 32 hours in this run.

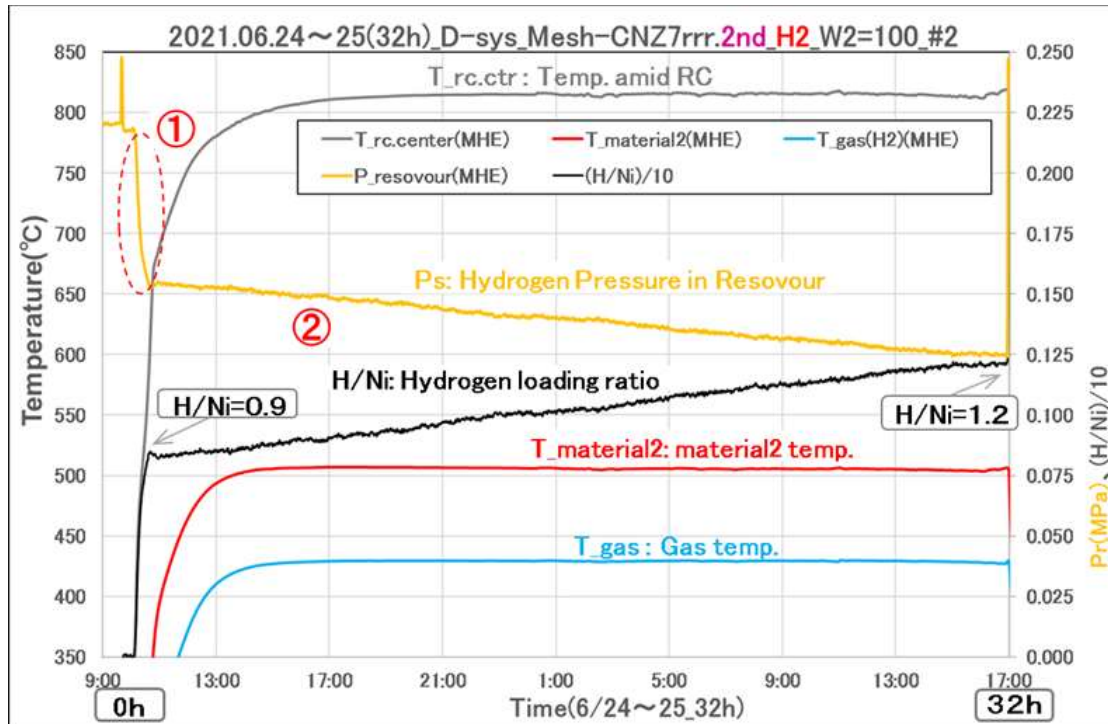


Fig.4; Typical example of raw data of temperatures and gas pressures.

(2) Characteristics of Excess Power Generation

We show typical example of raw data by calibration run with dummy sample, compared with data by MHE sample (Fig.4), in Fig. 5. Gas temperature data by TC6 for the MHE sample gave 20-25 °C increase from data by the calibration run. Estimated excess power level is in the range of 15-17 W that continued for 30 hours duration. Conversion of temperature increment data of TC6 to thermal power was done by using conversion ratio of temperature of calibration runs with dummy sample and W2 level change. Step response of excess power peak will be explained in the next section.

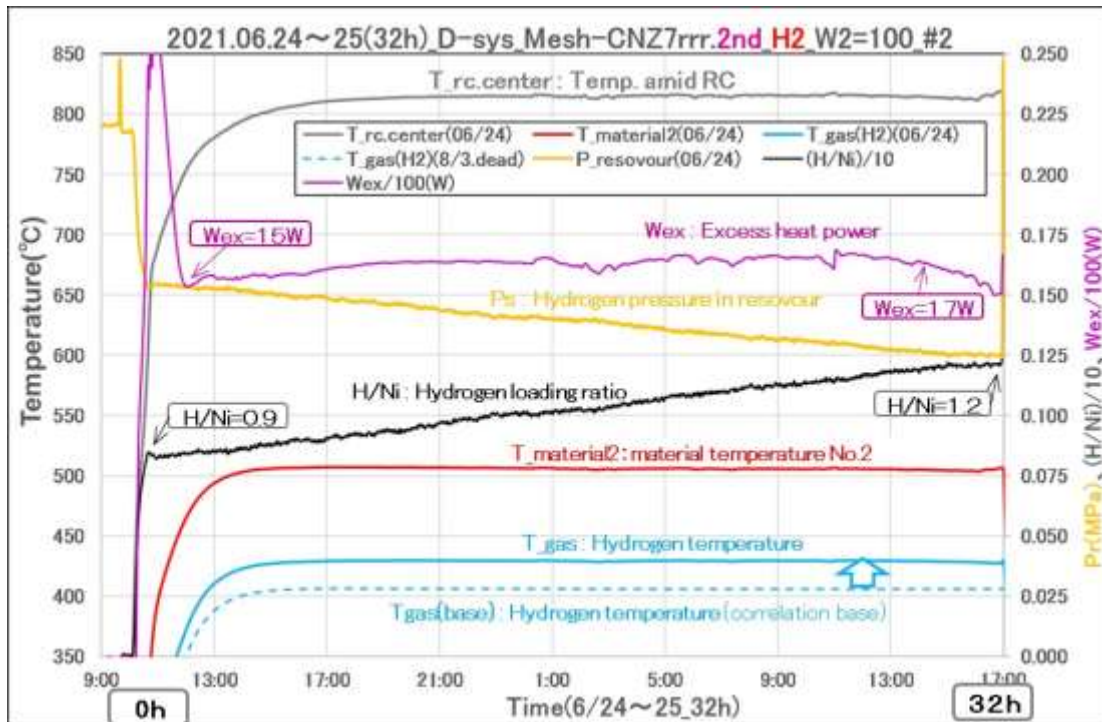


Fig.5; Typical example of data by calibration run with dummy sample (dot line) and data by reaction run with MHE sample (actual line)

(3) Rise-Up Reaction

Step responses of H/Ni loading ratio and excess thermal power after the start-up of W2 heater-on is shown in Fig.6. This is a part as for initial 2.5 hours of the 32 hours run of Fig.5. In the initial ① phase of ca. 10 min interval after W2 heater-on, excess power W_{ex} became negative (endothermic) with minus 6-8 W level. We can regard it by endothermic H-absorption by MHE powder sample. During this interval, there may happen small increase of H-absorption, but accurate estimation of absorption rate is difficult due to small change of P_s . P_s increased once after 10 min by RC temperature increment, and started to decrease by the fast phase H-absorption when RC gas temperature exceeded ca. 200 °C. During this interval, we speculate that endothermic H-absorption and exothermic MHE reaction on surface SNHs of powders⁹⁾ are competing to draw a complex variation. After about 10 min, H/Ni loading ratio increased and excess

power was drawing peak- out at 24-26 W (Initial ② of rise-up response). The fast phase H-absorption ends at around 40 min, but Wex broad peak lasts till ca. 60 min. This delay may have taken place due to heat capacity of MHE powder plus RC structure. This initial burst-like Wex peak is supposed to happen in the duration of endothermic H-absorption and steep exothermic heat generation by the MHE nuclear-like reaction.

After 60 min, Wex started to decrease to reach at “plateau Wex generation” (15-16 W in this case) and continue for more than 30 hours, associating the very slow H-absorption.

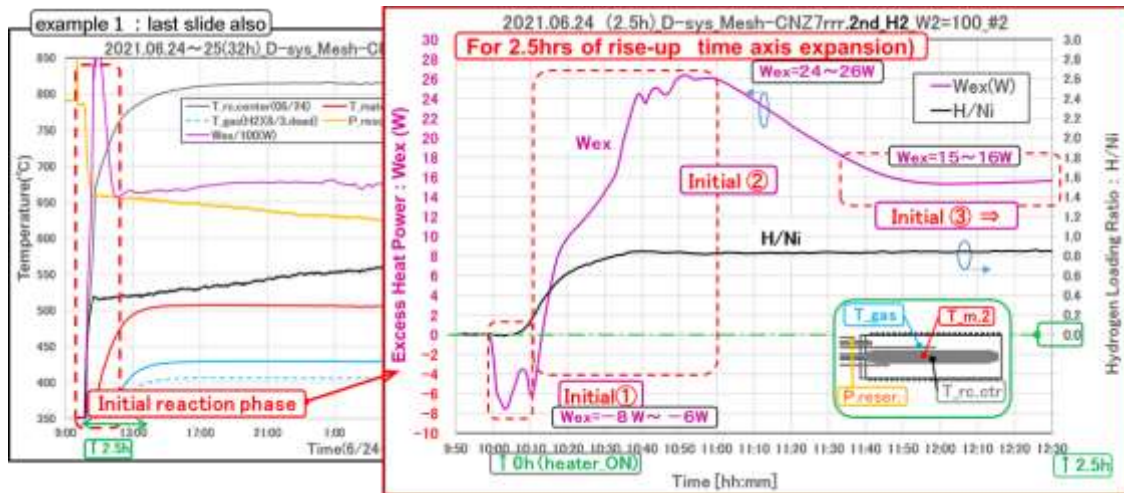


Fig.6; Steep response of H/Ni and Wex by MHE reaction in rise up period

(4) Confirmation of Reproducibility

Wex evolution has drawn typical pattern of evolution closely correlated to the evolution of H/Ni loading ratio, as shown in Fig.7. Initial heat peak (burst-like) started to decrease to reach at “plateau Wex generation” lasting long time as 30-70 hours typically. We compare two data in Fig.7, for different samples and different W2 heating powers. Left figure is for CNZ7rrr with W2=100W, while the right figure is for CNZ9rr with W2=160W. We confirm the reproducibility of AHE phenomenon with same patterns for Wex generation and H/Ni loading evolutions.

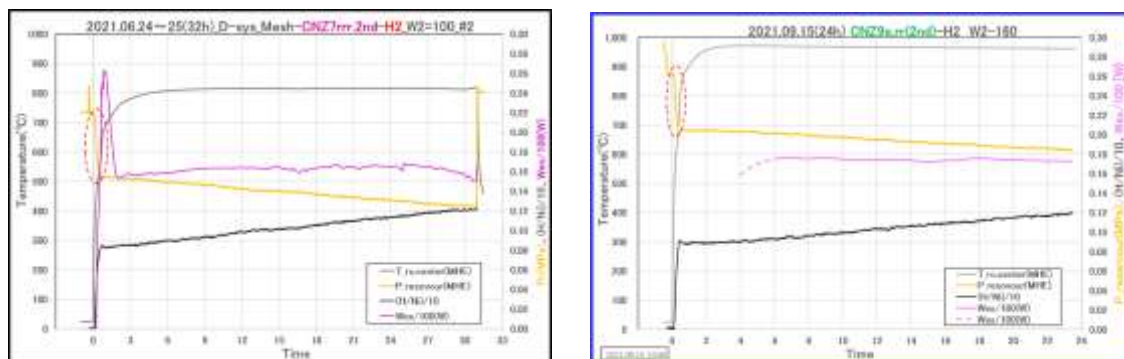


Fig.7; Confirmation of reproducibility of two Hydrogen absorptions

3-2. Saturation of H-Loading and Evolution of Excess Power

(1) Slow H-Loading Process

We have confirmed the reproducibility of AHE phenomenon with same patterns for Wex generation and H/Ni loading evolutions. In Fig.8, we show the procedure that H/Ni values went to near equilibrium very slowly. In this case, H-absorption saturated after about 50 hours. Excess temperatures in RC were however observed as decaying mode after about 40 hours. This decay trend is most sensitively seen in evolution of RC center temperature (T-rc.ctr), which is the most easily seen measure of AHE (anomalous heat effect) to watch the phenomenon. H/Ni loading ratio has still very slowly increased to 1.6 at 120 hours after the start of ET run.

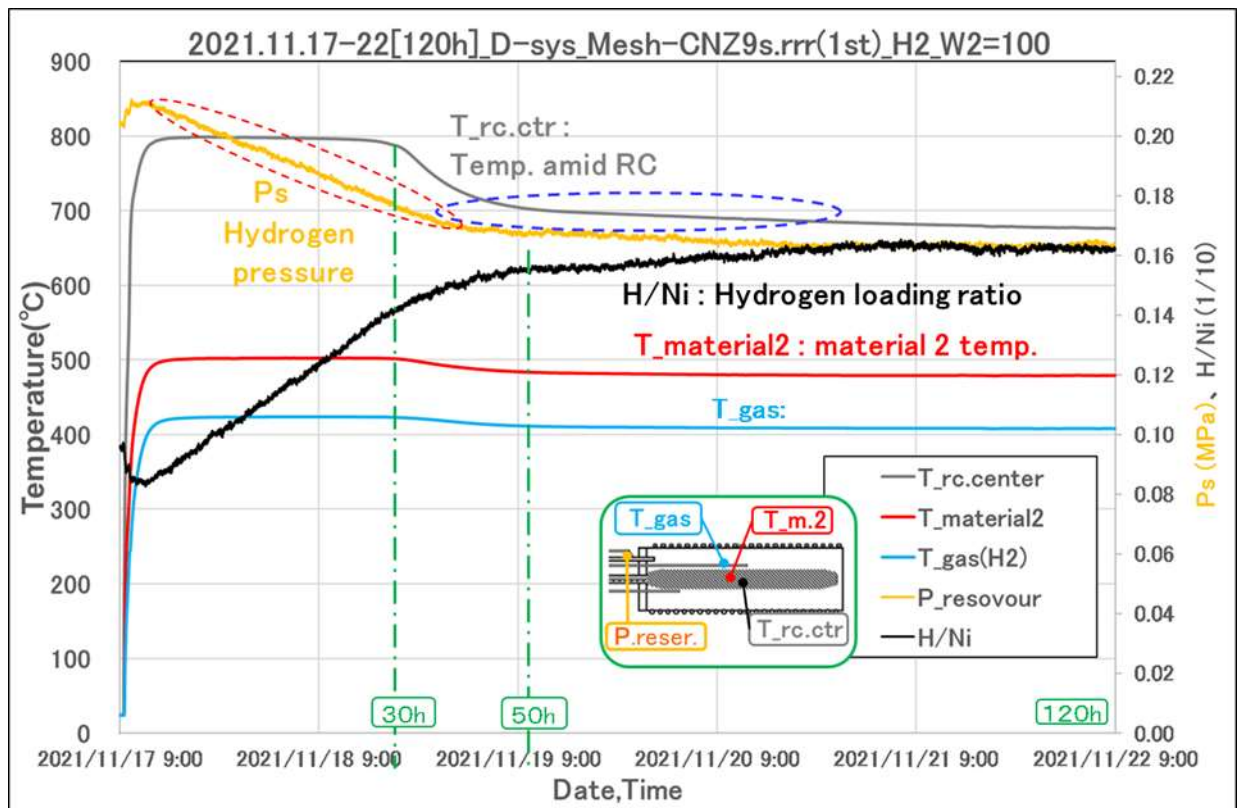


Fig.8; Saturation of Slow H-loading process and response of Temp. in RC

(2) Evolution of Excess Heat Power

In Fig.9, we show typical trend data of excess power generation after W2 heater-on. Wex continued for about 30 hours with 12 W level (①_Phase①). From 30 hours to 50 hours, Wex slowly decreased (②_Phase②). After 50 hours, low level Wex as 2-4 W continued further to the termination of run at 120 hours. From these data pattern/evolution, we understand that level of H-loading ratio as H/Ni is a key factor of excess heat power generation process. On the theoretical model of nuclear heat generation in close correlation with H/Ni loading ratio will be discussed in our ICCF24 paper⁹⁾ and other papers/documents^{7,8)}. Brief explanation of theory will be given in the end of this discussion section.

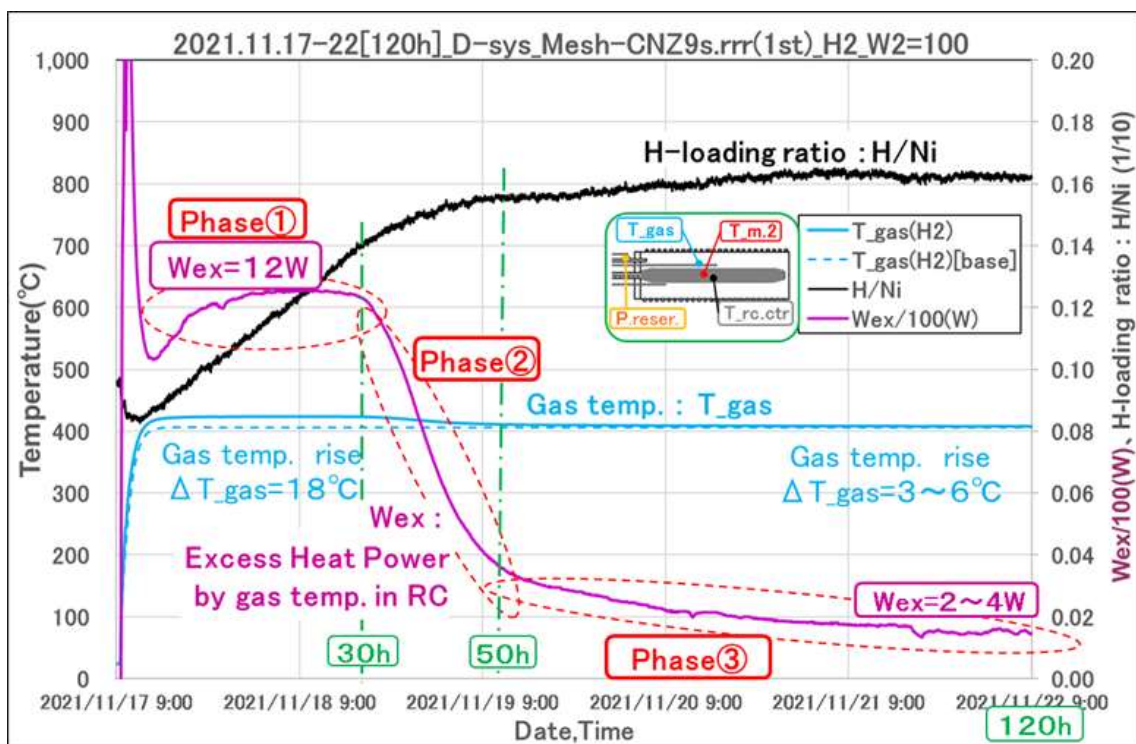


Fig.9; Saturation of Slow H-loading process and Evolution of excess power

(3) Confirmation of Reproducibility

We show typical trend data for confirmation of reproducibility of excess power generation in correlation with the very slow H-absorption phase, in Fig.10. The left figure is for CNZ7rrr sample with $W_2 = 100$ W heating, and the right figure is for CNZ9rr with $W_2 = 160$ W heating. H/Ni values are approaching to saturation at around 50 hours for the left, and 90 hours for the right, in correlation with rather high excess power “plateau” levels, respectively. Then Wex started to decrease in 50 (left) and 90 (right) hours to go to small Wex bias levels which continued till 120 (left) and 144 hours (right), respectively. Hydrogen loading ratios as H/Ni values increased to 1.6 (left) and 2.0 (right), respectively. Theoretical upper limit of H/Ni value for Ni-core meso-catalyst⁸⁾ is studied to be 3.5 (1.0 for O-site H-occupation, 2.0 for T-site H occupation and 0.5 at surface SNHs). Therefore, we speculate that not all Ni islands in used CNZ samples were of ideal core-shell structure in 2-20 nm meso-catalyst size. About 50 % (left) and 60 % (right) of MHE sample were effectively active. So far, we can increase nano-islands of samples to enhance total heat generation. Another point will be due to not very homogeneous temperature distribution in sample zone, since we have obtained the trend that the higher Wex observed the more increased temperature elevation.

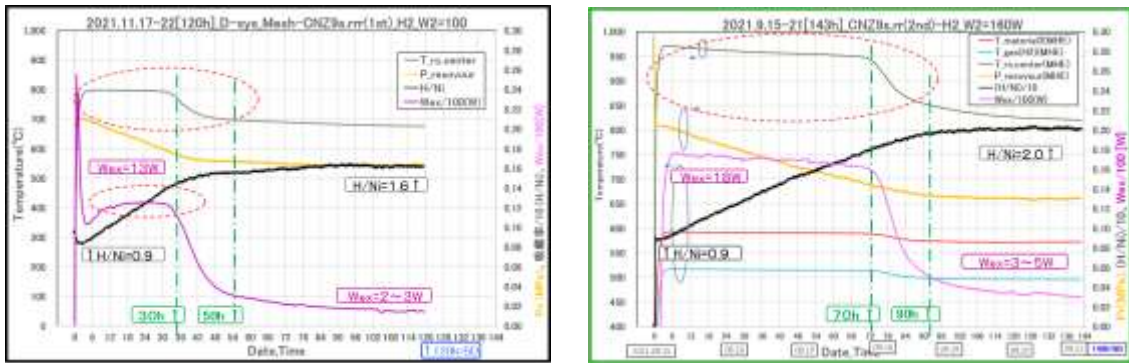


Fig.10; Confirmation of reproducibility of saturation of slow H-loading process, evolution of excess power and decrease to bias level

3-3. Re-Activation Phenomenon after MHE Heat Power Decrement

(1) RCV Close Operation and Pressure Response

We have met the new findings of MHE power re-activation treatment. When H/Ni loading ratio looked approaching the saturation, we can re-activate MHE excess power by RCV operation.

We temporarily close RCV for several hours to shut the H-gas feed from H-gas reservoir cylinder (8 L). As we described already, Pr decreasing speed by H-absorption in sample is magnified by about 25 times. We show typical data in Fig.11(a) and (b). By comparing intervals of RCV open (O) and RCV close (C), H-absorption speed into sample powder should be same, but rapid decrease of Pr by RCV close is clearly seen.

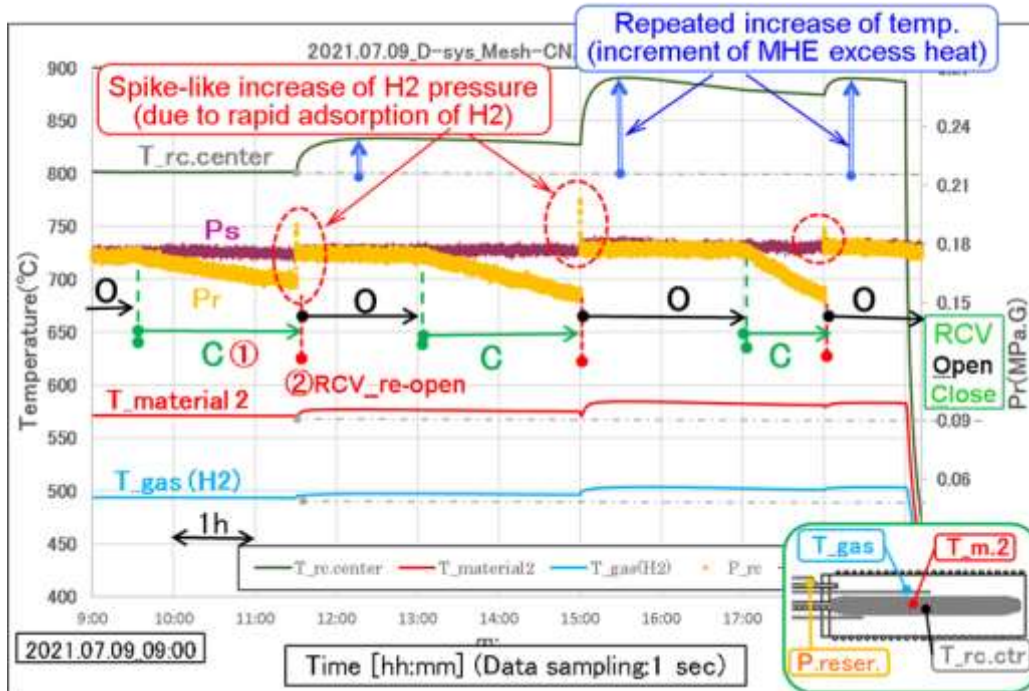


Fig.11(a); Re-activation of excess heat generation

(2) Re-Activation of AHE of MHE Heat Power

After several hours of RCV-close operation, we made RCV open to have observed rapid burst spike of Pr increment in a few seconds and associating rapid increase of temperatures in RC, most sensitively at RC center (by T-rc.ctr data). This boost up of MHE power continues for several hours. In Fig.11 (b_right), precise evolution of data per every second are shown. The Pr spike lasted for about 10 seconds. We conceive that some kind of triggering took place when RCV was re-opened. The triggering effect induced heat step (maybe 4H/TSC WS fusion at SNHs on sample powder) to suddenly heat MHE sample powder keeping “full” T-site loading.

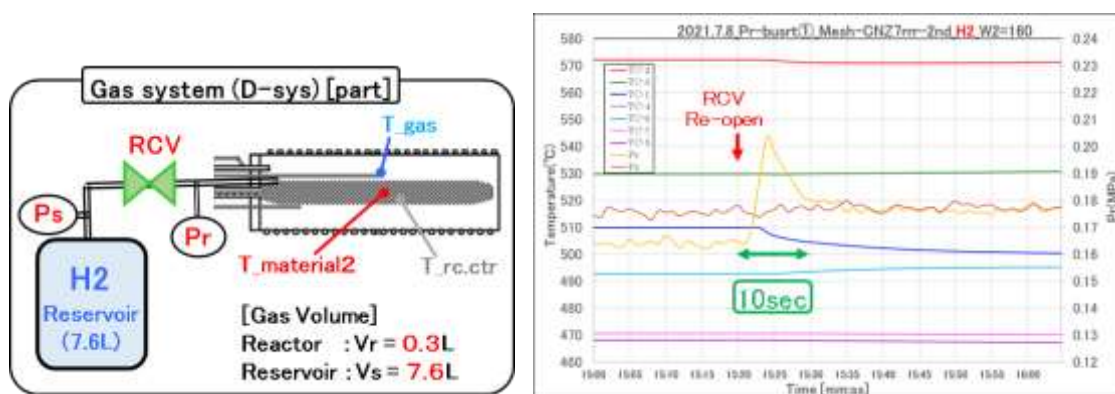


Fig.11(b. left); Gas system from reservoir to RC through RCV in D-system

Fig.11(b. right); Rapid increase of Pr after re-opening of RCV (10seconds)

Some portion of trapped H-atoms at T-sites may have been desorbed by the triggered heat step. Increased Pr burst (0.3 L in RC) was absorbed by gas flow to H-gas reservoir (8 L) to increase slightly equilibrium Ps pressure. Gas temperature in RC (T-gas) increased 5-15 °C (5-15 W boost up of excess thermal power). In parallel, we observed large increment as 50-70 °C at RC center (by T-rc.ctr) to provide us very clear information of the re-activation effect. In this run, we repeated the RCV-close-to-open operation three times. We observed Pr increase and Wex increase every time of RCV-open operation. Boost up Wex level by this re-activation operation has slowly decreased and returned to the initial low bias level of Wex in a day or so. H/Ni loading ratio decreased by the RCV-reopen on the level 0.1-0.2 and after a day it has recovered to the saturated value (1.6-2.0 in real runs) with low level Wex bias as 4-5 W.

(3) Confirmation of Reproducibility

We have confirmed repeatability of this re-activation method, by more than 10 times RCV-close-to-open operations. In Fig.12, example data of repeated operations of RCV-close-to-open method for different samples (CNZ7rrr for left figure and CNZ9s rr for right figure). This is therefore an important new finding for controlling continuation of MHE power level in very long heat producing operation in applications. Pr spike magnitudes and Wex boost-up levels are changing from trial to trial, and we need further studies on better controlling the method.

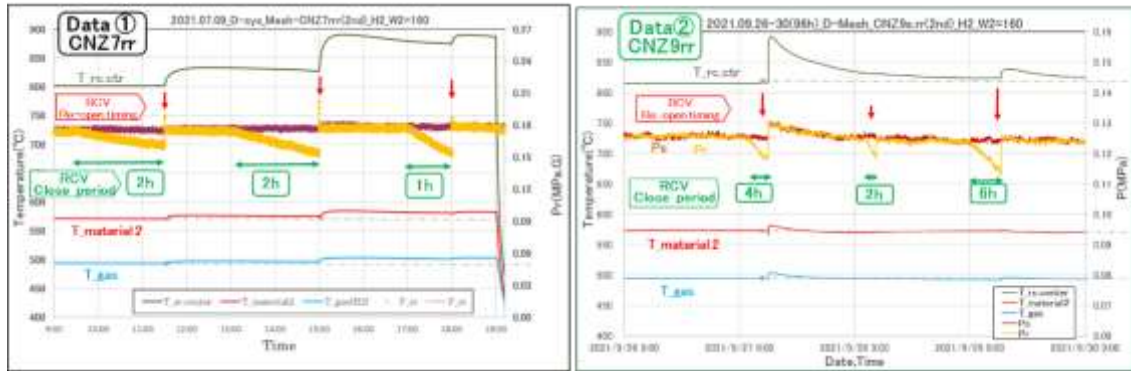


Fig.12; Confirmation of reproducibility of reactivation of excess heat generation

3-4. Brief Theoretical Explanation

After exceeding the turning point of $H/Ni=1.0$ (nominal value), excess thermal power was started to increase steeply, and a few days later it started to decrease at the near full $H/Ni \gg 1.0$ dependent on condition of the MHE sample-material under elevated temperature (highest temperature amid RC was over $900\text{ }^{\circ}\text{C}$) (Fig.9). H/Ni loading ratio was estimated by calculating the decrease of hydrogen pressure in the reaction chamber (RC) and in the reservoir tank, (Pr) and (Ps) respectively. The characteristics of H/Ni evolution shows that the absorption of hydrogen on the T-sites of the FCC lattice of Ni nano-islands in the MHE sample-material is important factor for the AHE excess thermal power generation in 200W/kg -sample level. And this is also the experimental evidence of the reported absorption mechanism of hydrogen into the Ni nano-meso-catalyst islands^{7,8,9} (Fig.13).

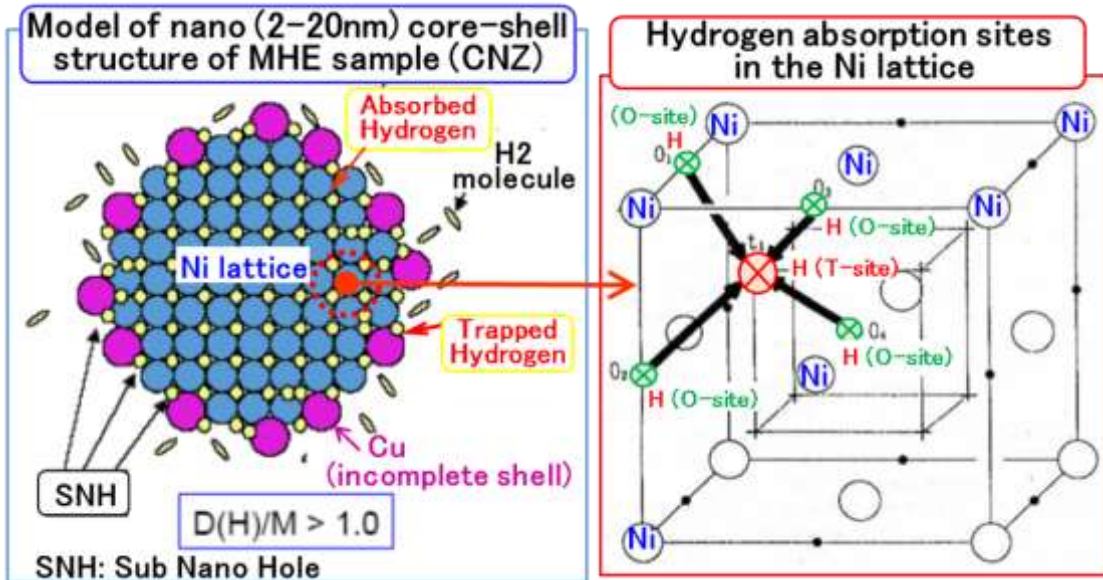


Fig.13; Absorption of hydrogen on the O-sites and T-sites in the FCC lattice of Cu-Ni nano-islands (core-shell structure) in the MHE sample-material

The conceivable mechanism of the observed re-activation is as follows. The re-feeding of hydrogen-gas with pressure difference between P_s and P_r would be some kind of stimulus toward the MHE reaction sites (SNHs^{6,7,8}) on the surface of Cu-Ni nano-islands. The first phase of on-surface MHE reactions makes the enough heat energy to desorb some part of the absorbed hydrogens at T-sites under H-loading saturated state. The desorbed hydrogens can make the rapid increase (burst) of reaction chamber gas pressure P_r . When amount of proton-empty T-sites becomes available (after some ten second of peak of P_r in real runs), the increase of temperatures of MHE sample-material zone by the MHE reaction can continue for a day with slowly decaying mode by increasing H/Ni ratio (recovering). Under this condition, the TSC model predicts that MHE reactions as 4H/TSC WS fusion (³He atoms and deuterons are ash) are taking place at T-sites by 4H/TSC formation from 4 protons of O-sites^{7, 8,9}). The re-activated MHE reaction rates were slowly decreased and the H/Ni loading was also returned to the previous full saturation level (nominal local value of 3.5). And before the reactivating valve operation and the temperatures of MHE sample-material in the RC also returned to the previous semi-equilibrium temperatures with low level AHE power (several watts in this study) at SNHs, which is long lasting bias.

VI. SUMMARY AND CONCLUDING REMARKS

We had new knowledge with two findings by new D-system experiments on MHE study

- 1) Findings of close Correlation of excess thermal power and H/Ni loading ratio :
 - After the fast rise-up H loading to Ni O-sites, exceeding H/Ni = 1.0 (nominal value), strong MHE reactions were induced.
 - Associating very slow H-loading to Ni T-sites, main part of excess thermal power by MHE reactions with (20~30W) lasted for a few days
 - After saturation of H-loading to T-sites, excess thermal power decreases to reach at rather constant excess power level (a few watts) continuing further
 - We confirmed that the phenomena is reproducible with different heating power for different MHE nano-composite samples.
- 2) Findings of MHE power re-activation method :
 - After saturation of H-loading to Ni nano-cores, artificial increment of excess power (re-activation) can be done by the discovery of RCV-close-to-open method.
 - For different MHE samples with different heating conditions, this re-activation process was many times repeatable.
 - The mechanism of MHE reactions here can be very well explained by the 4H/TSC WS fusion theory (see the following references ⁷⁻⁹)

References:

- [1] Akito Takahashi; Physics of Cold Fusion by TSC Theory, J. Condensed Matt. Nucl. Sci., 12, 191-198, 2013
- [2] See also: [\(PDF\) MHE nuclear-like thermal power generation and guiding TSC theory \(researchgate.net\)](#)

- [3] Akito Takahashi, Toyoshi Yokose, Yutaka Mori, Akira Taniike, Yuichi Furuyama, Hiroyuki Ido, Atsushi Hattori, Reiko Seto, Atsushi Kamei, Joji Hachisuka, “Latest Progress in Research on AHE and Circumstantial Nuclear Evidence by Interaction of Nano-Metal and H(D)-Gas”, *J. Condensed Matter Nucl. Sci.*, 33, 14-32, 2020
- [4] Akito Takahashi, Toyoshi Yokose, Yutaka Mori, Akira Taniike, Yuichi Furuyama, Hiroyuki Ido, Atsushi Hattori, Reiko Seto, Atsushi Kamei, Joji Hachisuka, “Enhancement of excess thermal power in interaction of nano-metal and H(D) gas”, Proc. JCF20, pp.9-27, 2020
- [5] Masahiko Hasegawa, Yutaka Mori, Akito Takahashi, Joji Hachisuka, Hiroyuki Ido, Reiko Seto, Akira Taniike, Yuichi Furuyama, “Comparison of AHE data between H₂ and He runs for CNZ7rrr Sample”, Presentation at JCF21 Meeting, December 2020, web conference of JCFRS:
(PDF) Comparison of AHE data between H₂ and He runs for CNZ7rrr sample - English version (researchgate.net)
- [6] Yutaka Mori, Akito Takahashi, Masahiko Hasegawa, Joji Hachisuka, Yuichi Furuyama; New MHE Experiments by D-System, JCF-22 Meeting (this meeting), 2022
- [7] Akito Takahashi; Physics of Cold Fusion by TSC Theory, *J. Condensed Matt. Nucl. Sci.*, 12, 191-198, 2013
- [8] Akito Takahashi; (PDF) MHE nuclear-like thermal power generation and guiding TSC theory (researchgate.net) See also referred papers in this Research-Gate paper.
- [9] Akito Takahashi, Masahiko Hasegawa, Yutaka Mori; Understanding of MHE excess power generation patterns by TSC theory, Proc. ICCF24, July 26-28 2022, USA, to be published in JCMNS.
Preprint will be uploaded in Research-Gate Akito Takahashi site.

Energy Generation using Nano-sized Multilayer Metal Composites with Hydrogen Gas; Intentional Induction of Heat Burst Phenomenon

Yasuhiro Iwamura¹, Takehiko Itoh^{1,2}, Tomonori Takahashi², Shinobu Yamauchi², Mari Saito², S. Murakami² and Jirohta Kasagi¹

¹Research Center for Electron Photon Science, Tohoku University, Sendai, 982-0826, Japan

²CLEAN PLANET Inc., Tokyo, 105-0022, Japan

E-mail: iwamura@lms.tohoku.ac.jp

Abstract

An innovative heat generation method using Ni based nano-sized metal multilayer thin films with hydrogen has been investigated by our team. Anomalously large heat generation up to about 20keV/H, which was too high to be explained by known chemical reactions, was induced by heating up the metal multilayer thin film that absorbed hydrogen gas in advance.

Spontaneous heat burst phenomena during excess energy generation has been observed, which was reported at JCF21. In this study, we reported that we succeeded in intentionally inducing such a heat burst phenomenon. For example, a heater input of 25.8 W could be reduced to 25.0 W and then returned to the original 25.8 W after 3 minutes to cause a heat burst phenomenon in which the surface temperature rises 20°C to 30°C for several minutes. Considering that the pressure in the chamber is less than 10^{-4} Pa, the energy released in this heat burst cannot be explained by any known chemical reactions such as hydrogen combustion. This phenomenon has been observed frequently, although it depends on the state of sample. At present, we assume that the temperature distribution change due to the perturbation in input power and hydrogen diffusion and concentration are involved in intentional induction of heat burst phenomenon.

1. Introduction

Our research team has been studying innovative methods of generating heat using Ni-based nano-sized multilayer metal [1]-[5]. This experimental method was developed based on the experiments on permeation-induced transmutation using deuterium and palladium multilayers [6]-[9] and on anomalous heat generation using nanoparticles [10]-[13].

The permeation-induced transmutation phenomenon, which is completely different from conventional transmutation by nuclear reactors or accelerators. D₂ gas permeation through a nano-structured multilayer thin film composed of Pd and CaO thin film and Pd substrate with a target element induces nuclear transmutation reactions [6]-[9]. It was firstly observed at Mitsubishi Heavy Industries [6] and successfully replicated by other institutes such as Toyota R&D center [14]. Typical target element is Cs and produced element is Pr. Transmutation reactions of Sr, Ba, W into Mo, Sm, Pt were also observed by this method. In this research, deuterium diffusion through nano-sized multilayer thin film was a key factor and the elemental analysis was key technique.

NEDO (New Energy and Industrial Technology Development Organization) research project on anomalous heat effects using Ni, Pd, Cu, Zr nano particles was done from Oct.

2015 to Oct. 2017 [10]-[13]. Anomalous heat generation, which is too much to be explained by any known chemical process, was observed. Qualitative reproducibility was confirmed between the Kobe University and Tohoku University. In the paper [13], coincident burst events of the reaction chamber pressure and gas temperature were observed many times using Cu, Ni and Zr nanoparticles with H₂ gas. It suggested heat burst energy releases in the reaction chamber. In these experiments, nano-sized particles and diffusion of hydrogen and deuterium were one of key factors to observe the heat effects and precise heat estimation was crucial.

Combining above important factors and methods to induce transmutation and heat generation reactions, we developed a present method using a nano-sized metal multilayer composite and hydrogen gas. During the anomalous heat experiments, we discovered that spontaneous heat bursts occur during excess heat generation. Even the energy generated by a single heat burst was too large to be explained by the chemical reactions of the materials in the vacuum chamber. By precisely analyzing the experimental conditions under which this spontaneous heat burst phenomenon occurred, we attempted to intentionally cause heat generation bursts. This paper focuses on heat burst phenomena and discusses the fact that even a single heat burst phenomenon cannot be explained by known chemical reactions and the significance of observing heat burst phenomena in heat measurement.

2. Experimental

Experimental method is basically the same with the paper [1]. Experimental set-up is shown in Fig.1. Two nano-sized metal multilayer composite samples, which were composed of Ni, Cu, CaO thin films on bulk Ni (25 mm × 25 mm × 0.1 mm), placed in the center of the chamber. H₂ gas and its pressure were monitored by a Pirani gauge. The chamber was evacuated by a turbo molecular pump. The multilayer samples were heated up by a ceramic heater in which a thermocouple (TC; Pt-PtRh13%) was embedded.

In the papers [1]-[2], the surface temperature of a sample was measured by an infrared radiation thermometer (IR-CAQ3CS; Chino Corp.). Now, we can measure surface temperatures for the two nano-sized metal multilayer composite samples by introducing two thermometer detectors. They were made of In GaAs and dual wavelength mode, 1.55 μm and 1.35 μm, were usually used. During the surface temperature measurement, it was possible to measure the emissivity of the sample surface by switching between single wavelength mode and dual wavelength mode. Heater input power was supplied by a DC power source in constant voltage mode. The input voltage and current were measured both by voltage and current monitors provided by the power supply and an independent voltmeter and amperemeter, respectively. Input power is calibrated using the voltmeter and the amperemeter readings. Gamma-rays and neutrons were monitored by a NaI (TI) scintillation counter (TCS-1172; Hitachi, Ltd.) and He-3 counter (TPS-1451; Hitachi Ltd.) during all experiments for safety reasons.

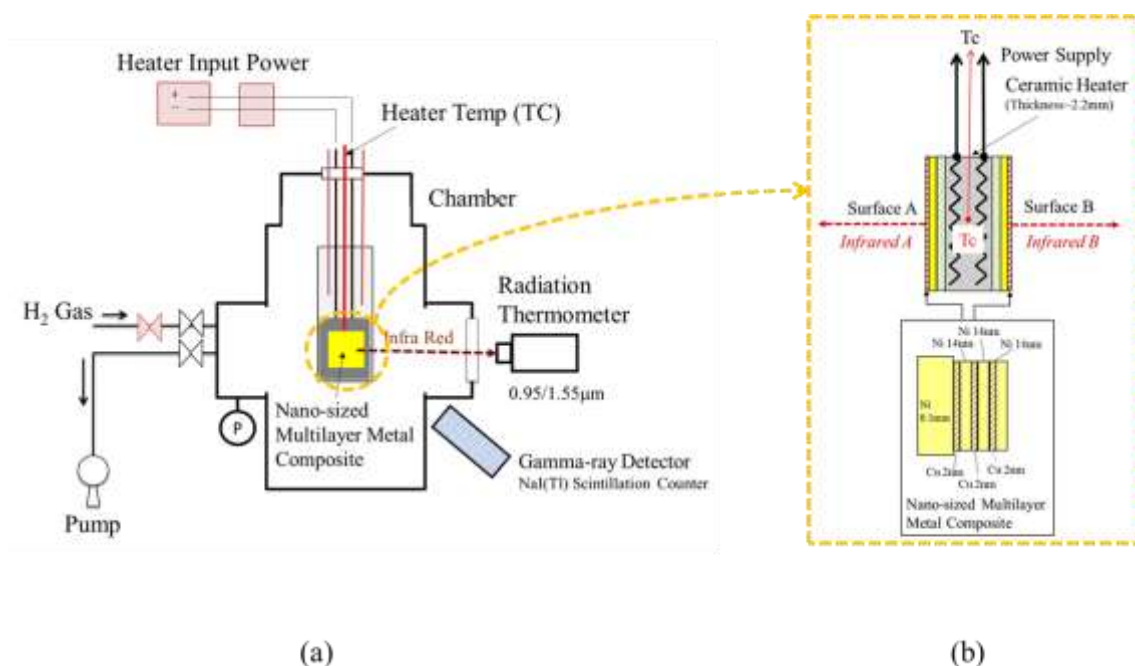


Figure 1. Experimental set-up; (a) schematic of experimental apparatus, (b) detail drawing around nano-sized multilayer metal composite [1].

A detailed drawing of the Ni based nano-sized metal multilayer composite is shown in Fig. 1(b). It was composed of a Ni Plate (25 mm square and 0.1 mm thick) and Cu-Ni multilayer thin film (20 mm diameter circle and about 100 nm thick). These samples were fabricated by the Ar ion beam method, or the magnetron sputtering method. Two nano-sized metal multilayer composite samples were heated by the ceramic heater (25 mm square and 2.2 mm thick) through SiO₂ plates (0.3 mm thick). If certain energy generation reactions occur on the surface of the samples, the temperature of the embedded thermocouple will rise. Simultaneously, infrared emission detected by the radiation thermometer, which corresponds to the surface temperature of the sample, would increase. Photos of the experimental set-ups and STEM image of Cu-Ni multilayer thin film are shown in Fig. 2.

The experimental procedure is as follows. Two nano-sized metal multilayer composites were placed in the chamber and baked for 2-3 days at heater temperature 900°C to remove H₂O and other hydrocarbons from the surface under vacuum conditions.

According to general knowledge, Cu and Ni diffuse into each other during the baking process, forming a Cu-Ni alloy. However, in our multilayer film, Cu and Ni are not simply alloyed, especially when CaO, Y₂O₃, etc. are added to Ni. The cause of this phenomenon is still under investigation, but it might be due to the effect of oxygen formed on the surface during the sputtering process.

After the baking process, H₂ gas was introduced into the chamber up to about 200 Pa at 250°C. To change the hydrogen loading conditions, the pressure of H₂ gas was sometimes increased up to 30 kPa. H₂ gas was loaded for about 16 hours. Then, H₂ gas was evacuated by the turbo molecular pump and simultaneously the samples were heated up by the ceramic heater up to 500~900°C. These processes trigger heat generation reactions and anomalous heat. Typically, after 8 hours, the heater input was turned down

and the samples were cooled down to 250°C. These processes (H₂ loading, heating up and cooling down samples) were repeated several times, with different heating temperatures or H₂ loading pressure.

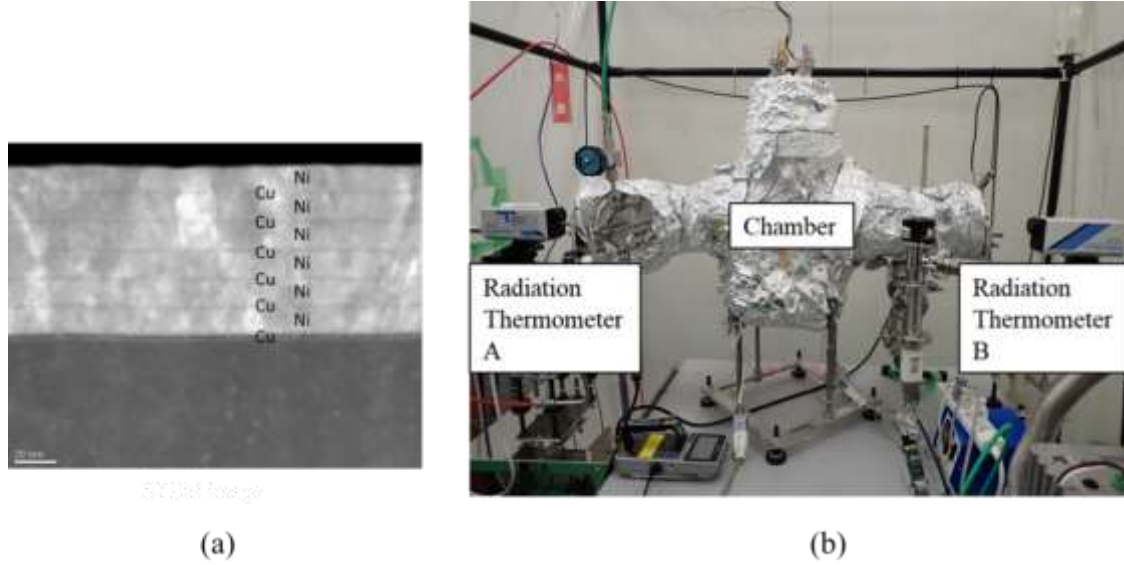


Figure 2. Photos of experimental apparatus and cross-sectional view of nano-sized metal multilayer composites; (a) STEM (Scanning transmission electron microscope) image of Cu-Ni multilayer thin film, (b) outer view of the present experimental set-ups.

During the above experimental procedure, hydrogen atoms are supposed to diffuse from the Ni plate through the nano-sized metal multilayer to the surface. The diffusion mechanism of hydrogen atoms is well known as “quantum diffusion” at low temperature [15]. Hydrogen atoms are hopping from a site to another site in metal. We assume that hydrogen flux is one of the key factors to induce condensed matter nuclear reactions and the hydrogen flux is intentionally arranged by the present experimental method. Hydrogen flux J from the nano-sized metal multilayer composite to the chamber is caused by gradient of hydrogen concentration and gradient of temperature as shown in eq. (1)[16].

$$J = -nD \left(\nabla c + \frac{cQ^* \nabla T}{k_B T^2} \right), \quad (1)$$

where n is the number of lattice atoms per unit volume, c is hydrogen concentration defined as the hydrogen/host-metal atom ratio, D is diffusion coefficient and Q^* is the heat of transport.

3. Results and Discussion

3.1 Excess Heat Evaluation

Excess Heat is evaluated based on the model described in Fig.3(a) and the following equation (2).

$$k_{eff} \frac{T_C - T_W}{L_{eff}} A_{eff} + A_S \sigma \{ \varepsilon_A (T_{SA}^4 - T_W^4) + \varepsilon_B (T_{SB}^4 - T_W^4) \} + A_{Rloss} \varepsilon_{Rloss} \sigma (T_{Rloss}^4 - T_W^4) = P_{in} + H_{ex} \quad (2)$$

where k_{eff} is equivalent thermal conductivity, T_c is the thermocouple temperature embedded in the ceramic heater, T_w is wall temperature of the chamber, L_{eff} and A_{eff} are effective length and effective surface area between the sample holder and wall, respectively. A_s is surface area of the sample, T_s is the surface temperature, ε is the emissivity of the sample, σ is the Stefan–Boltzmann constant. subscript A and B means surface A and B, respectively. A_{Rloss} , ε_{Rloss} and T_{Rloss} are effective surface area; effective emissivity and effective surface temperature for radiation loss except from the sample surface, which is mainly derived from the sample holder. P_{in} is the electrical heater input and H_{ex} is excess power. This equation is obtained under the following assumptions.

- 1) Thermal conduction via H_2 gas is negligible as H_2 pressure is low enough.
- 2) Radiation from chamber wall is negligible because T_w is room temperature.
- 3) The electrical input power is constant.

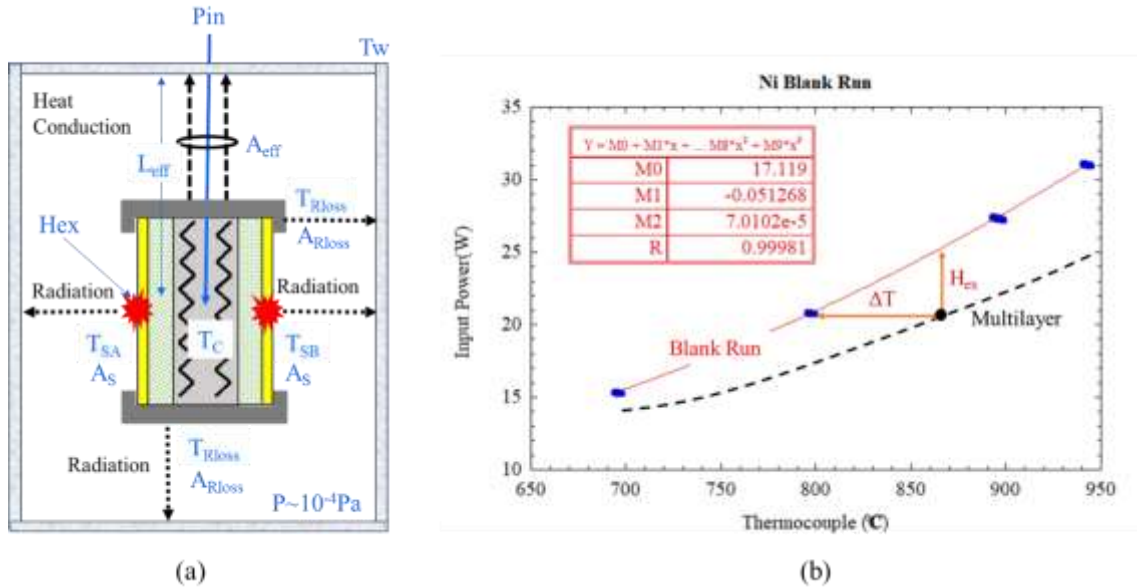


Figure 3. Method for excess heat evaluation; (a) model of excess heat evaluation, (b) relationship between input power(W) and thermocouple temperature (TC) for a blank run and a multilayer run.

A blank run, in which same sized Ni bulk samples without multilayer thin films were used, was performed with the same procedure described above. Figure 3(b) shows

the relationship between input power given to the ceramic heater and heater temperature detected by the thermocouple. As the radiation loss term from the sample holder is the same for Ni bulk and multilayer samples for the same temperature, generated excess heat power is supposed to be evaluated based on the blank run result as shown in Fig.3(b). Equation (2) for Ni bulk (subscript “0”) is written as

$$k_{eff} \frac{T_{C0} - T_W}{L_{eff}} A_{eff} + A_S \sigma \{ \varepsilon_{A0} (T_{SA0}^4 - T_W^4) + \varepsilon_{B0} (T_{SB0}^4 - T_W^4) \} + A_{Rloss} \varepsilon_{Rloss} \sigma (T_{Rloss0}^4 - T_W^4) = P_{in}. \quad (3)$$

In the papers [2]-[5], excess heat analysis was executed based on the assumption that ε is constant for Ni based nano-sized metal multilayer composite and Ni bulk as a first step of data analysis.

Emissivity ε can be measured by switching two wavelengths mode and single wavelength mode. Actual measured emissivity was in the range of 0.1-0.2 at surface temperature 700-750 °C, depending on the condition of the sample such as oxidation of surface or surface roughness, the vacuum of the experimental apparatus. However, the difference in emissivity between Ni bulk and Ni multilayer composite samples is within 0.05 (< 5 %), and the assumed condition is satisfied. It would be possible to consider that emissivity was almost the same for the Ni bulk and multilayer composite samples.

Excess heat H_{ex} is written based on the equations (2) for multilayer composite and Ni bulk (subscript “0”) samples.

$$H_{ex} = k_{eff} \frac{T_C - T_{C0}}{L_{eff}} A_{eff} + A_S \sigma \{ \varepsilon_A T_{SA}^4 - \varepsilon_{A0} T_{SA0}^4 + \varepsilon_B T_{SB}^4 - \varepsilon_{B0} T_{SB0}^4 - T_W^4 (\varepsilon_A - \varepsilon_{A0}) \} + A_{Rloss} \varepsilon_{Rloss} \sigma (T_{Rloss}^4 - T_{Rloss0}^4) \approx k_{eff} \frac{T_C - T_{C0}}{L_{eff}} A_{eff} + A_S \sigma \{ \varepsilon_A T_{SA}^4 - \varepsilon_{A0} T_{SA0}^4 + \varepsilon_B T_{SB}^4 - \varepsilon_{B0} T_{SB0}^4 \} + A_{Rloss} \varepsilon_{Rloss} \sigma (T_{Rloss}^4 - T_{Rloss0}^4) \quad \because T_{SA,B}^4 \gg T_W^4 \quad (4)$$

Now, we assume the following relations based on our experimental data. It is possible that T_{SA} and T_{SB} can be expressed as liner function of T_C within the experimental parameters.

$$\varepsilon_A \approx \varepsilon_{A0}, \quad \varepsilon_B \approx \varepsilon_{B0}, \quad T_{SA} \approx \alpha_A T_C + \beta_A, \quad T_{SB} \approx \alpha_B T_C + \beta_B, \quad T_{Rloss} \approx \alpha_{Rloss} T_C + \beta_{Rloss}.$$

ΔT is defined as

$$\Delta T = T_C - T_{C0}. \quad (5)$$

Therefore, the following expression is obtained.

$$H_{ex} \approx \Delta T \left\{ \frac{k_{eff}}{L_{eff}} A_{eff} + A_S \varepsilon_{A0} \sigma \alpha_A (T_{SA} + T_{SA0}) (T_{SA}^2 + T_{SA0}^2) + A_S \varepsilon_{B0} \sigma \alpha_B (T_{SB} + T_{SB0}) (T_{SB}^2 + T_{SB0}^2) + A_{Rloss} \varepsilon_{Rloss} \sigma (T_{Rloss} + T_{Rloss0}) (T_{Rloss}^2 + T_{Rloss0}^2) \right\}. \quad (6)$$

This equation shows that excess heat can be written as a function of ΔT . Therefore, excess heat evaluation by the Ni bulk calibration curve shown in Fig.3(b) is valid under the assumptions described above.

3.2 Experimental Results

Before describing heat burst phenomena, a typical example of anomalous heat generation, already published [2], is shown in Fig.3. Red and blue lines mean excess heat and pressure of the chamber, respectively.

At the beginning of the experiment, hydrogen gas was introduced to the chamber and absorbed into the Ni based nano-sized multilayer metal composite at 250°C. The pressure for each experiment gradually decreased as shown in the Fig. 3. The amount of hydrogen absorbed by the sample could be estimated based on the pressure change and temperature of the chamber.

After about 6×10^4 sec, H₂ gas was evacuated and simultaneously each sample was heated up rapidly by the ceramic heater. After that, excess heat generation more than input power was triggered by the rapid heating and hydrogen diffusion. Excess heat is calculated using the previously described method. For example, the first excess heat is about 5W at a heater temperature of about 870°C for an input of 19W. The input power was stable during a one cycle; for example, 19 W was applied to the ceramic heater from about 6×10^4 sec to about 9×10^4 sec.

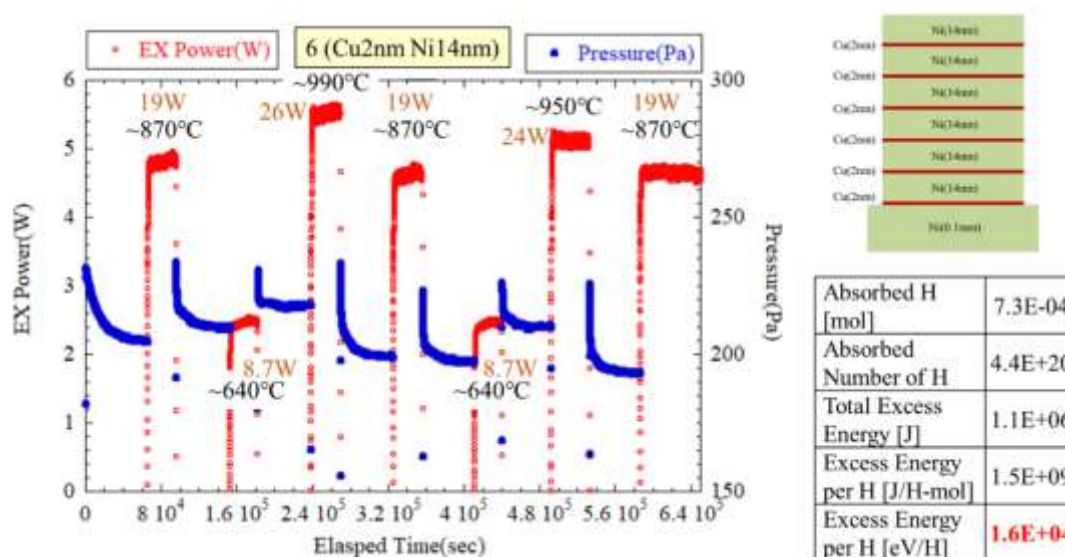


Figure 4. Example of anomalous heat generation [2].

From the decrease in pressure in the vacuum chamber, the total amount of hydrogen absorbed in this sample can be calculated as 7.3×10^{-4} mol or 4.4×10^{20} as shown on the right side of the Fig.4. By integrating this excess heat with time, the total energy released in this experiment can be calculated as 1.1 MJ. It is difficult to assume that all of the absorbed hydrogen is involved in the excess heat generation, and much of it is simply

released from the sample due to heating, but here we divide the total energy by the amount of hydrogen absorbed to avoid overestimation. This yields a value of 16 keV/H or 1.5 GJ/H-mol.

In normal chemical reactions, the amount of energy generated per hydrogen is on the order of eV. This is because chemical reactions can only release energy at the level of electron binding energy. Compared to this, the value of 16 keV/H just obtained is an order of magnitude higher, even though it is an underestimate. Released energy per hydrogen cannot be explained by any known chemical process and suggests that the observed heat generation might be of nuclear origin.

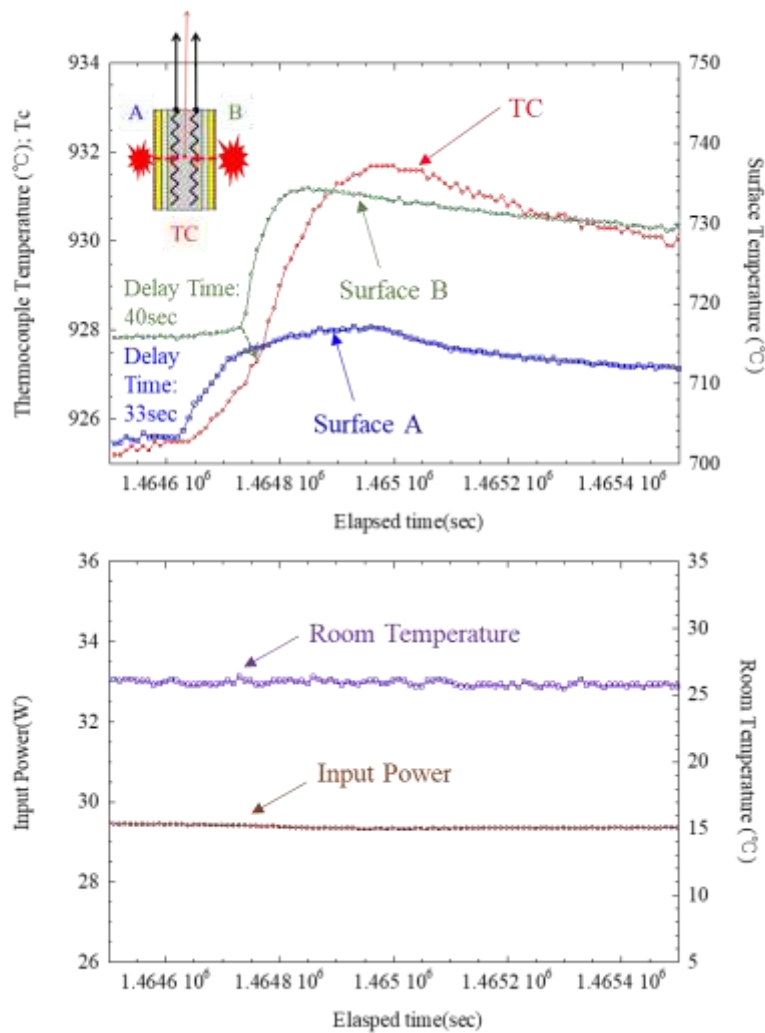


Figure 5. An example of spontaneous heat burst, which occurred at the surface A at first and afterwards at the surface B. Their heat bursts induced the rise of Tc. Input power and room temperature were constant during these events [1].

Next, an example of a spontaneous thermal burst is described. As shown in Fig. 5, a heat burst occurred suddenly on surface A, and the heat propagated to the thermocouple (TC) at the center of the ceramic heater, followed by a heat burst on surface

B, which further propagated to the TC. Input power and room temperature were constant during these events. Therefore, the heat burst events were not caused by the change of electrical input power or heat coming in from the environment. The samples consisted of 6 layers of Cu (2 nm) and Ni (14 nm) fabricated by magnetron sputtering on Ni bulk.

Delay time from the spontaneous heat burst at surface A and B to the thermocouple was about 33 and 40 sec, respectively. Based on the specific heat and size data for the sample, ceramic heater and sample holder materials (Al_2O_3 and SiO_2), the time constant when heat is generated on the sample surface can be calculated to be approximately 36 seconds (see [1]). Therefore, the delay time obtained from the experiment is almost the same, and it is consistent to assume that the heat burst occurred near the sample surface. This example gives us clear evidence that heat release reactions occurred in the near surface region of the nano-sized multilayer metal composite with hydrogen gas.

When analyzing the phenomenon of spontaneous sudden heat bursts described above, it was observed that there were some cases where the heat burst phenomenon occurred after small deviations in input power caused by fluctuations in the outside temperature, etc. Therefore, we tried to reproduce the heat burst phenomena by perturbing the electrical input power. As a result, it became possible to intentionally induce heat burst phenomena.

An example of a heat burst phenomenon induced by an intentional perturbation of input electrical power is shown in Fig. 6 (a). At the beginning, 25.8 W was input, and then decreased to 25.0 W. Then the TC and surface temperature A and B decreased gradually. When the input was returned to the original input of 25.8 W, the surface temperature A, B, and Tc all increased and became larger than the values at the original input of 25.8 W. At maximum, Tc increased by about 9°C , surface A by about 17°C , and surface B by about 25°C . The increases in surface A and B temperatures were larger and steeper than that of Tc as shown in Fig. 6 (a). It can be considered that heat burst energy generated at the surface A and B, which is induced by the intentional perturbation of input power, propagated to the thermocouple.

On the other hand, an example of no heat burst phenomenon induced by a similar perturbation is shown in Fig. 6 (b). In this case, when the input power, which was initially 26.3 W, was reduced to 25.8 W, the thermocouple and surface temperatures A and B gradually decreased as in Fig. 6(a). Then, when the input power was returned to 26.3 W, the heat burst phenomenon did not occur, and the thermocouple and surface temperatures A and B returned to their original values.

The same experimental setup was used for these two examples, but the compositions of the samples were different. Figure 6 (a) is a 6-layer CuNi_7 sample, and Figure 6 (b) is a 6-layer CuNi_7 sample with CaO inserted into the Ni layer. The conditions under which this phenomenon occurs are being investigated in detail. According to experimental results, it depends on (1) the composition and state of the sample, (2) the surface temperature of the sample, and (3) the amount and time range of the input power perturbation. At present, we assume that the temperature distribution change due to the perturbation in input power and hydrogen diffusion and concentration are involved in intentional induction of heat burst phenomenon.

The research implications of heat bursts are as follows. Usually, in the case of heat measurement as shown in this paper, the heat generation is evaluated using a calibration curve, and there are many cases where people question whether the heat

dissipation characteristics are different between the time of calibration and the time of the heat generation experiment due to variations in the way the sample is mounted, etc. We are constantly checking various measurements to see if there are any changes in the heat dissipation characteristics from experiment to experiment. We conclude that the heat burst phenomena cannot be explained by the difference in the heat dissipation characteristics between a calibration and an experiment. The observation of the heat burst phenomena increases the reliability of the heat measurement experiment.

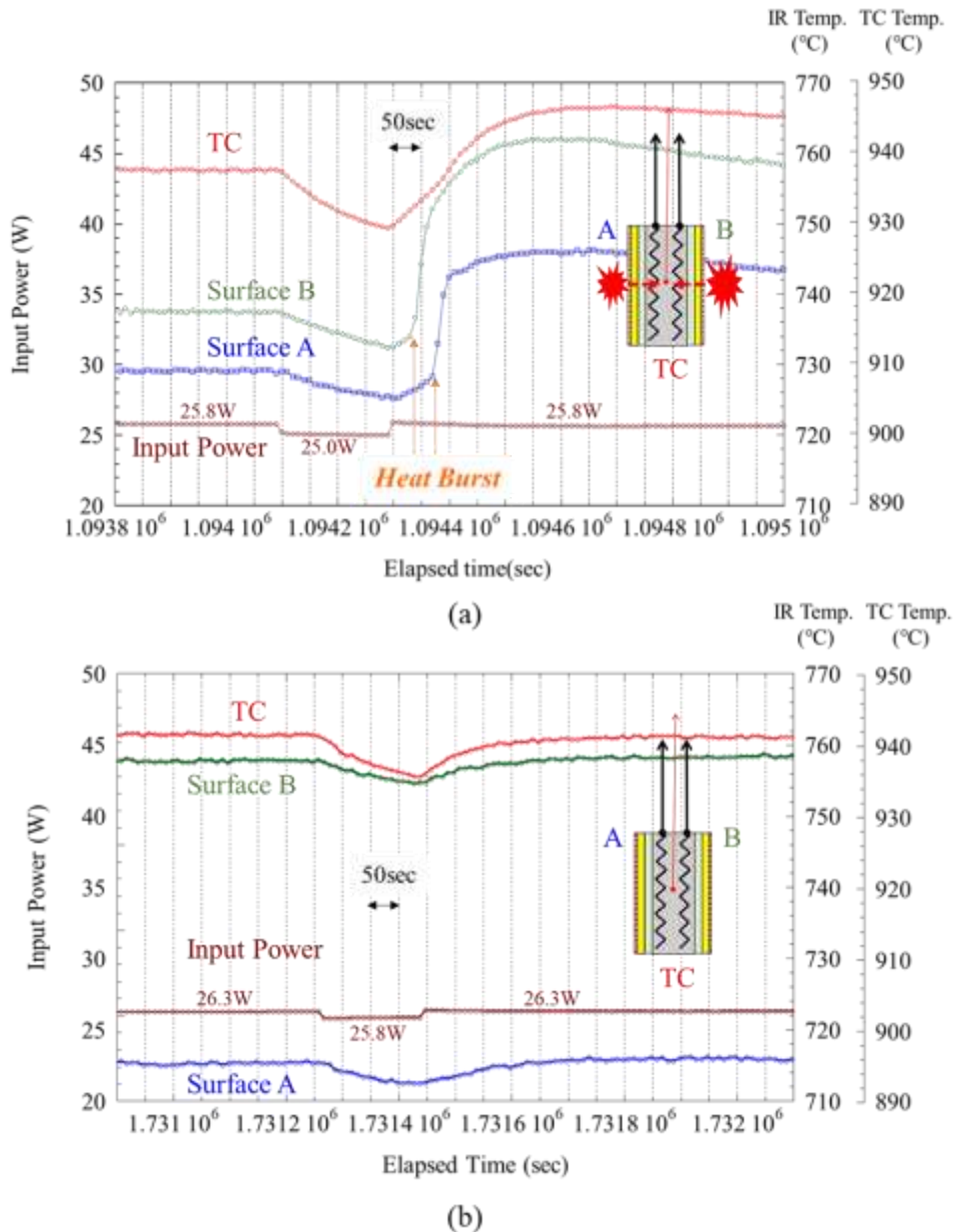


Figure 6. Intentional heat burst induced by a perturbation in input power: (a) an example of heat burst phenomena induced by the intentional perturbation in input electrical power, (b) an example of no heat burst phenomena.

Next, we examine the possibility that the observed heat burst phenomenon was caused by some chemical reactions. Figure 7 plots the change in excess power during the intentionally induced heat burst shown in Fig. 6. At about 1.0944×10^5 sec, a heat burst induced by the perturbation of input power. About 5.5 W excess heat was obtained before the input power perturbation and it increased up to 6.5 W after the perturbation in input power and gradually decreased. The excess increase due to the heat burst lasted for at least 1.2×10^4 seconds. 12 kJ energy release by the one heat burst can be calculated by integrating excess power with time.

Whether the energy obtained from this single heat burst can be explained by chemical reactions is discussed below. During the heat release experimental cycle, all the hydrogen introduced for absorption was evacuated, and the degree of vacuum was less than 1×10^{-4} Pa when the heat burst phenomenon was observed. Therefore, the number of moles of residual gas was less than 4×10^{-10} mol. Chemical reactions that could generate heat under these circumstances are as follows.

- (1) When the residual gas in the chamber is all oxygen and the absorbed hydrogen is oxidized and generates heat.
- (2) When the residual gas is oxygen and Ni metal is oxidized.
- (3) When the residual gas is a mixture ($\text{H}_2:\text{O}_2=2:1$) and its combustion energy energizes the surfaces of the two samples.

It is known that the combustion reaction of hydrogen is about 290 kJ/mol and the heat of formation of nickel oxide is about 240 kJ/mol. Since the number of moles of residual gas in the chamber was less than 4×10^{-10} mol, the heat generated in each case can be calculated less than 10^{-3} J. It is completely negligible if we compare the energy increased by the heat burst: 12kJ. This clearly shows that at least the chemical reactions (1)-(3) cannot explain the heat burst phenomenon observed in this study.

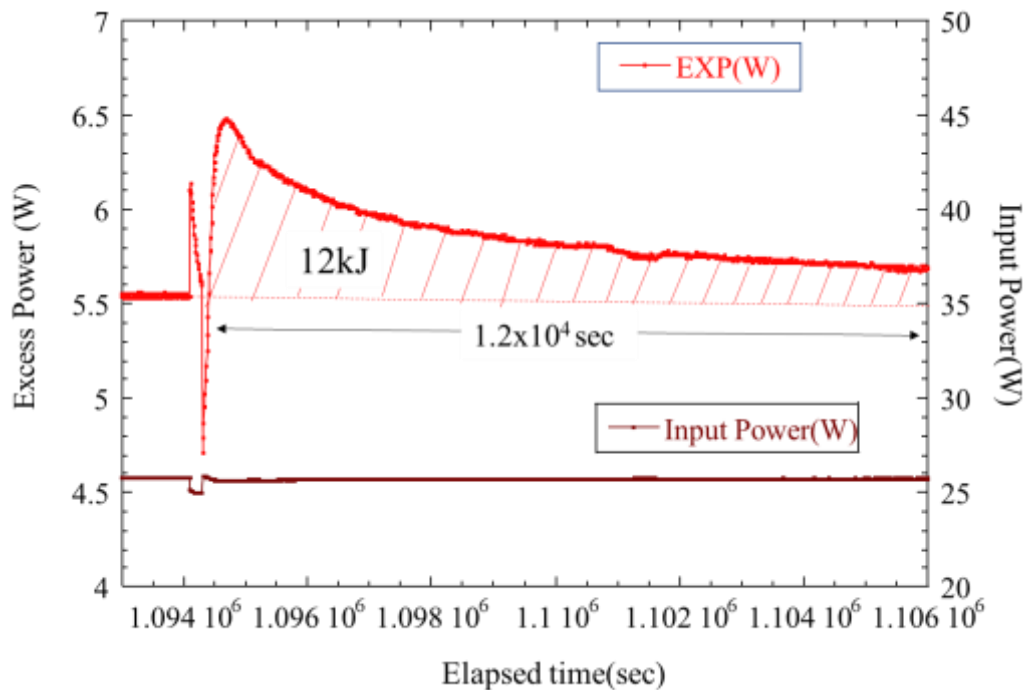


Figure 7. Released energy by a single heat burst reactions.

4. Concluding Remarks

We have been conducting research and development with an experimental method using Ni based nano-sized metal multilayer thin films with hydrogen. Anomalously large heat generation up to about 20keV/H, which was too high to be explained by known chemical reactions, was induced by heating up the metal multilayer thin film that absorbed hydrogen gas in advance.

As reported at JCF21, sudden spontaneous heat burst phenomena during excess energy generation has been observed. In this paper, we described that we succeeded in intentionally inducing such a heat burst phenomenon. An example of intentional heat burst phenomenon induced by a perturbation in input power is shown in this paper. Considering that the pressure in the chamber is less than 10^{-4} Pa, the energy released in this heat burst cannot be explained by any known chemical reactions such as hydrogen combustion. This phenomenon has been observed frequently, although it depends on the state of sample. The observation of the intentional heat burst phenomena dispelled concerns that the observed excess heat might be due to a deviation of Ni bulk calibration curve. In other words, it contributed to improving the reliability of heat measurements. We are currently investigating the conditions under which this heat burst phenomenon occurs, which is expected to contribute to the clarification of the mechanism of induced abnormal heat reactions.

Acknowledgements

The authors acknowledge Mr. H. Yoshino, Dr. T. Hioki, Mr. Y. Endo and Mr. S. Hirano who are the members of CLEAN PLANET Inc., for their significant assistance. The authors also thank Mr. Y. Shibasaki and Prof. H. Kikunaga of Tohoku University for their support. This work is supported by CLEAN PLANET Inc., Research Center for Electron Photon Science of Tohoku University Electron Photon, the Thermal & Electric Energy Technology Foundation and Tanaka Kikinzoku Memorial Foundation.

References

- [1] Y. Iwamura, T. Itoh, M. Saito, S. Murakami and J. Kasagi, "Evidence for Surface Heat Release Reaction over Nano-sized Multilayer Metal Composite with Hydrogen Gas", *Proceedings of the 21st Meeting of Japan CF Research Society*, JCF21, December 11-12, 2020, Online Meeting, p.1-14.
- [2] Y. Iwamura, T. Itoh, J. Kasagi, S. Murakami and M. Saito, "Excess Energy Generation using a Nano-sized Multilayer Metal Composite and Hydrogen Gas", *J. Condensed Matter Nucl. Sci.* **33** (2020) 1–13.
- [3] Y. Iwamura, "Heat generation experiments using nano-sized metal composite and hydrogen gas", *Cold Fusion: Advances in Condensed Matter Nuclear Science*, Ed. Jean-Paul Biberian, Elsevier, Amsterdam, (2020)157-165.
- [4] S. Murakami, T. Itoh, Y. Iwamura, M. Saito and J. Kasagi, "Excess Energy Generation Experiments using a Nano-sized Multilayer Metal Composite and Hydrogen Gas", *Proceedings of the 20th Meeting of Japan CF Research Society*, JCF20, December 13-14, 2019, Reference Hakata Eki-Higashi Rental Room, Fukuoka, Japan p.86-96.

- [5] M. Saito, T. Itoh, Y. Iwamura, S. Murakami and J. Kasagi, “Elemental Analysis for Elucidation of the Anomalous Heat Generation Phenomena”, Proceedings of the 20th Meeting of Japan CF Research Society, JCF20, December 13-14, 2019, Reference Hakata Eki-Higashi Rental Room, Fukuoka, Japan p.74-85.
- [6] Y. Iwamura, M.Sakano and T.Itoh, Elemental Analysis of Pd Complexes: Effects of D₂ Gas Permeation, *Jpn. J. Appl. Phys.* **41** (2002) 4642-4650.
- [7] Y. Iwamura, T. Itoh, N. Gotoh and I. Toyoda, Detection of Anomalous Elements, X-ray and Excess Heat in a D₂-Pd System and its Interpretation by the Electron-Induced Nuclear Reaction Model, *Fusion Technology*, **33** (1998) 476-492.
- [8] Y. Iwamura, T. Itoh, M. Sakano, N. Yamazaki, S. Kuribayashi Y. Terada, T. Ishikawa, D. Sekiba, H. Yonemura and K. Fukutani, Observation of Low Energy Nuclear Transmutation Reactions Induced by Deuterium Permeation through Multilayer Pd and CaO thin Film, *J. Condensed Matter Nucl. Sci.* **4** (2011) 132–144.
- [9] Y. Iwamura, T. Itoh and S. Tsuruga, Transmutation Reactions Induced by Deuterium Permeation through Nano-structured Pd Multilayer Thin Film, *Current Science*, Vol. 108, NO. 4 (2015) 628-632.
- [10] A. Kitamura, A. Takahashi, R. Seto, Y. Fujita, A. Taniike and Y. Furuyama, “Effect of Minority Atoms of Binary Ni-Based Nano-Composites on Anomalous Heat Evolution under Hydrogen Absorption”, *J. Condensed Matter Nucl. Sci.*, **19** (2016) 1-10.
- [11] A. Kitamura, A. Takahashi, K. Takahashi, R. Seto, T. Hatano, Y. Iwamura, T. Itoh, J. Kasagi, M. Nakamura, M. Uchimura, H. Takahashi, S. Sumitomo, T. Hioki, T. Motohiro, Y. Furuyama, M. Kishida, H. Matsune, “Excess heat evolution from nanocomposite samples under exposure to hydrogen isotope gases”, *International Journal of Hydrogen Energy* **43** (2018) 16187-16200.
- [12] Y. Iwamura, T. Itoh, J. Kasagi, A. Kitamura, A. Takahashi and K. Takahashi, “Replication Experiments at Tohoku University on Anomalous Heat Generation Using Nickel-Based Binary Nanocomposites and Hydrogen Isotope Gas”, *J. Condensed Matter Nucl. Sci.* **24** (2017) 191–201.
- [13] Y. Iwamura, T. Itoh, J. Kasagi, A. Kitamura, A. Takahashi, K. Takahashi, R. Seto, T. Hatano, T. Hioki, T. Motohiro, M. Nakamura, M. Uchimura, H. Takahashi, S. Sumitomo, Y. Furuyama. M. Kishida and H. Matsune, Anomalous Heat Effects Induced by Metal Nano-composites and Hydrogen Gas, *J. Condensed Matter Nucl. Sci.* **29** (2019) 119–128.
- [14] T. Hioki et.al, Inductively Coupled Plasma Mass Spectrometry Study on the Increase in the Amount of Pr Atoms for Cs-Ion-Implanted Pd/CaO Multilayer Complex with Deuterium Permeation, *Jpn. J. Appl. Phys.* **52** (2013) 107301.
- [15] Y. Fukai, Evidence for Quantum Diffusion of Hydrogen in Ta: Quench-Recovery Experiments Revisited, *Japanese Journal of Applied Physics*, Vol.23, No.8 (1984) 596-598.
- [16] H. Wipf, Electro- and Thermo-Transport of Hydrogen in Metals, *Hydrogen in Metals II*, Ed. by G. Alefeld and J. Völkl, Springer-Verlag, Berlin, Heidelberg (1978) 273-304.

Heat generation of metal composite powder caused by the pulse flow of hydrogen gas

Tomotaka Kobayashi¹, Ken Naitoh¹, Junsuke Shigemura¹, Daiki Okada¹,
Yoshiki Nomura¹

¹Waseda University, Tokyo, Japan

E-mail: winningshot1996@asagi.waseda.jp

Abstract Anomalous heat generations in exposure of nickel or palladium powder to hydrogen or deuterium gas were reported in the previous research. Especially, we focused on the heat generation during hydrogen gas absorption by metal composite powder. In our previous report, we developed a reaction system with small chamber and conducted the fundamental experiment of the anomalous heat effect. About 10 K of temperature increase was observed when hydrogen gas is absorbed by Pd-Ni-Zr composite powder at about 500 K. In this report, we conducted the experiments of anomalous heat generation (absorption of hydrogen gas by nickel powder and Pd-Ni-Zr composite powder) with the pulse flow of hydrogen gas. As a result, about 35 K of temperature rise was observed in the experiment using Pd-Ni-Zr composite powder under the condition: 240°C of initial temperature and 0.9 MPa of the gas pressure. In addition, the tendency was observed that temperature rise during experiment is increased than that of the experiments without the pulse flow.

Keywords: Anomalous heat, Metal composite powder, Hydrogen gas, Pulse flow

1. Introduction

It is known that anomalous heat is generated when hydrogen or deuterium is absorbed by nickel or palladium [1-4]. In the previous research, anomalous heat generation is observed in several patterns: long time exposure of metal powder (Ni or Pd) to hydrogen (or deuterium) gas [1,2], hydrogen (or deuterium) gas absorption by mixed oxides of Pd and Zr [3], electrolysis using Ni film [4], and so on.

Our purpose is to develop a new energy generator using the anomalous heat, which is accelerated by very high compression obtained by collision of the high-speed multi-jets repeatedly [5-9]. Therefore, we focused on the heat generation during hydrogen gas absorption by metal composite powder.

In our previous report, we developed a reaction system with small chamber (Fig. 1)

and conducted the fundamental experiment of the anomalous heat effect. About 10 K of temperature increase was observed when hydrogen gas is absorbed by Pd-Ni-Zr composite powder at about 500 K (Fig. 2). [10]

In this report, we conducted the experiments of anomalous heat generation (absorption of hydrogen gas by nickel powder and Pd-Ni-Zr composite powder [11]) with the pulse flow [12] of hydrogen gas to confirm the effect of the pulse flow on the anomalous heat generation.

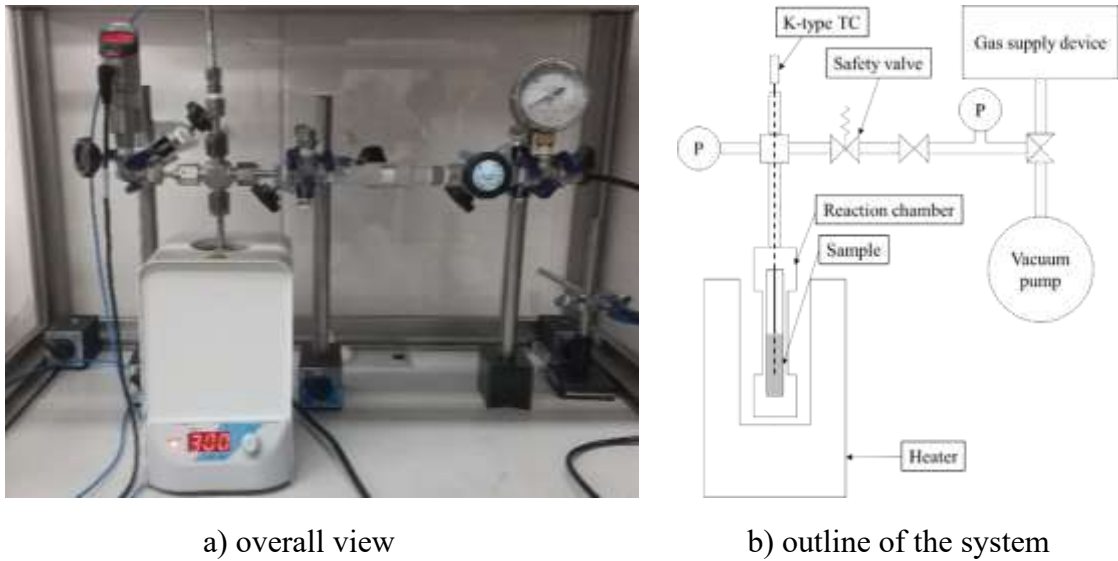


Fig. 1. Reaction system in our previous report [10]

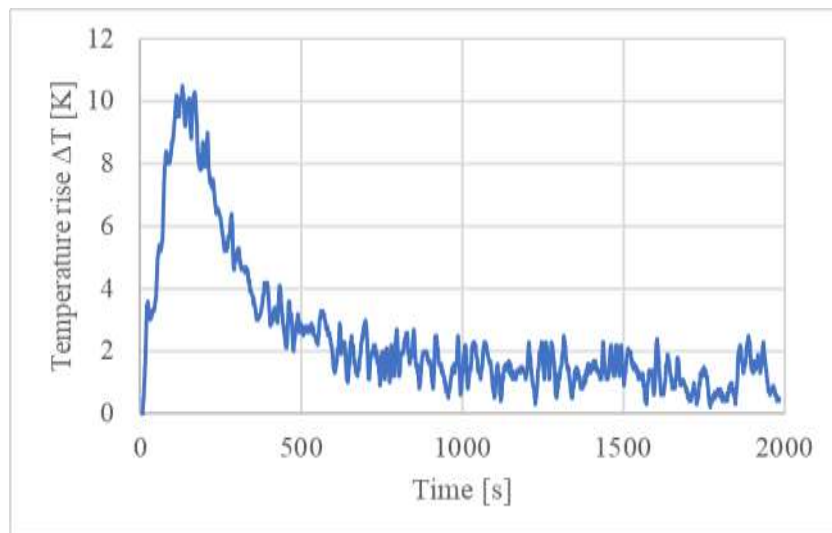


Fig. 2. Experimental result in our previous report [10]

2. Experimental device

Outline of the reaction system is shown in Fig. 3. The system is constructed of heater, reaction chamber, K-type thermocouple, safety valve, two pressure gauges, solenoid valve, hand valve, three-way valve, gas supply device, and vacuum pump.

The reaction chamber having about 2 mL volume is made of stainless steel (SUS316L). The heater is used for preheating the reaction chamber. It can be heated in range of 100 - 300 °C. The K-type thermocouple, whose tip is embedded in the sample, is used for measuring the sample temperature. The gas supply device is used for providing gas (nitrogen or hydrogen) while the experiments. The maximum pressure of provided gas allowable for the gas supply device is 1.0 MPa. The pressure of the gas provided in the reaction chamber is measured by the pressure gauges. The safety valve opens when the pressure in the chamber exceeds 1.0 MPa to prevent the breaking down of the system. The vacuum pump is used for evacuation. The ultimate pressure of the vacuum pump is 1.6 Pa.

In this report, a solenoid valve (YS302AH88M9BC3, made by KONAN ELECTRIC CO., LTD.) is installed in the reaction system. The solenoid valve enables to conduct the experiment with pulse flow of hydrogen gas.

Specification of the reaction system is shown in Table 1.

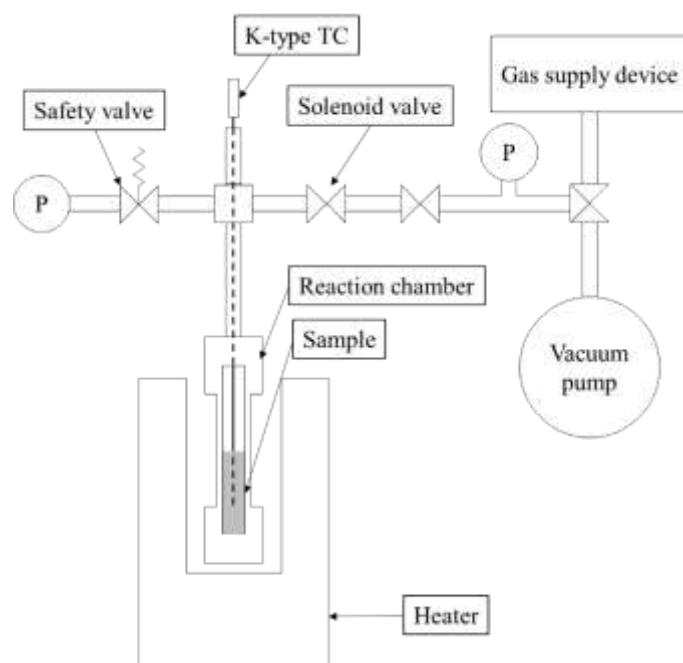


Fig. 3. Outline of the reaction system

Table 1. Specification of the reaction system

Material of reaction chamber	SUS316L
Volume of reaction chamber	2 mL
Ultimate pressure of vacuum pump	1.6 Pa
Maximum pressure of loading gas	1.0 MPa
Maximum temperature of heater	300 °C

3. Procedure of the experiment

The procedure of the experiment is shown in Fig. 4. First, the sample (nickel powder or Pd-Ni-Zr composite powder [11]) is set in the reaction chamber. Then, the chamber is evacuated by the vacuum pump. After that, the chamber is preheated by the heater. After the preheating, hydrogen (or nitrogen for the control experiment) gas is loaded to upstream side of the solenoid valve. After that, solenoid valve is opened, and pulse flow of the hydrogen (or nitrogen) gas enters into the chamber. The temperature increase of the sample is measured by the K-type thermocouple. At the end of the experiment, the loaded gas is exhausted, and the chamber is vacuumed again not to leave the loaded gas in the chamber.

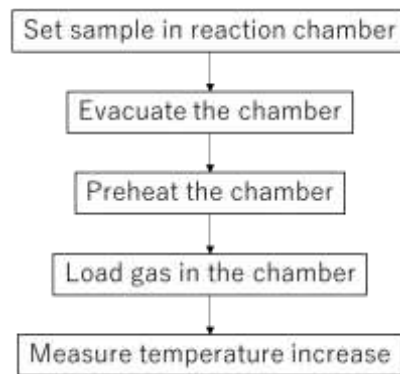


Fig. 4. Procedure of the experiment

4. Experimental result

Experimental conditions are shown in table 2. In the experiments, 3.0 g of nickel powder (NFP201S, made by JFE MINERAL COMPANY, LTD.) and Pd-Ni-Zr composite powder ([PNZ10r, provided by Technova Inc.](#)) [6] were used as a sample.

The experiments were conducted using hydrogen gas, and nitrogen gas as the control experiment. (The experiment using nitrogen gas is done before hydrogen gas.) The experiments were conducted in the range of loaded gas pressure 0.12 - 0.9 MPa and initial temperature of sample 95-240 °C. In this report, the experiments were conducted under

both conditions with and without pulse flow of hydrogen gas.

Table 2. Experimental conditions

Sample	Nickel powder or Pd-Ni-Zr composite powder
Sample mass	3.0 g
Kind of gas	Hydrogen or Nitrogen (control experiment)
Gas pressure	0.12 – 0.9 MPa
Initial temperature	95 – 240 °C

Figure 5 shows the result of the experiment (using 3.0 g of Nickel powder, 0.5 MPa of gas pressure, 240 °C of initial temperature, without the pulse flow). An orange line for nitrogen gas loaded and a blue line for hydrogen gas loaded in Fig. 5a show the time-histories of temperature for the Nickel sample, while Fig. 5b shows the temperature rise ΔT from the control experiment for nitrogen gas loaded, i.e., the temperature difference between cases of hydrogen and nitrogen loaded. In the experiment, temperature rise began about 400 seconds after hydrogen gas loading. About 4 K of temperature rise was observed about 500 seconds after the beginning of the temperature rise.

Figure 6 shows the result of the experiment (using 3.0 g of Nickel powder, 0.5 MPa of gas pressure, 240 °C of initial temperature, with the pulse flow). Fig. 6a show the time-histories of temperature for the sample and Fig. 6b shows the temperature rise ΔT . In the experiment, temperature rise began about 300 seconds after hydrogen gas loading. About 3.5 K of temperature rise was observed about 300 seconds after the beginning of the temperature rise.

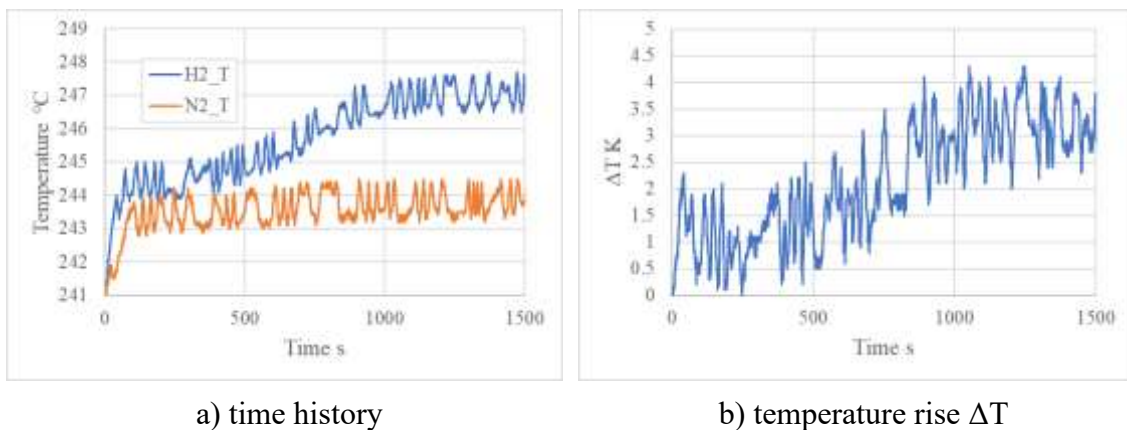
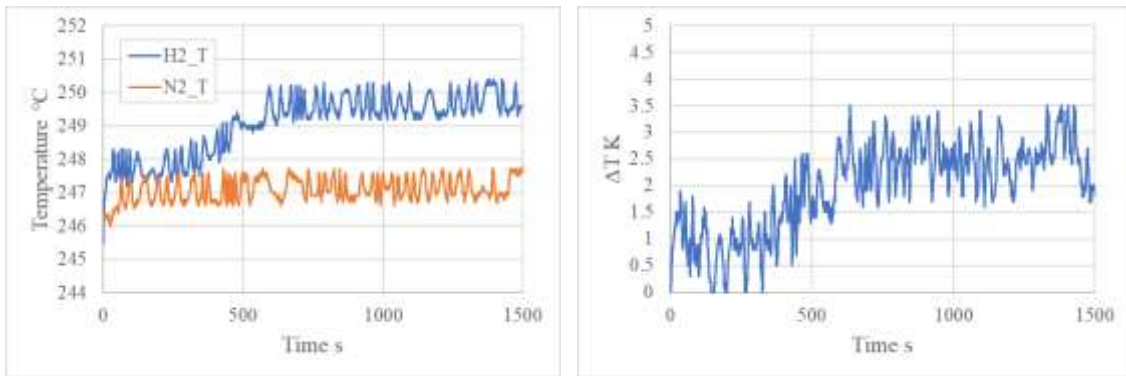


Fig. 5. Result of the experiment (Ni 3.0 g, 240°C, 0.5 MPa, without pulse flow)
(Kobayashi et al., *ICCF-23*, 2021)



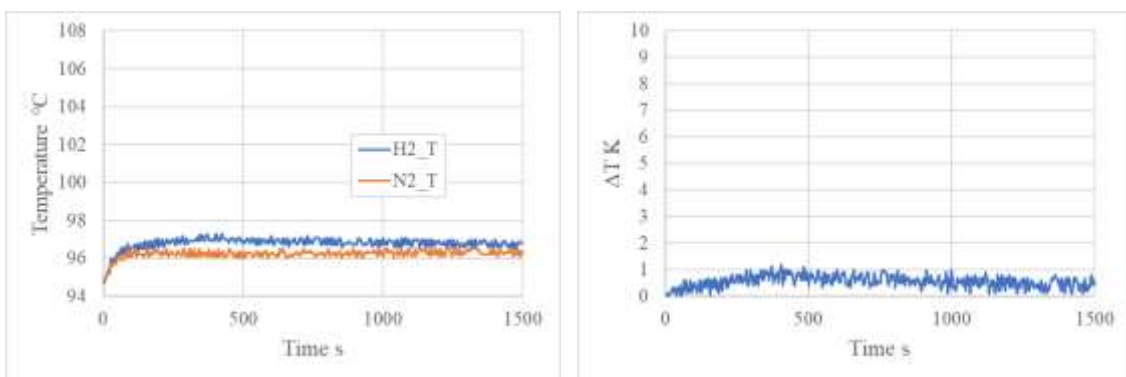
a) time history

b) temperature rise ΔT

Fig. 6. Result of the experiment (Ni 3.0 g, 240°C, 0.5 MPa, with pulse flow)

Figure 7 shows the result of the experiment (using 3.0 g of Pd-Ni-Zr composite powder, 0.12 MPa of gas pressure, 95 °C of initial temperature, without the pulse flow). Fig. 7a show the time-histories of temperature for the sample and Fig. 7b shows the temperature rise ΔT . In the experiment, temperature rise began just after hydrogen gas loading. However, no obvious difference from the control experiment.

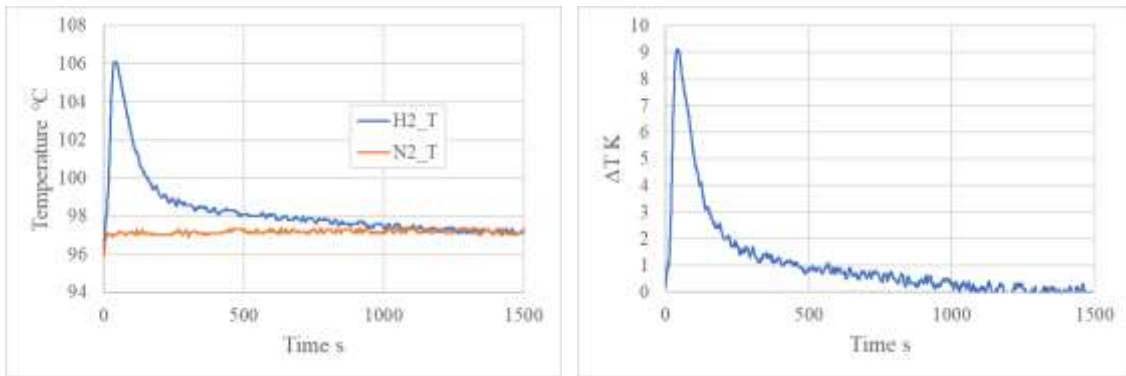
Figure 8 shows the result of the experiment (using 3.0 g of Pd-Ni-Zr composite powder, 0.12 MPa of gas pressure, 95 °C of initial temperature, with the pulse flow). Fig. 8a show the time-histories of temperature for the sample and Fig. 8b shows the temperature rise ΔT . In the experiment, temperature rise began just after hydrogen gas loading. About 9 K of temperature rise was observed about 40 seconds after the beginning of the temperature rise.



a) time history

b) temperature rise ΔT

Fig. 7. Result of the experiment (Pd-Ni-Zr 3.0 g, 95°C, 0.12 MPa, without pulse flow)



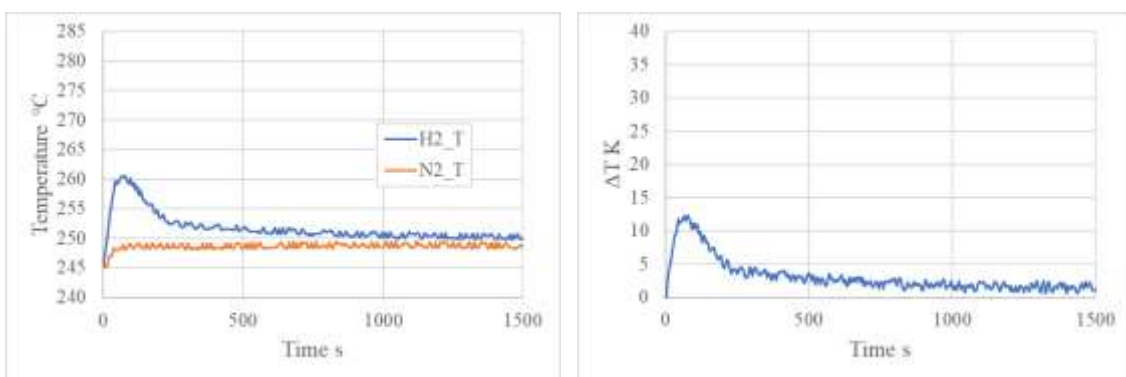
a) time history

b) temperature rise ΔT

Fig. 8. Result of the experiment (Pd-Ni-Zr 3.0 g, 95°C, 0.12 MPa, with pulse flow)

Figure 9 shows the result of the experiment (using 3.0 g of Pd-Ni-Zr composite powder, 0.9 MPa of gas pressure, 240 °C of initial temperature, without the pulse flow). Fig. 9a show the time-histories of temperature for the sample and Fig. 9b shows the temperature rise ΔT . In the experiment, temperature rise began just after hydrogen gas loading. About 12 K of temperature rise was observed about 80 seconds after the beginning of the temperature rise.

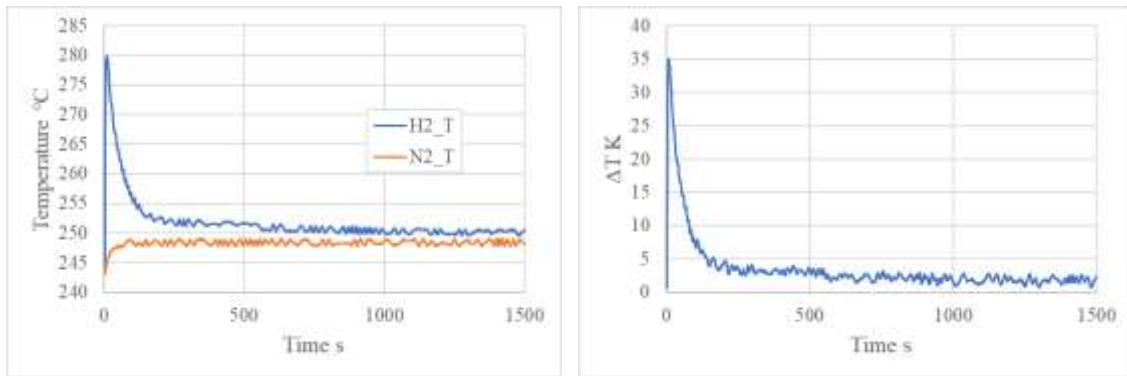
Figure 10 shows the result of the experiment (using 3.0 g of Pd-Ni-Zr composite powder, 0.9 MPa of gas pressure, 240 °C of initial temperature, with the pulse flow). Fig. 10a show the time-histories of temperature for the sample and Fig. 10b shows the temperature rise ΔT . In the experiment, temperature rise began just after hydrogen gas loading. About 35 K of temperature rise was observed about 10 seconds after the beginning of the temperature rise.



a) time history

b) temperature rise ΔT

Fig. 9. Result of the experiment (Pd-Ni-Zr 3.0 g, 240°C, 0.9 MPa, without pulse flow)



a) time history

b) temperature rise ΔT

Fig. 10. Result of the experiment (Pd-Ni-Zr 3.0 g, 240°C, 0.9 MPa, with pulse flow)

5. Effect of the pulse flow of hydrogen gas on the temperature rise

5.1. Effect on the temperature rise of Nickel powder

According to the Figs. 5 and 6, temperature rise ΔT in the experiments (using 3.0 g of Nickel powder, 0.5 MPa of gas pressure, 240 °C of initial temperature) were about 4 K (without the pulse flow) and 3.5 K (with the pulse flow). In this case, obvious difference was not observed in the temperature rise in the experiments (using nickel powder) with and without the pulse flow of hydrogen gas.

5.2. Effect on the temperature rise of Pd-Ni-Zr composite powder

According to the Figs. 7 and 8, temperature rise ΔT in the experiments (using 3.0 g of Pd-Ni-Zr composite powder, 0.12 MPa of gas pressure, 95 °C of initial temperature) were < 1 K (without the pulse flow) and about 9 K (with the pulse flow). In this case, temperature rise was observed only in the experiment with the pulse flow, while almost zero temperature rise without the pulse flow.

According to the Figs. 9 and 10, temperature rise ΔT in the experiments (using 3.0 g of Pd-Ni-Zr composite powder, 0.9 MPa of gas pressure, 240 °C of initial temperature) were about 12 K (without the pulse flow) and about 35 K (with the pulse flow). In this case, larger temperature rise was observed in the experiment with the pulse flow.

Summarizing the above, the temperature rises in the experiments using Pd-Ni-Zr composite powder were increased by the pulse flow of hydrogen gas, and larger temperature rise was observed under the condition of higher gas pressure and initial temperature.

6. Conclusion

The experiments of anomalous heat generation (absorption of hydrogen gas by nickel powder and Pd-Ni-Zr composite powder) with the pulse flow of hydrogen gas were conducted.

As a result, about 3.5 K of temperature rise in the experiment using nickel powder and about 35 K using Pd-Ni-Zr composite powder. In the experiments using the nickel powder, the effect of the pulse flow of hydrogen gas in the temperature rise was not observed. On the other hand, in the experiments using the Pd-Ni-Zr composite powder, the temperature rise was increased by the pulse flow of hydrogen gas under the two experimental conditions. In addition, larger temperature rise was observed under the condition of higher gas pressure and initial temperature.

Acknowledgements

This work was supported by Grant-in-Aid for JSPS Fellows (21J21973) and the grant of The Thermal & Electric Energy Technology Foundation (TEET). We appreciate Technova Inc. for the useful discussion and for providing the sample of Pd-Ni-Zr powder. Sincere thanks are also due to the other members of the Naitoh Laboratory for their help.

References

- [1] Y. Iwamura et al., “Anomalous Heat Effects Induced by Metal Nano-composites and Hydrogen Gas”, *J. Condensed Matter Nucl. Sci.* 29, 119-128, 2019.
- [2] Y. Arata and Y. Zhang, “The Establishment of Solid Nuclear Fusion Reactor”, *J. High Temp. Soc.* 34, 85-93, 2008.
- [3] A. Kitamura et al., “Anomalous effects in charging of Pd powders with high density hydrogen isotopes”, *Physics Letters A*, 373(35), 3109–3112, 2009. doi:10.1016/j.physleta.2009.06.061
- [4] G. H. Miley and J. A. Patterson, “Nuclear transmutations in thin-film nickel coatings undergoing electrolysis”, *J. New Energy* 1, p.5, 1996.
- [5] T. Kobayashi and K. Naitoh, “Quasi-stability theory with multi-dimensional Taylor expansion: revealing transmutation of atoms in cold fusion”, *22nd International Conference on Condensed Matter Nuclear Science (ICCF22) Book of Abstracts*, 18-19, 2019.
- [6] A. Takahashi et al., “Latest Progress in Research on AHE and Circumstantial Nuclear Evidence by Interaction of Nano-Metal and H(D)-Gas”, *J. Condensed Matter Nucl. Sci.* 33, 14-32, 2020.
- [7] R. Konagaya et al., “Development of weak cold-fusion engine (Fusine) assisted by

- molecular chemical reaction: based on double focusing-compression over 1,000 bar and 7,000 K due to pulsed supermulti-jets colliding”, *22nd International Conference on Condensed Matter Nuclear Science (ICCF22) Book of Abstracts*, p.15, 2019.
- [8] K. Naitoh et al., “Fundamental Experimental Tests toward Future Cold Fusion Engine Based on Point-compression due to Supermulti-jets Colliding with Pulse (Fusine)”, *J. Condensed Matter Nucl. Sci.* 24, 236-243, 2017.
- [9] T. Kobayashi, K. Naitoh, Y. Wake, Y. Naridomi, A. Takahashi, R. Seto, H. Ido, J. Hachisuka, “Development of reaction system with small chamber for fundamental experiments measuring anomalous heat effect”, *Proc. of JCF20*, 1-8, 2020.
- [10] T. Kobayashi, J. Shigemura, K. Naitoh, Y. Mori, R. Seto, J. Hachisuka, “Temperature and pressure dependence of anomalous heat generation occurring in hydrogen gas absorption by metal powder”, *J. Condensed Matter Nucl. Sci.*, 2021 accepted.
- [11] A. Takahashi et al., “Latest Progress in Research on AHE and Circumstantial Nuclear Evidence by Interaction of Nano-Metal and H(D)-Gas”, *J. Condensed Matter Nucl. Sci.*, 33, 14-32, 2020.
- [12] R. Konagaya, K. Naitoh, T. Kobayashi, Y. Isshiki, et al., “Two Prototype Engines with Colliding and Compression of Pulsed Supermulti-Jets through a Focusing Process, Leading to Nearly Complete Air Insulation and Relatively Silent High Compression for Automobiles, Motorcycles, Aircrafts, and Rockets”, SAE Technical Paper, 2020-01-0837, 2020. doi:10.4271/2020-01-0837

Recent Progress of Deuterium/Hydrogen Desorption Experiments Using Pd-Ni Samples

S. Narita*, M. Endo, H. Matsushashi, N. Yanagidate, A. Shoji

Iwate University
Morioka, Iwate, 020-8551, Japan

*narita@iwate-u.ac.jp

Abstract

We conducted deuterium absorption and desorption experiments using Pd-based metal complex samples fabricated by depositing metal membranes. In particular, in the deuterium desorption experiment with a Ni membrane coated sample of Pd, we observed a short-period of intermittent fluctuations in temperature, which indicates peculiar migration and densification of deuterium at the Pd-Ni interface. In addition, a large increase in the sample temperature was observed with simultaneous gas release from the sample. We recently modified the experimental conditions to obtain more accurate temperature measurements and better reproducibility. Moreover, we conducted experiments with hydrogen, in addition to our previous experiments with deuterium. As a result, temperature and pressure behaviors similar to those reported in previous studies were observed for both deuterium and hydrogen experiments with high reproducibility. The maximum excess heat was estimated to be a few hundred microjoules.

1. Introduction

Excess heat evolution has been observed in hydrogen (H) and deuterium (D) loading/unloading processes in Pd-Ni and Cu-Ni systems [1–8]. These studies have revealed that the following conditions are important for inducing a low-energy nuclear reaction in condensed matter:

- 1) Complex metals, such as composite particles or multilayers.
- 2) Nano-structures of samples, such as fine particles or thin membranes.

We conducted deuterium absorption and desorption experiments using Pd-based metal complex samples based on the experiment invented by Yamaguchi et al. [9]. In this study, various samples of Pd foils coated with metal membranes, such as Pd/Ni, Pd/Zr, Pd/Ni/Zr, Pd/Ag, and Pd/Ti, were used. In particular, for the sample of Pd coated with the Ni membrane, we observed a short-period intermittent fluctuation in temperature, which might indicate that prompt deuterium diffusion occurred bidirectionally between the Pd foil and the membrane [10–12]. Although we did not obtain any results indicating that

significant excess heat was generated, the associated peculiar migration and densification of deuterium at the Pd-Ni interface may be related to the excess heat generation phenomenon reported in other experiments [4,5].

Experiments were conducted to elucidate the mechanism of the observed phenomena. Recently, we modified our experimental apparatus to obtain more accurate temperature measurements and evaluate heat generation. Moreover, we conducted experiments with hydrogen, in addition to our previous experiments with deuterium. In this paper, we reported the latest experimental results obtained using the modified apparatus.

2. Experiment

The sample was prepared using the following procedure. A fine structure was formed on the surface of the Pd foil ($t = 0.1$ mm) via etching with an Ar ion beam. The surface morphology was investigated using AFM analysis, which revealed several projections with heights of approximately 200 nm, and TEM analysis, which revealed a semi-spherical shape of size 50–200 nm [12]. A Ni membrane ($t \sim 100$ nm) was then deposited onto the etched surface by Ar⁺ sputtering.

The fabricated Pd-Ni sample was exposed to hydrogen or deuterium gas under a pressure of 5 atm for approximately 24 h for loading. The loading ratio H/Pd or D/Pd was typically 0.65–0.75. Subsequently, the sample was placed in the chamber and evacuated to $\sim 10^{-4}$ Pa. A DC power supplier supplied a constant current (0.75 A) to stimulate deuterium out-diffusion from the sample via Joule heating. The sample temperature, pressure in the chamber, and voltage/current applied to the sample were monitored every 0.1 s during the desorption experiment, which continued for approximately 24 h.

We recently modified the experimental setup as follows. The sample temperature was measured using a thermocouple; however, the contact state between the thermocouple and the sample sometimes changed during the desorption experiment, resulting in incorrect temperature measurements. We also used an infrared (IR) radiation thermometer (Chino:IR-CAEJCS). The IR thermometer has another advantage in terms of the time response of the temperature change (~ 0.1 s). In addition, a camera was used to observe the sample deformation during the experiment. Yamaguchi et al. observed heat generation correlated with sample deformation in experiments with Pd multilayer samples. The deformation is considered to be caused by internal stresses generated by the diffusion of hydrogen in the sample and the embrittlement of the sample metal. A model has been proposed in which the phase transition of the sample results in localized densification of hydrogen in the sample, causing nuclear reaction [9].

A schematic of the experimental setup is shown in Fig. 1, and the new sample holder

is shown in Fig. 2.

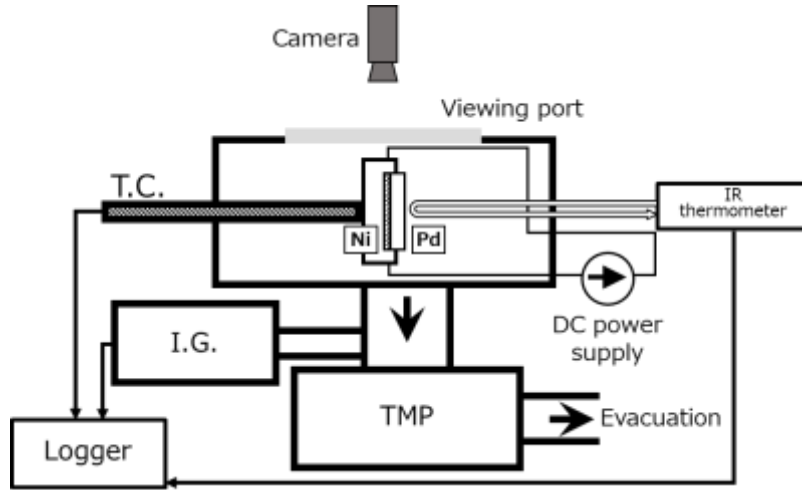


Fig. 1. Schematic of the experimental setup.

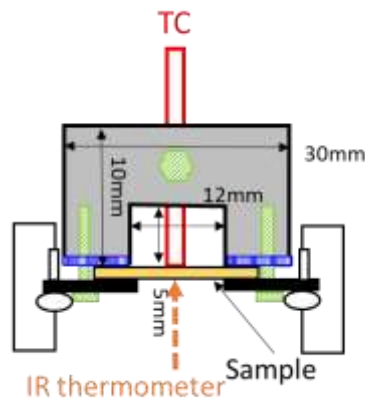


Fig. 2. Sample holder.

3. Results and Discussion

Fig. 3 shows the temporal changes in temperature, pressure, and voltage in two typical desorption experiments with deuterium (Pd/Ni-D-1 and Pd/Ni-D-2), and Fig. 4 shows the magnified view of these changes just after the start of the experiment. Heat generation and gas desorption were observed intermittently during the first few hours of almost all the experiments. This behavior was observed only in the early stages of the experiment, probably because all deuterium in the sample was desorbed within the first few hours. The pressure and voltage changes appear to be synchronized, which indicates that the

sample resistance increased during desorption. Presumably, this is the same phenomenon observed in previous experiments, where deuterium densifies in the sample and is then released [12]. It can be observed that changes in the infrared thermometer follow changes in pressure and voltage. This indicates that the infrared thermometer was more responsive than the thermocouple.

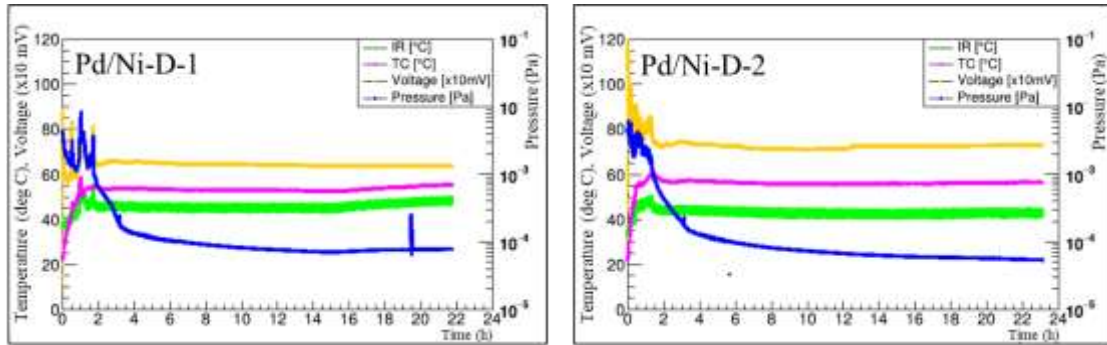


Fig. 3. Time dependence of temperature, pressure, and voltage in deuterium desorption.

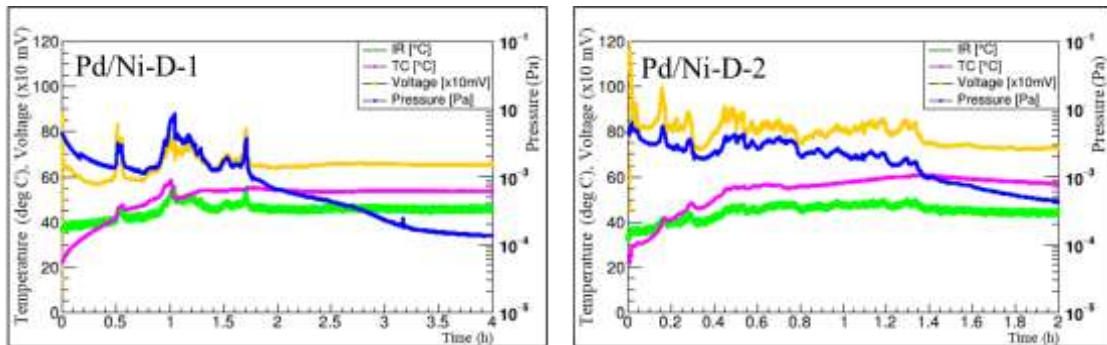


Fig. 4. Time dependence of temperature, pressure, and voltage in deuterium desorption, just after the start of the experiment.

Figs. 5 and 6 show the time dependence of temperature, pressure, and voltage in hydrogen desorption experiments for approximately 24 h and enlarged views of the first few hours of the experiments, respectively, for two typical runs (Pd/Ni-H-1 and Pd/Ni-H-2). Similar behavior was observed in the hydrogen experiments as in the deuterium experiments.

For reference, experiments were conducted using unloaded samples. The results are shown in Fig. 7. No significant changes in temperature or pressure were observed. Therefore, the temperature changes observed in the loaded samples, whether hydrated or deuterated, can be attributed to reactions related to H/D diffusion or adsorption.

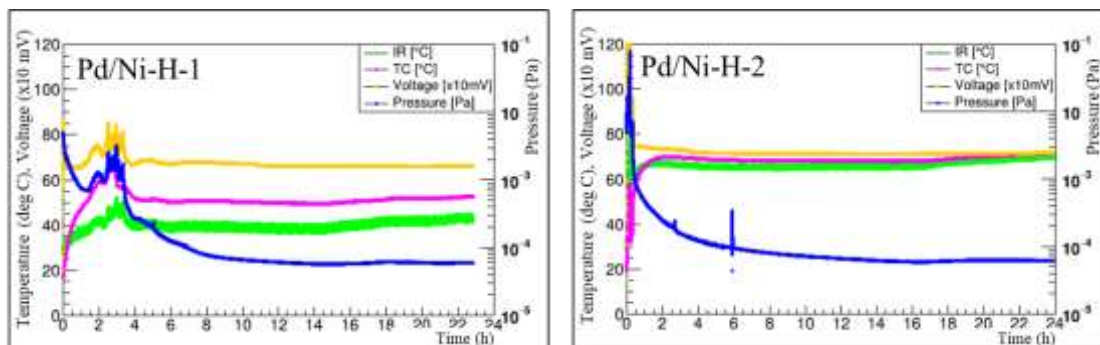


Fig. 5. Time dependence of temperature, pressure, and voltage in hydrogen desorption.

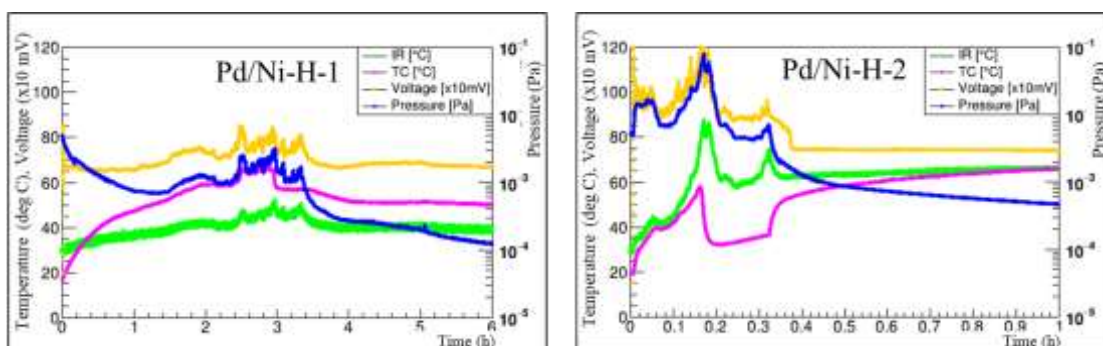


Fig. 6. Time dependence of temperature, pressure, and voltage in hydrogen desorption, just after the start of the experiment.

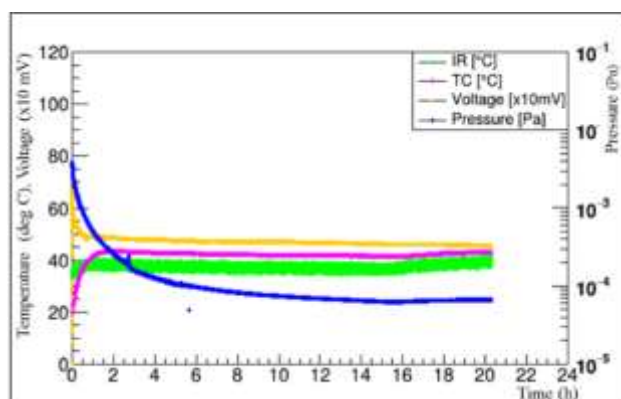


Fig. 7. Time dependence of temperature, pressure, and voltage in reference experiment.

We investigated the heat balance for the observed temperature and the following processes:

- 1) Joule heating due to the fluctuation of the electric power applied.
- 2) Heat by H/D dissolution into Pd.
- 3) Excess heat by unknown processes.

Here, the heat values for each process are expressed as J_1 , J_2 , and J_3 , respectively. The heat derived from the observed temperature change ΔT can be expressed as follows:

$$mC\Delta T = J_1 + J_2 + J_3, \quad (1)$$

where m denotes the weight of the Pd foil and C denotes the specific heat of Pd. J_1 was estimated from the relationship between the change in the input power and sample temperature for the calibration run performed in advance. J_2 can be calculated by the amount of deuterium desorbed while simultaneously changing the temperature, which can be obtained by monitoring the pressure inside the chamber. However, this effect should be small, and J_2 is considered negligible. Here, the heat of solution/dissolution with H/D migration between Pd and Ni should be considered, but it is ignored because the effect is small. Therefore, the excess heat, J_3 , was estimated, and the results for both the deuterium and hydrogen experiments are shown in Fig. 8.

No difference was observed between the experiments with deuterium and hydrogen. The IR thermometer fluctuated between ± 0.1 J and appeared to be sensitive to the J_3 calculation. J_3 reached maximum values of 0.1–0.4 J in each experiment. Particularly, in the experiment for Pd/Ni-H-2, a high value of J_3 was observed (~ 0.4 J) simultaneously with a large amount of gas release. The excess heat obtained here was significantly smaller than that reported in other experiments [2,3,8]. It is necessary to verify these differences by comparing the experimental conditions of each experiment. It is possible that the reactions that cause heat generation differ from each other. In particular, other experiments have been conducted at temperatures of several hundred degree celsius, which may be a critical requirement for inducing a reaction. Our experiments could only be performed at temperatures below 100 °C due to restrictions on the heat resistance of the equipment. Further improvements to the equipment need to be considered. Analysis of the sample images taken during the experiment showed no obvious deformation of the sample during large temperature increases.

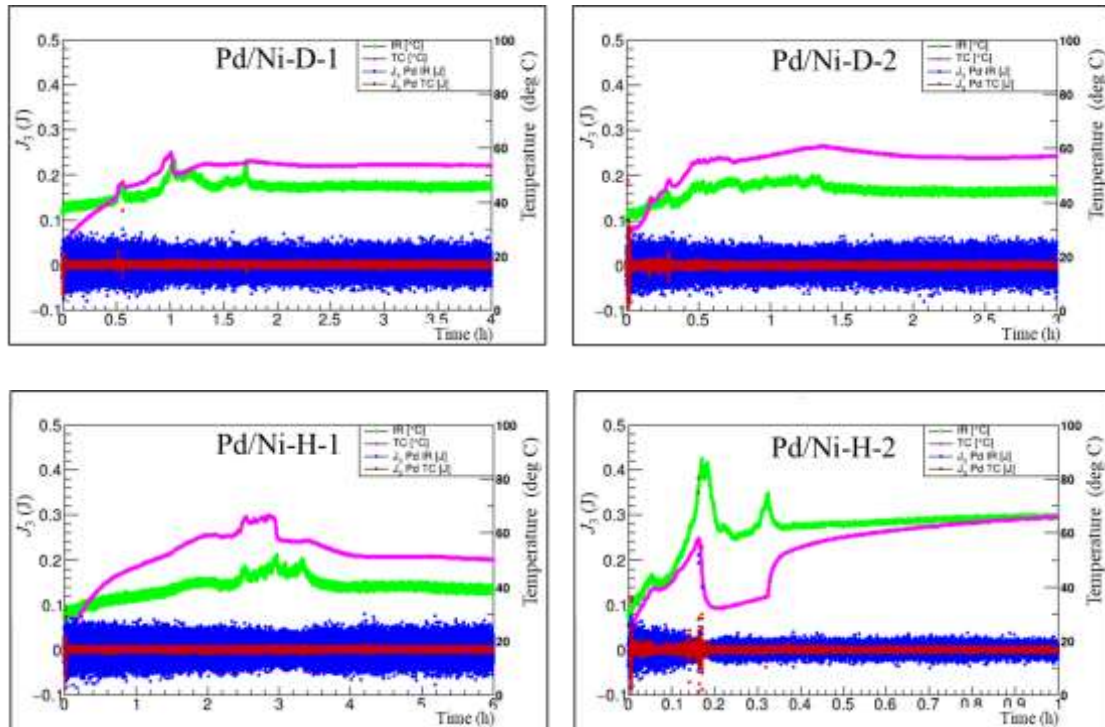


Fig. 8. Excess heat obtained by the temperature measured by a thermocouple (red) and IR thermometer (blue) for the deuterium experiments (top plots) and hydrogen experiments (bottom plots).

4. Summary

We performed deuterium and hydrogen desorption experiments using Pd foil with Ni surface coating and our recently modified experimental setup. Consequently, intermittently increasing temperatures and simultaneous increases in temperature and pressure were observed with high reproducibility within a few hours after the start of the desorption experiment. This phenomenon was also observed in previous studies. The maximum excess heat, estimated from the measured temperatures, was approximately 0.4 J. More accurate temperature measurements and calibration data are required to improve the evaluation of the excess heat. In the future, experiments on various sample types and conditions will be conducted to enhance excess heat. Such studies are expected to clarify the trigger conditions and mechanisms for inducing reactions at the origin of heat generation.

References

- [1] A. Kitamura et al., Proc. of JCF18 (2018) 14.
- [2] A. Kitamura et al., Int. J. Hydrogen Energy 43 (2018) 16187.

- [3] Y. Iwamura et al., Proc. of JCF18 (2018) 32.
- [4] A. Takahashi et al., Proc. of JCF19 (2019) 1.
- [5] T. Yokose et al., Proc. of JCF19 (2019) 18.
- [6] A. Takahashi et al., J. Condensed Matter Nucl. Sci. 33 (2020) 14.
- [7] Y. Iwamura et al., J. Condensed Matter Nucl. Sci. 33 (2020) 1.
- [8] Y. Iwamura et al., Proc. of JCF21 (2021) 1.
- [9] E. Yamaguchi et al., Jpn. J. Appl. Phys., 29 (1990) L666.
- [10] Y. Sato et al., Proc. of JCF18, (2018) 1.
- [11] M. Endo et al., Proc. of JCF19, (2019) 53.
- [12] M. Endo et al., Proc. of JCF20, (2020) 61.

Computer Simulation on the Metal Hydride Band Gaps of Pd, Ni and Cu Metal Lattices

Hidemi Miura

Izumi-ku, Sendai. 981-3109, Japan

Abstract: It has been recently reported if thermal motion of electrons with energy larger than ~ 0.5 eV in metals produce electron neutrino pairs, and if the produced electron neutrinos have the kinetic energy of ~ 0.1 eV, they could cause Low Energy Nuclear Reaction (LENR). If semiconductor-like electronic band gaps of 0.5 to 1.0 eV are generated, electrons which transit from conduction bands to valence bands on the band gaps could replace the thermal electrons in this LENR idea. In order to confirm these band gaps occur, the electronic band and the electronic density of state (DOS) of face centered cubic (FCC) metal lattices such as Pd, Ni and Cu metals, and as a comparison with these metals, those of Pt, Ag, Au and Al metals and others were investigated by using ABINIT, the first principle molecular dynamics method with a personal computer. As a result, the band gaps across the Fermi levels were observed when eight H atoms entered the O sites and T sites of the unit cell of Pd, Ni and Pt metal lattices, and four H atoms entered those of Cu, Ag, and Au metal lattices. Above all, the metal hydride band gaps of Pd, Ni and Cu metal lattices were observed to occur with the gap energy of 0.5 to 1.0 eV.

Keywords: computer simulation, electronic band, electronic density of state, metal hydride band gap

1. Introduction

A lot of experiments and theories have been reported on the Low Energy Nuclear Reaction (LENR) of condensed matter. Among them, we also have investigated the phonon states of the face centered cubic (FCC) metal lattices when H atoms enter them and the total energy when H atoms move between the O sites and T sites of them by computer simulation using a personal computer (PC) ^{1, 2)}.

It has been recently reported by Parkhomov if thermal motion of electrons with energy larger than ~ 0.5 eV in metals produce electron neutrino pairs, and if the produced electron neutrinos have the kinetic energy of ~ 0.1 eV, they could cause the LENR ³⁾. The emission of electron neutrinos from excited atoms is being studied in theories and experiments ⁴⁾. On the other hand, the electronic band and the electronic density of states (DOS) of metal hydrides have been investigated, and found that the Fermi level in palladium hydride (PdH) shifts to the direction of high energy of the electronic band, the hydrides of La and Ce, etc. of rare earth metal transit into insulators ⁵⁾ and NiH₂ and CuH transit into semiconductor states ⁶⁾. However, since these investigations have been done on the metal hydrides with stable H atoms, in relation to the LENR, it will also be necessary to investigate on the metal hydrides with unstable H atoms which rapidly or excessively enter metals. At that time, when H atoms enter metals such as Pd, the Fermi levels would

shift to the direction of high energy of the electronic band and the band gaps of 0.5 to 1.0 eV of semiconductor states could be generated. Although the probabilities of electron neutrino pair production from the electron transition of the band gaps by weak interactions are very small, if some enhancement mechanism of the electron transition will work, electrons which transit from conduction bands to valence bands on the band gaps could replace the thermal electrons in the LNER of Parkhomov.

In order to confirm that metals which occlude H atoms become the metal hydrides to generate the semiconductor states or band gaps, the electronic band and the electronic DOS were investigated by ABINIT, the first principle molecular dynamics method using a PC. Calculations were done for FCC metals with H atoms which entered O sites and T sites, such as Pd metal which rapidly occlude H atoms to form the metal hydride, Ni and Cu metals which are less likely to form the metal hydrides than Pd metal and as a comparison with these metals, Pt, Ag, Au and Al metals which hardly form the metal hydrides. In addition, the electronic band and the electronic DOS of Ti metal of FCC structure forming the metal hydride with occluded H atoms were calculated in the same way, although Ti metal has hexagonal close-packed (HCP) structure with no occluded H atom. Further, those of palladium oxide (PdO) which is different from FCC in the lattice structure were calculated. And those of Pd metal hydride with an impurity atom such as He or Li in one of the O sites of the unit cell were also calculated.

Although H atoms which entered the FCC metals can move quickly between the O sites and the T sites, electrons around the H atoms could more quickly follow the changes caused by the movement of the H atoms. Metals such as Pd, Ni, Pt, Cu, Ag and Au, which were used for the calculations, have originally the small (0 or nearly 0) total electronic DOS regions at the energy of 5 to 10 eV higher than the Fermi levels. When H atoms enter the metal, the number of electronic bands increases according to the amount of electrons carried with the H atoms. Therefore, the new electronic bands are generated in the valence band of the lower energy region than the Fermi level and the higher energy region around the Fermi level due to interactions between the electrons of lattice metals and those of entered H atoms. If H atoms in the metal increases in some extent, the Fermi level shifts to the direction of high energy and enters the band gap or small (0 or nearly 0) total electronic DOS region, and the metal hydride would transit into the semiconductor state.

As a result of the calculations, the band gaps across the Fermi levels were observed to be generated when eight H atoms entered the O sites and T sites of the unit cell of Pd, Ni and Pt metal lattices and four H atoms entered those of Cu, Ag and Au metal lattices. Above all, as the band gaps of energy 0.5 to 1.0 eV it was confirmed that the metal hydride band gaps of $\text{Pd}_4\text{H}_3\text{O}+5\text{H}_\text{T}$ with three H atoms in the O sites and five H atoms in the T sites, and $\text{Pd}_4\text{H}_4\text{O}+4\text{H}_\text{T}$ with four H atoms in the O sites and four H atoms in the T sites occurred. Furthermore, those of $\text{Ni}_4+8\text{H}_\text{T}$ with eight H atoms in the T sites, and those of $\text{Cu}_4+4\text{H}_\text{T}$ with four H atoms in the T sites occurred. On the other hand, those of $\text{Ag}_4+4\text{H}_\text{T}$ occurred as the band gaps wider than 1.0 eV, and those of $\text{Ni}_4\text{H}_4\text{O}+4\text{H}_\text{T}$ and $\text{Au}_4+4\text{H}_\text{T}$ occurred narrower than 0.5 eV. And the small (0 or nearly 0) total electronic DOS regions across the Fermi levels were observed on $\text{Pd}_4+8\text{H}_\text{T}$, etc., but those were not

observed on Ti and PdO metal lattices. However, even near the Fermi level, the band gap or small (0 or nearly 0) total electronic DOS region was not observed on Al metal lattice. When an impurity atom such as He or Li entered one of the O sites of the unit cell of Pd hydride metal lattice, the Fermi level shifted to the direction of high energy, and the band gap or small (0 or nearly 0) total electronic DOS region occurred according to the amount of outermost electrons of the impurity atom and those of occluded H atoms. Therefore, the generation of band gaps in the metal hydride would not depend on only occluded H atoms.

2. Calculations

2.1 Software and Hardware Used for Calculations

Calculations were carried out by ABINIT, the first principles electronic state simulation program. This program was based on Density Functional Theory of the local density approximation using plane waves for the basis function and norm preservation type pseudo potentials with semi core^{7, 8)}. And it worked on a PC with 4 cores / 8 ways CPU and 32 GB main memory.

2.2 Metals Used for Calculations

The electronic band and the electronic DOS of the FCC metal lattices with H atoms in the O sites and T sites, such as Pd metal which rapidly occlude H atoms to form the metal hydrides, Ni and Cu metals which are less likely to form the metal hydrides than Pd metal and, as a comparison with these metals, Pt, Ag, Au and Al metals which hardly form metal hydrides, were calculated. In addition, those of Ti metal which has HCP structure with no occluded H atom and transit to FCC structure forming the metal hydride with occluded H atoms, and those of PdO which is different from FCC structure, were investigated.

2.3 Unit Cell of Metal Lattice Used for Calculations

Fig. 1 shows the unit cell of Cu metal lattice with H atoms occluded in the O sites as an example of the FCC metal lattices such as Pd, Ni, Cu, Pt, Ag, Au and Al metals used for calculations. Ti metal transits to the FCC metal hydrides when H atoms occluded in the T sites of them. Calculations were done as the bulk metals changing the lattice constants of these FCC metals under the periodic boundary conditions.

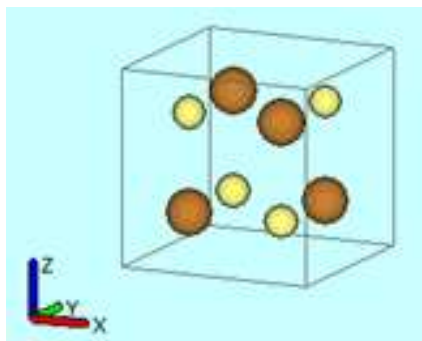


Fig. 1 Unit Cell of Cu_4H_4 (CuH)
as an example of FCC metal lattice
Sphere of brown: Cu atom
Sphere of yellow: H atom

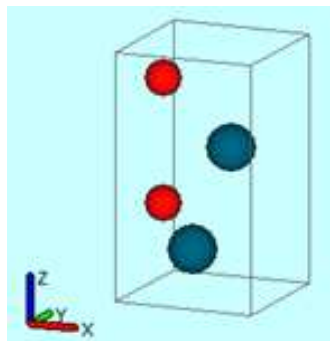


Fig. 2 Unit Cell of Pd_2O_2 (PdO)
as an example
Sphere of bleu: Pd atom
Sphere of brown: O atom

Fig. 2 shows the unit cell of PdO metal lattice which is different from FCC structure. PdO is a powder-shaped metal and consists of asymmetrical O sites and T sites, but calculations were done as if H atoms enter the center of each asymmetrical O sites and T sites in the same way to the FCC metal lattices.

2.4 Methods of Calculations

Calculations were done by increasing H atoms one by one in the O sites of the unit cell of four atoms of Pd, Ni, Cu, Pt, Ag, Au or Al metal, and then by increasing H atoms one by one in the T sites of the unit cell. Furthermore, calculations were oppositely done by increasing H atoms one by one in the T sites of the unit cell of four Ti metal atoms, and then by increasing H atoms one by one in the O sites of the unit cell. The lattice constant was used the value when the total energy of the unit cell of Pd, Ni, Cu, Pt, Ag, Au or Al metal with H atoms in the O sites became the minimum, and when that of Ti metal with H atoms in the T sites became the minimum.

It is known that while H atoms enter stably the O sites of Pd, Ni, Cu of FCC lattice metals, they lose their stability when the distance of two H atoms in the metal lattices are smaller than $\sim 2.1 \text{ \AA}$. Therefore, if some H atoms have already entered the O sites, and the other H atoms entered later the T sites adjacent to them, the H atoms which entered the T sites later would become unstable and go out them. However, calculations were done as if the whole H atoms in the unit cell keep stable short while the electrons move around them. As for Pd metal lattice, although calculations were done using the lattice constants when the total energy of the unit cell with H atoms not only in the O sites but also T sites became minimum, both electronic total DOS near the Fermi level were almost the same. Furthermore, as for Pd metal lattice, three different types of pseudo potentials were used to inspect the typical case, but the whole electronic total DOS were almost the same. As for Ti metal lattice, the lattice constants when the total energy of the unit cell with H atoms not in the T sites but in the O sites became the minimum were used, and the pseudo potential of HCP, not FCC, was used as it was. As for PdO metal lattice, calculations were similarly done by increasing H atoms one by one in the asymmetrical O sites and T sites of the unit cell. Moreover, as for Pd metal lattice, the electronic band and the electronic DOS were calculated with an impurity atom such as He or Li in one of the O sites of the unit cell of the metal hydride lattice. Although each impurity atom possibly enters the T sites of Pd metal lattice if its atomic radius is small, calculations were done in the same way as it enters the O sites.

3. Results

3.1 Pd Metal Lattices

As examples of the calculation results, Fig. 3 shows (a) the electronic band and (b) the electronic DOS of Pd₄H₄O of the unit cell with four H atoms in the O sites. The Fermi level referenced to 0 eV is in the valence band. The bonding band at $\sim -9 \text{ eV}$ and the antibonding band at $\sim 6 \text{ eV}$ were formed by interactions between the 4d orbitals of Pd atoms and the 1s orbitals of H atoms.

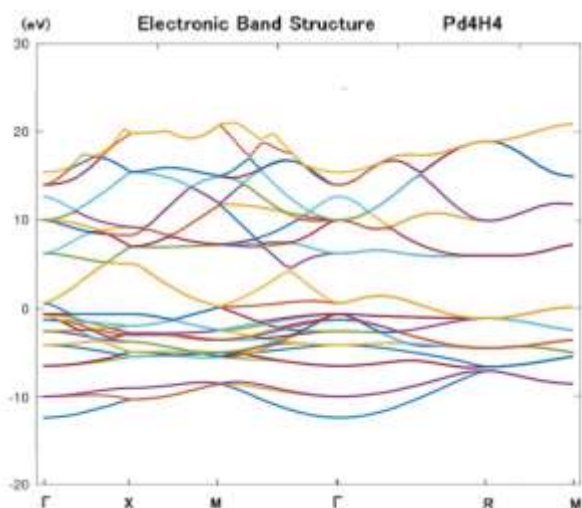
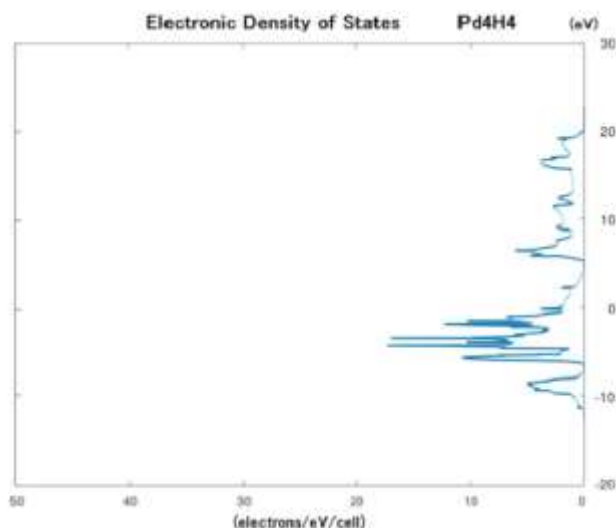


Fig. 3 (a) Electronic Band of Pd₄H₄_O
 Horizontal axis: wavenumber of electron
 (Symmetrical points are indicated.)
 Vertical axis: energy of electron
 Each band is color-coded for easy viewing.



(b) Electronic DOS of Pd₄H₄_O
 Horizontal axis: density of States
 Vertical axis: energy of electron

As examples of band gaps of 0.5 to 1.0 eV, Fig. 4 shows (a) the electronic band and (b) the electronic DOS of Pd₄H₄_O+4H_T of the unit cell with four H atoms in the O sites and four H atoms in the T sites. The Fermi level referenced to 0 eV is in the band gap. The bonding band at ~ -9 eV was almost at the same place of Pd₄H₄_O, but the antibonding band shifted down to ~ 0.9 eV from ~ 6 eV of Pd₄H₄_O.

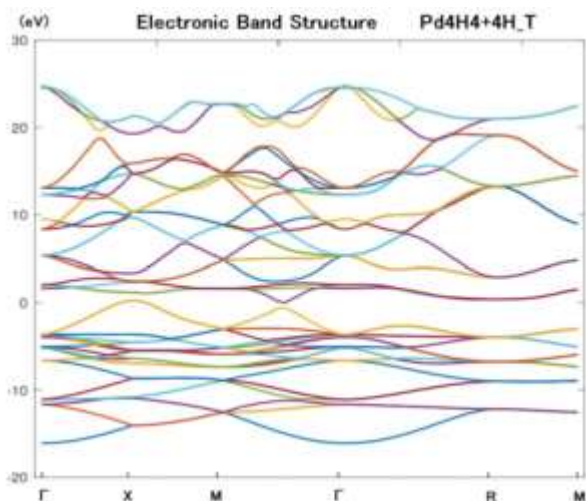
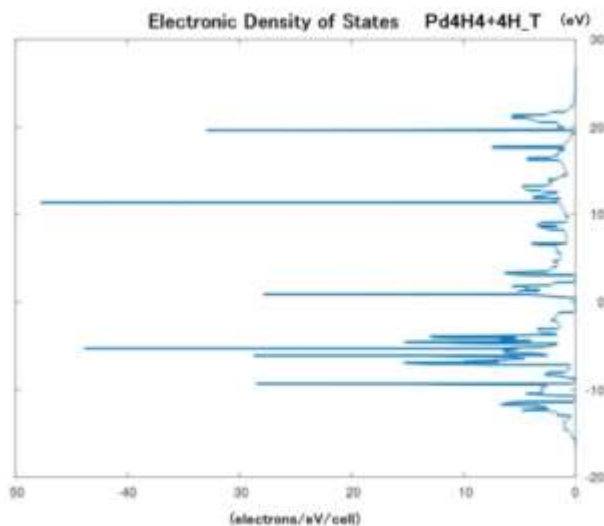


Fig. 4 (a) Electronic Band of Pd₄H₄_O+4H_T
 Horizontal axis: wavenumber of electron
 (Symmetrical points are indicated.)
 Vertical axis: energy of electron
 Each band is color-coded for easy viewing.



(b) Electronic Band of DOS of Pd₄H₄_O+4H_T
 Horizontal axis: density of states
 Vertical axis: energy of electron

Fig. 5 shows the enlarged view of the neighborhood of the Fermi level of the electronic DOS of Pd₄H₄_O+4H_T. Blue line indicates the total electronic DOS, orange line indicates the partial electronic DOS of 4d electron orbitals of Pd atoms, yellow line

indicates those of 1s electron orbitals of H atoms in the O sites, green line indicates those of 1s electron orbitals of H atoms in the T sites and light blue line indicates (overlapping) those of 2s and 2p electron orbitals of H atoms in the O sites and T sites.

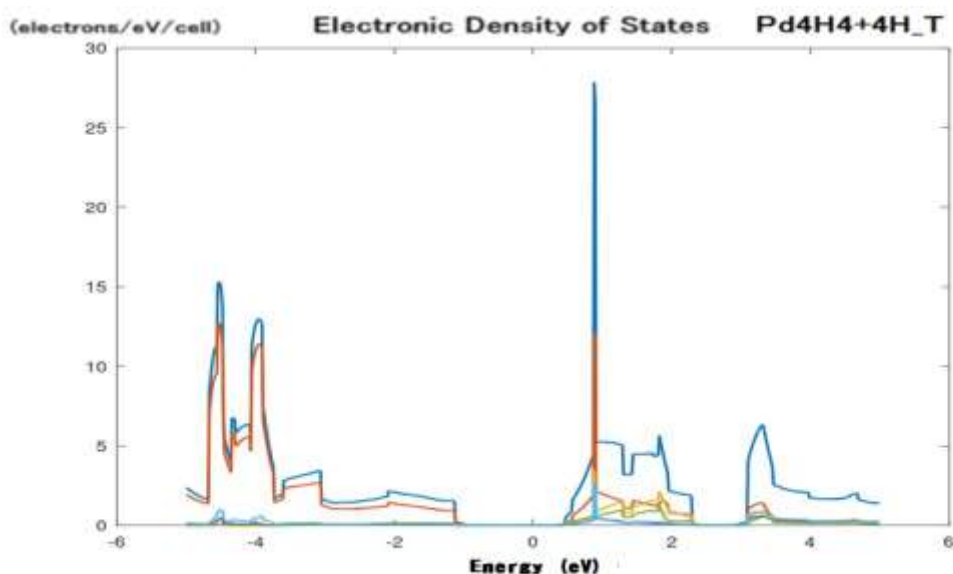


Fig. 5 Electronic DOS of Pd₄H₄_O+4H_T (neighborhood of Fermi Level)

Blue line: the total electronic DOS,
 Orange line: the partial electronic DOS of 4d electron orbitals of Pd atoms,
 Yellow line: those of 1s electron orbitals of H atoms in the O sites,
 Green line: those of 1s electron orbitals of H atoms in the T sites,
 Light blue line: those of 2s and 2p electron orbitals of H atoms in the O sites and T sites

The partial electronic DOS of 4d electron orbitals of Pd atoms occupied the most of the total electronic DOS in the valence band lower than the Fermi level. And the contribution of the partial electronic DOS of 1s/1p and 2s/2p electron orbitals of H atoms increased in the total electronic DOS of the conduction band higher than the Fermi level. On the other hand, a sharp peak appeared at ~ 0.9 eV higher than the Fermi level, where the partial electronic DOS of the various electron orbitals overlapped each other by the interactions between 4d orbitals of Pd atoms and s and p electron orbitals of H atoms. (These sharp peaks appeared with intervals of ~ 10 eV in the electronic DOS of Pd₄H₄_O+4H_T (Fig.4 (b)).) No sharp peak appeared in the electronic DOS of Pd₄H₄_O (Fig.3 (b)). Electrons could be probably excited through this sharp peak near the Fermi level and transit to the lower level over the band gap. Although the similar peaks also appeared in Ni₄H₄_O+4H_T and Cu₄+4H_T, the peak in Pd₄H₄_O+4H_T was the largest.

Table 1 shows the lattice constants when the total energy of the unit cell of Pd metal lattice with H atoms in the O sites become the minimum, and the band gaps or small (0 or nearly 0) total electronic DOS regions with H atoms in the O sites and T sites. The total electronic DOS smaller than 0.0001 electrons/eV/cell are written by the lower limits and upper limits without any parentheses, which mean band gaps. And the total electronic DOS smaller than 0.01, 0.1 and 0.2 electrons/eV/cell are written by the lower limits and upper limits with parentheses of [], () and (()), respectively.

Table 1 Lattice Constants, Band Gaps or Small Total DOS Regions of Pd₄H_{m+n}T

	Lattice Constant									
	[eV; Based on Fermi level]									
	Pd4H0 (Pd)		Pd4H1(PdH _{0.25})		Pd4H2(PdH _{0.5})		Pd4H3(PdH _{0.75})		Pd4H4 (PdH)	
	3.87 Å		3.93 Å		3.98 Å		4.02 Å		4.07 Å	
	6.79	7.80	6.40	6.95	5.65	5.90	4.34	5.16	2.98	4.63
+ H1_T	6.72	6.95	[5.88	6.04]	[4.76	5.03]	3.42	3.86	2.48	2.91
+ H2_T	[6.14	6.38]	5.27	5.35	3.70	3.79	(2.85	3.27)	1.93	2.12
+ H3_T	4.75	5.95	3.82	4.21	2.80	3.38	1.68	2.27	0.80	1.46
+ H4_T	3.04	5.04	2.64	3.34	1.85	2.34	0.80	1.45	-0.75	0.13
+ H5_T	[3.30	3.51]	2.40	2.66	[1.39	1.62]	-0.63	[0.01]	-1.20	-0.91
+ H6_T	1.96	2.74	1.41	1.95	((-0.22	0.12))	-1.52	-1.15	-1.49	-1.23
+ H7_T	0.95	1.31	(-0.34	0.10)	(-1.05	-0.68)	-1.90	-1.33	-1.77	-1.40
+ H8_T	[-0.51	0.27]	(-1.64	-1.15)	-1.82	-1.29	-2.00	-1.15	-2.22	-1.68

Criteria : < 0.0001 electrons/eV/cell [< 0.01 electrons/eV/cell]
 (< 0.1 electrons/eV/cell)
 ((< 0.2 electrons/eV/cell))

If H atoms in Pd metal lattices increased in some extent, the Fermi levels shifted to the direction of high energy and to the originally small (0 or nearly 0) total electronic DOS regions at the energy of 6 to 8 eV higher than the Fermi levels. Consequently the band gaps or the small total electronic DOS regions across the Fermi levels occurred when eight H atoms entered the O sites and T sites of the unit cell of Pd metal lattices, which were displayed in shades.

3.2 Comparison of Ni, Pd and Pt Metal Lattices

Table 2 compares the band gaps or small (0 or nearly 0) total electronic DOS regions of Ni, Pd and Pt metal lattices when H atoms enter the O sites and T sites of the unit cell of them. Adding to the band gaps or the small total electronic DOS regions referred above, those smaller than 0.4 electrons/eV/cell are written by the lower limits and upper limits with [()].

Table 2 Comparison of Important Band Gaps or Small Total DOS Regions of Ni, Pd and Pt Metal

	Lower Limit			Upper Limit	
	Energy Gap etc.				
Ni4 + H8_T	-0.34	0.51	Ni4H1 + H7_T	(-0.19	0.36)
	ΔE = 0.85			(ΔE = 0.55)	
Pd4 + H8_T	[-0.51	0.27]	Pd4H1 + H7_T	(-0.34	0.10)
	ΔE = 0.78			(ΔE = 0.44)	
Pt4 + H8_T	(-0.01	0.19)	Pt4H1 + H7_T	((-0.14	0.26))
	ΔE = 0.20			[(ΔE = 0.41)]	
Ni4H3 + H5_T	(-0.14	0.25)	Ni4H4 + H4_T	-0.20	0.17
	ΔE = 0.39			ΔE = 0.37	
Pd4H3 + H5_T	-0.63	[0.01]	Pd4H4 + H4_T	-0.75	0.13
	ΔE = 0.64			ΔE = 0.88	

Criteria : < 0.0001 electrons/eV/cell [< 0.01 electrons/eV/cell]
 (< 0.1 electrons/eV/cell)
 ((< 0.2 electrons/eV/cell))
 [(< 0.4 electrons/eV/cell)]

Above all, the metal hydride band gaps of Pd₄H₃_O+5H_T of 0.64 eV with three H atoms in the O sites and five H atoms in the T sites, and that of Pd₄H₄_O+4H_T of 0.88eV with four H atoms in the O sites and four H atoms in the T sites were observed as the band gaps of 0.5 to 1.0 eV and of smaller than 0.0001 electrons/eV/cell (partially 0.01 electrons/eV/cell). Furthermore, that of Ni₄+8H_T of 0.85 eV with eight H atoms in the T sites, and that of Ni₄H₄_O+4H_T of 0.37 eV with four H atoms in the O sites and T sites respectively, were observed as the band gaps smaller than 0.0001 electrons/eV/cell but narrower than 0.5 eV.

3.3 Cu Metal Lattices

Table 3 shows the lattice constants when the total energy of the unit cell of Cu metal lattice with H atoms in the O sites become the minimum, and the band gaps or small (0 or nearly 0) total electronic DOS regions with H atoms in the O sites and T sites. Adding to the band gaps or the small total electronic DOS regions referred above, those smaller than 0.6 electrons/eV/cell are written by the lower limits and upper limits with ((()))

Table 3 Lattice Constants, Band Gaps or Small Total DOS Regions of Cu₄H_m+nH

	Cu ₄ H ₀ (Cu)		Cu ₄ H ₁ (CuH _{0.25})		Cu ₄ H ₂ (CuH _{0.5})		Cu ₄ H ₃ (CuH _{0.75})		Cu ₄ H ₄ (CuH)	
	3.57 Å		3.63 Å		3.70 Å		3.76 Å		3.80 Å	
	[(4.18 4.41)]	[(2.82 3.35)]	[(2.16 2.39)]	[(1.46 1.72)]	[(0.19 0.29)]	[(0.19 0.29)]	[(0.19 0.29)]	[(0.19 0.29)]	[(0.19 0.29)]	[(0.19 0.29)]
+ H1_T	[(2.81 3.02)]	(((1.76 2.19)))	[(0.92 1.12)]	((-0.19 0.05))	((-0.93 -0.68))					
+ H2_T	((1.97 2.39))	[(1.11 1.35)]	[(−0.47 0.02)]	(−0.86 −0.60)	((−1.35 −0.80))					
+ H3_T	(1.53 1.75)	((−0.39 −0.03))	[(−1.37 −0.63)]	−1.19 −0.95	−1.46 −1.31					
+ H4_T	−0.55 0.17	−1.29 −0.93	−1.41 −1.19	−2.44 −1.36	−2.54 −1.64					
+ H5_T	((−0.99 −0.66))	[−1.56 −1.31]	−1.49 −1.12	−2.68 −2.01	−2.64 −2.04					
...					

Criteria : < 0.0001 electrons/eV/cell [< 0.01 electrons/eV/cell]
 (< 0.1 electrons/eV/cell)
 ((< 0.2 electrons/eV/cell))
 [(< 0.4 electrons/eV/cell)]
 (((< 0.6 electrons/eV/cell)))

If H atoms in Cu metal lattices increased in some extent, the Fermi levels shifted to the direction of high energy and to the originally small (0 or nearly 0) total electronic DOS regions at the energy of 4 to 5 eV higher than the Fermi levels. Consequently the band gaps or the small total electronic DOS regions across the Fermi levels occurred when four H atoms entered O sites and T sites of the unit cell of Cu metal lattices, which were displayed in shades.

3.4 Comparison of Cu, Ag, Pt and Ti Metal Lattices

Table 4 compares the band gaps or small (0 or nearly 0) total electronic DOS regions of Cu, Ag and Au metal lattices when H atoms enter O sites and T sites of the unit cell of them, further that of Ti metal lattice for reference.

Table 4 Comparison of Important Band Gaps or Small Total DOS Regions of Cu, Ag, Au and Ti Metals

Cu4+H4_T	-0.55	0.17	Cu4H4	(-0.19	0.29)	Lower Limit	Upper Limit				
	$\Delta E = 0.72$							$\Delta E = 0.48$		Energy Gap etc.	
Ag4+H4_T	-1.02	0.40									
	$\Delta E = 1.42$										
Au4+H4_T	-0.46	-0.05	Ti4H8_T.fcc	(-0.68	-0.30)	[eV; Based on Fermi level]					
	$\Delta E = 0.41$							$\Delta E = 0.38$			

Criteria : < 0.0001 electrons/eV/cell (< 0.1 electrons/eV/cell)

Above all, the metal hydride band gap of Cu₄+H₄_T of 0.72 eV with four H atoms in the T sites was observed as the band gap of 0.5 to 1.0 eV and of smaller than 0.0001 electrons/eV/cell. Furthermore, that of Ag₄+H₄_T of 1.42 eV was observed as the band gap wider than 1.0 eV, and that of Au₄+H₄_T of 0.41 eV was observed as the band gap narrower than 0.5 eV, both of which were smaller than 0.0001 electrons/eV/cell. Further, the small total electronic DOS regions not across the Fermi levels were observed on Ti metal lattice.

3.5 Other Metal Lattices

The small (0 or nearly 0) total electronic DOS regions were observed in PdO metal lattices, but those were not observed even near the Fermi levels in Al metal lattices. As for Ti metal, there was a problem in the use of pseudo potential of HCP structure with no H atom for the metal hydride of FCC structure with H atoms in the T sites. And as for PdO metal, there was another problem that although PdO was a powder-shaped metal and consisted of asymmetrical O sites and T sites, calculations were done as if H atoms enter the center of them respectively, in the same way to the FCC metal lattices.

When an impurity atom such as He or Li entered one of the O sites of the unit cell of Pd hydride metal lattice, the Fermi level shifted to the direction of high energy by the amount of outermost electrons of the impurity atom and those of occluded H atoms, the band gap or small total electronic DOS region across the Fermi level occurred. Therefore, the generation of band gaps in the metal hydrides would not depend on only occluded H atoms. Calculation results related to the impurity atoms were shown in Appendix(Table5).

4. Discussion

4.1 Changes of Electronic State in Metal Lattices

Metals such as Pd, Ni, Pt, Cu, Ag, and Au, which were used for the calculations, had originally the small (0 or nearly 0) total electronic DOS regions at the energy of 4 to 8 eV higher than the Fermi levels. When H atoms entered the O sites and T sites of the metal lattice, a bonding band appeared in the lower energy region of the valence band and an antibonding band appeared in the higher energy region around the Fermi level due to the interaction between the orbital electrons of lattice metal atoms and those of occluded H atoms, and the Fermi level shifted to the direction of high energy of the electronic band. Consequently, when eight H atoms entered the unit cell of Ni, Pd and Pt metal lattices, which were the elements of group 10 in the periodic table written in Table 1 and Table 2, the Fermi levels entered the band gaps or small (0 or nearly 0) total electronic DOS

regions of them. Similarly, when four H atoms entered the unit cell of Cu, Ag and Au metal lattices, which were the elements of group 11 in the periodic table written in Table 3 and Table 4, the Fermi levels entered the band gaps or small (0 or nearly 0) total electronic DOS regions of them. When twice as many H atoms enter Ni, Pd and Pt atom metals of the elements of group 10 in the periodic table as Cu, Ag and Au metals of the elements of group 11 in the periodic table, elements of both groups would become the same electronic state in which the band gaps across the Fermi levels would be temporarily phase transitioned semiconductor states. Above all, the metal hydride band gaps of Pd₄H₃_O+5H_T of 0.64 eV and Pd₄H₄_O+4H_T of 0.88 eV of Pd metal lattice, Ni₄+8H_T 0.85 eV of Ni metal lattice and Cu₄+4H_T of 0.72 eV of Cu metal lattice were observed.

In this simulation, the metal hydride band gaps of Pd, Ni and Cu metal lattices were investigated when H atoms entered the O sites and T sites of them. Similar result would be expected when deuterium (D) atoms enter those metal lattices, although some differences in calculation results would take place between H and D isotopes. These metal hydride band gaps across the Fermi levels would occur in the process of movement of H/D atoms which entered the metal lattices rapidly or excessively by electrolysis, gas permeation and agitation with vibration blades ⁹⁾, etc.

4.2 Process of LENR Caused by Metal Hydride Band Gaps

The LENR would be caused in the following processes, in which electron neutrinos and electron antineutrinos are produced by the electron transition from the metal hydride band gaps with the premise,

(1) Experiments were conducted in which neutrinos collided with electrons bound in atoms to expel electrons. From this, it was theoretically inferred that changes in the bound state of electrons in atoms cause the production of neutrino pairs. An electron neutrino is considered to have the mass smaller than 0.28 eV ¹⁰⁾, so the electron neutrino pair production could occur in the electron transition of the band gap larger than ~ 0.6 eV.

(2) Photons are mostly produced by the electron transition from the band gaps, and the probabilities of electron neutrino pair production by weak interactions are very small. Therefore, in order for the LENR to be caused by neutrino pair production through the electron transition from these band gaps, some kind of enhancement of the electron transitions will be necessary.

4.2.1 Generation of Metal Hydride Band Gaps

It is considered that the metal hydride band gaps of Pd, Ni and Cu metal lattices were confirmed when H/D atoms entered the O sites and T sites of them in this simulation.

4.2.2 Electron Excitations by H/D Atoms

In this simulation, the metal hydride band gaps of 0.5 to 1.0 eV semiconductor state across the Fermi levels were confirmed when H/D atoms entered Pd, Ni and Cu metal lattices. Although almost all of electrons in the metal at room temperature (~ 300 K) have energy smaller than ~ 0.05 eV, H/D atoms possibly get changed the energy of ~ 0.5 eV

when they move between the O sites and T sites ²⁾, which could cause the valence electrons to jump the metal hydride band gaps of Pd, Ni and Cu metal lattices.

4.2.3 Electron Transitions and Accumulation of Electron Excitations

Electrons would transit from the excited states of the metal hydride band gaps to the low energy states across the Fermi levels, mostly emitting photons. If H/D atoms diffuse and move in the metal lattice increase, the chances of interaction of them also increase. Therefore, electrons being excited to the higher energy of conduction bands become more than those transit to the lower energy of valence bands to accumulate the excited states of conduction bands of the metal hydride band gaps.

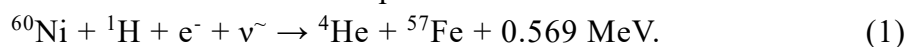
4.2.4 Enhancement of Electron Transitions

Electrons would transit the metal hydride band gaps of 0.5 to 1.0 eV across the Fermi levels, mostly emit photons. These photons are considered to be the infrared radiations of energy smaller than ~ 1.0 eV or wavelength longer than ~ 1.0 μm . If the wavelength is sufficiently longer than the lattice constant of metal lattices, a lot of adjacent band gaps would be coherently excited to emit collectively many photons in some enhancement mechanism such as superradiance. The more photons emitted by superradiance would cause the more neutrinos produced, although the probabilities by weak interactions are very small, or the more electrons excited by the rest photons.

4.2.5 Efficient LENR by Produced Electron Neutrinos and Antineutrinos

The electron neutrino production would be mostly proportional to the number of photons in the lattice metal. And the significant number of electron neutrinos would be produced. The kinetic energy of the produced electron neutrino or electron antineutrino is the remaining half of the transition energy of the electron minus the mass of the produced neutrino pair. If the transition energy of the electron is less than ~ 1.0 eV, the kinetic energy of the generated electron neutrino or electron antineutrino becomes smaller than ~ 0.2 eV. As a result, the spread of the neutrino's wave function (the degree of de Broglie wavelength) is on the order of micrometers, neutrinos cause many interactions over a wide range, and the LENR occurs efficiently even if the probability of a weak interaction process is low. Produced electron neutrinos and electron antineutrinos would be considered to interact with quarks in H/D atoms (proton (p) / deuteron (d)) by weak interactions to cause the LENR.

For example, a proton (quark) of H/D atom, an electron and the produced electron antineutrino would interact by weak interactions and collide all together as “a pseudo neutron ($1\text{H/D} + e^- + \bar{\nu}$)” on another nucleus such as a lattice metal nucleus. This type LENR has been shown in the report of Parkhomov ³⁾.



4.3 Traces of LENR on the Surface of Solids Such as Metals

When the electron transition is enhanced by superradiance, electron neutrinos and

electron antineutrinos are thought to be produced along several narrow cones due to the high directivity of superradiance. In the case of solids such as metals, the generated heat and the produced atomic elements by the LENR might leave traces of geometric patterns such as circles and ellipses on the surface of solids, and the generated melts or products might erupt from small areas of the surface of solids.

5. Summaries

It has been recently reported by Parkhomov if thermal motion of electrons with energy larger than ~ 0.5 eV in metals produce electron neutrino pairs, and if the produced electron neutrinos have the kinetic energy of ~ 0.1 eV, they could cause the LENR. Therefore, if H atoms enter metals such as Pd, and if temporarily the semiconductor-like band gaps of 0.5 to 1.0 eV are generated, electrons which transit the band gaps could replace the thermal electrons in the LENR of Parkhomov. In order to confirm these band gaps occur, the electronic band and the electronic DOS of FCC metal lattices such as Pd, Ni and Cu metals, comparing with Pt, Ag, Au and Al metals and others, were investigated by using ABINIT, the first principle molecular dynamics method with a PC. As a result, it was confirmed that the band gaps across the Fermi levels were generated when eight H atoms entered the O sites and T sites of the unit cell of Pd, Ni and Pt metal lattices, and four H atoms entered those of Cu, Ag and Au metal lattices. Above all, the metal hydride band gaps of Pd, Ni and Cu metal lattices were observed to occur with the gap energy of 0.5 to 1.0 eV to cause the LENR.

In this simulation, the metal hydride band gaps of Pd, Ni and Cu metals were investigated when H atoms entered the O sites and T sites of them. Similar result would be expected when D atoms enter those metal lattices, although some differences in calculation results would take place between H/D isotopes. These metal hydride band gaps across the Fermi levels would occur in the process of movement of H/D atoms which entered the metal lattices rapidly or excessively by electrolysis, gas permeation and agitation with vibration blades, etc. The LENR would be caused in the following processes, in which the electron neutrinos and electron antineutrinos are produced by the electron transition from the metal hydride band gaps,

- (1) Generation of Metal Hydride Band Gaps,
- (2) Electron Excitations by H/D Atoms,
- (3) Electron Transitions and Their Accumulation of Electron Excitations,
- (4) Enhancement of Electron Transitions,
- (5) Efficient LENR by Produced Electron Neutrinos and Antineutrinos.

It is considered that the realization of these processes involves technical difficulties. However, if electrons transit the metal hydride band gaps of 0.5 to 1.0 eV, the LENR would probably occur due to the enhancement of the electron transition with such as superradiance and the increase of neutrino interactions with spread of neutrino wave functions.

References

- 1) H. Miura, Computer Simulation of Hydrogen Phonon States in Palladium Metal, Proc. of 15th Meeting of Japan CF Research Society, p. 100 (2014)
- 2) H. Miura, Computer Simulation of Transition Energy of H atoms in Cu, Ag and Au Metal Lattices, Proc. of JCF 20, 47 (2019)
- 3) A. G. Parkhomov, Weak Interactions as Essence of LENR, International Journal of Unconventional Science, E4, 3-5 (2019).
- 4) M. Yoshimura, Neutrino Pair Emission from Excited Atoms, Phys. Rev. D 75, 113007 (2007).
- 5) A. Fujimori, et al, Electronic Structure of Cerium Hydrides: Augmented-Plane-Wave Linear-Combination-of-Atomic-Orbitals Energy Bands, Phys. Rev. B 22, 3573 (1980).
- 6) H. Smithson, et.al, First-Principles Study of the Stability and Electronic Structure of Metal Hydrides, Phys. Rev. B 66, 144107 (2002).
- 7) X. Gonze, et.al, Computer Phys. Commun. 180, 2582-2615 (2009).
"ABINIT : First-principles approach of materials and nanosystem properties."
- 8) X. Gonze, et.al, Zeit. Kristallogr. 220, 558-562 (2005).
"A brief introduction to the ABINIT software package."
- 9) H. Miura, Water Cluster Related to OHMASA-GAS, Proc. of JCF 18, 93 (2017).
- 10) Thomas S.A., et al, Upper Bound of 0.28 eV on Neutrino Masses from the Largest Photometric Redshift Survey, Phys. Rev. Lett., 105(3):031301 (2010). .

Appendix

Table 5 Comparison of Impurity Atom Occluded Pd Hydride Band Gaps or Small Total DOS Regions

								Lattice Constant	
								Lower Limit	Upper Limit
								[eV; Based on Fermi level]	
1	2	3 ~ 12	13	14	15	16	17	18	
①	②		③	④	⑤	⑥	⑦	⑧ (⑩)	
1	Pd4H4+4H_T							~He1H3+5H_T	
	-0.75 0.13 ΔE = 0.88								-0.58 0.07 ΔE = 0.65
2	~Li1H3+4H_T	~Be1H3+3H_T	~B1H3+2H_T		~C1H3+1H_T	~N1H3	~O1H3+7H_T	~F1H3+6H_T	~Ne1H3+5H_T
	-0.52 0.05 ΔE = 0.57	-0.69 0.02 ΔE = 0.71	(-0.16 0.30) ΔE = 0.46		-0.34 0.36 ΔE = 0.70	(-0.18 0.11) ΔE = 0.29	(-0.33 -0.27) ΔE = 0.06	(-0.10 0.13) ΔE = 0.23	-0.57 0.24 ΔE = 0.81
3	~Na1H3+4H_T	~Mg1H3+3H_T	~Al1H3+2H_T		~Si1H3+1H_T	~P1H3	~S1H3+7H_T	~Cl1H3+6H_T	~Ar1H3+5H_T
	-0.36 0.02 ΔE = 0.38	-0.53 0.17 ΔE = 0.70	((-0.09 0.13) ΔE = 0.22)		-0.28 0.40 ΔE = 0.68	(-0.45 0.35) ΔE = 0.80	— — ΔE = 0.00	(-0.10 -0.06) ΔE = 0.04	-0.35 0.11 ΔE = 0.46
4	~K1H3+4H_T	~CaH3+3H_T	Transition Metal	~Ga~	~Ge~	~As~	~Se~	~Br~	~Kr~
	(-0.50 0.28) ΔE = 0.78	(-0.39 0.34) ΔE = 0.73		~	~	~	~	~	~

Criteria : < 0.0001 electrons/eV/cell (< 0.1 electrons/eV/cell)
(< 0.2 electrons/eV/cell)

① ~ ⑩ : Number of Outermost Electrons